Migration of allogenic T cells in intestinal lymphoid structures during acute Graft-versus-Host Disease.

Migration allogener T-Zellen in intestinalen lymphoiden Strukturen während der akuten Graft-versus-Host Reaktion.

Doctoral thesis for a doctoral degree
at the Graduate School of Life Sciences,
Julius-Maximilians-Universität Würzburg,
Section Infection and Immunity

submitted by

Katja Julika Jarick (née Ottmüller)

from

Hamburg

Würzburg 2019

Submitted on: ……..……..
Office stamp

Members of the Promotionskomitee:

Chairperson:	Prof. Dr. Georg Gasteiger
Primary Supervisor:	Prof. Dr. Dr. Andreas Beilhack
Supervisor (Second):	Prof. Dr. Manfred Lutz
Supervisor (Third):	Prof. Dr. Michael Sixt
Supervisor (Fourth):	Prof. Dr. Joachim P. Spatz

Date of Public Defense: ……..……

Date of Receipt of Certificates: …….

I. Affidavit

I hereby confirm that my thesis entitled 'Migration of allogenic T cells in intestinal lymphoid structures during acute Graft-versus-Host Disease.' is the result of my own work. I did not receive any help or support from commercial consultants. All sources and / or materials applied are listed and specified in the thesis.

Furthermore, I confirm that this thesis has not yet been submitted as part of another examination process neither in identical nor in similar form.

Place, Date Signature

Eidesstattliche Erklärung

Hiermit erkläre ich an Eides statt, die Dissertation „Migration allogener T-Zellen in intestinalen lymphoiden Strukturen während der akuten Graft-versus-Host Reaktion." eigenständig, d.h. insbesondere selbständig und ohne Hilfe eines kommerziellen Promotionsberaters, angefertigt und keine anderen als die von mir angegebenen Quellen und Hilfsmittel verwendet zu haben.

Ich erkläre außerdem, dass die Dissertation weder in gleicher noch in ähnlicher Form bereits in einem anderen Prüfungsverfahren vorgelegen hat.

Ort, Datum Unterschrift

II. Acknowledgements

I would like to take the opportunity to thank the people who helped me accomplish the completion of this thesis.

First of all, I would like to thank Prof. Andreas Beilhack for accepting me to his group and to entrust me with this exciting project. Thank you for your insightful personal and scientific guidance, the liberty of action and the motivation, which always encouraged me to continue and think independently.

Thank you to Prof. Manfred Lutz, Prof. Michael Sixt and Prof. Joachim Spatz for being on my thesis committee. The wise scientific input during the meetings was of great value for me and considerably contributed to shaping my questions and aims in this project.

I would also like to thank Prof. Dr. Mark Miller and his team for teaching me how to perform intravital microscopy of the intestine. I am thankful for the help I received from Prof. Katrin Heinze, Mike Friedrich, Jürgen Pinnecker and Oğuzhan Angay due to the collaboration about advanced imaging techniques and analyses. Thanks for being accessible and for your input and keen interest in this project.

I would like to thank Dr. Christian Brede, Dr. Ana-Laura Jordán-Garrote and Dr. Jorge Amich for introducing me into the world of experimental cell transplantation and to help me find my place in the lab. Big thanks to Lukas Scheller and Josefina Peña who greatly contributed to this project during their MD and Master theses. It was and is a pleasure to work with you, thank you for the trust you have put in me. I am thankful to Dr. Zeinab Mokhtari for the inspiring and fruitful discussions, your enthusiasm, your perspective on migration analysis and your friendship.

Thank you Dr. Duc-Dung Le, Haroon Shaikh, Sina Thusek, Musga Qureischi, Carolin Graf and Estibaliz Arellano for the great team atmosphere, the experimental group efforts and the fun times in the lab and afterwards. Thank you to Dr. Andreas Brandl, Dr. Julia Delgado-Tascón, Julia Hartweg – also for her comforting friendship –, Tim Steinfatt and all members of the Beilhack Laboratory for discussions and help. I would also like to thank Dr. Duc-Dung Le, Julia Hartweg, Marcel Jarick and Haroon Shaikh for their careful proofreading and feedback.

I would like to thank my parents Dagmar and Kai, my brother Jan and my grandmother Gisela to support, motivate and spur my professional progress. Special thanks go to my husband Marcel for always being the rock in my turbulent waters, and his infinite love and support in all situations.

III. Table of contents

IV. List of Figures

V. List of Tables

VI. List of Abbreviations

AF	Alexa Fluor
aGvHD	acute Graft-*versus*-Host Disease
B6	C67BL/6
BABB	benzyl-alcohol/benzyl benzoate
BALB	Bagg albino
CCL	C-C motif chemokine ligand
CCR	C-C motif chemokine receptor
CD	cluster of differentiation
Cy	cyanine
EDTA	ethylenediaminetetraacetic acid
FACS	fluorescence-activated cell sorting
FCS	fetal calf serum
FITC	fluorescein isothiocyanate
GFP	green fluorescent protein
GvHD	Graft-*versus*-Host Disease
HBSS	Hank's buffered salt solution
IEL	intraepithelial lymphocytes
IL	interleukine
ILF	isolated lymphoid follicle
IU	international units

LP	long-pass
LPL	lamina propria lymphocytes
MAdCAM	mucosal-associated cell adhesion molecule
MHC	major histocompatibility complex
PBS	phosphate-buffered saline
PerCP	peridinin-chlorophyll-protein complex
RPMI	Roswell Park Memorial Institute
S1P	sphingosine-1-phosphate
S1PR1	sphingosine-1-phosphate receptor 1
TCR	T cell receptor
Th1	T helper cell type 1
Th2	T helper cell type 2
XCL	C-motif chemokine ligand

VII. Contribution statement

This thesis was conducted at the University Hospital of Würzburg in the laboratory of Prof. Dr. Dr. Andreas Beilhack. Experimental work has been performed by myself, and technical support was given by Lukas Scheller, Julia Hartweg, Sina Thusek, Dr. Duc-Dung Le, Maria Ranecky, Haroon Shaikh and Musga Qureischi. Lukas Scheller performed the RNAseq experiments under supervision of myself and Prof. Dr. Dr. Andreas Beilhack. Bioinformatic analyses of the exported cell tracks were performed by Dr. Zeinab Mokhtari (all members of the Beilhack Laboratory).
Mike Friedrich, Jürgen Pinnecker and Katrin Heinze supported this work through maintenance of the light sheet- and two-photon microscopes (Rudolf Virchow Center, University of Würzburg). Parts of this thesis were published previously in the Journal 'Frontiers in Immunology'. Authors: Katja J. Jarick, Zeinab Mokhtari, Lukas Scheller, Julia Hartweg, Sina Thusek, Duc-Dung Le, Maria Ranecky, Haroon Shaikh, Musga Qureischi, Katrin G. Heinze, Andreas Beilhack (2018). Title: Photoconversion of Alloreactive T Cells in Murine Peyer's Patches During Acute Graft-Versus-Host Disease: Tracking the Homing Route of Highly Proliferative Cells In Vivo. *Frontiers in Immunology* 2018. 9(1468).

VIII. Summary

T cell infiltration into the intestine occurs after priming and activation in the mesenteric lymph nodes and Peyer's patches and subsequent trafficking via the blood circulation. We hypothesized that additionally to the vascular trafficking route, a fraction of T cells in the Peyer's patches directly migrate into the adjacent *lamina propria* of the small intestine. To test this hypothesis, we employed a mouse model of acute Graft-*versus*-Host Disease to study the direct T cell migration from the Peyer's patches to the adjacent *lamina propria*.

First, we analyzed the border of Peyer's patches on histological sections and found that the Peyer's patch is not enclosed by a capsule or basement membrane. Thus, the tissue architecture allows for direct access to the surrounding tissue. With whole-mount light sheet fluorescence microscopy we quantified a three-dimensional gradient of T cells around Peyer's patches on day 2.5 and day 3 after transplantation. This gradient evened out at day 4 and day 6 when high numbers of T cells started to evenly infiltrate the intestine from the blood circulation. We confirmed that gradient-forming T cells around Peyer's patches resided within the tissue parenchyma of the *lamina propria* and not inside lymphatic vessels.

To positively prove that the recently activated donor T cells around Peyer's patches have egressed directly from that patch, we established a protocol for intravital photoconversion of T cells inside Peyer's patches. 12 h after photoconversion inside a single Peyer's patch, photoconverted T cells resided only around this particular Peyer's patch and not elsewhere in the small intestine. This indicated that the T cells did not infiltrate via the blood but migrated to the adjacent *lamina propria* of the small intestine. Dynamic intravital two-photon microscopy revealed that these T cells next to the Peyer's patch migrated in a random pattern. This suggested that these cells did not follow a positive chemoattractive gradient once they had reached the *lamina propria*. Laser-capture microdissection combined with RNA sequencing of the mucosa near the Peyer's patch identified a wide range of migration-promoting factors. These included chemokines, co-stimulatory receptors and migration-associated intracellular molecules, which are candidates to promote this direct migration from Peyer's patches.

Altogether, we demonstrate for the first time that additionally to the vascular trafficking route, a fraction of T cells migrates directly from the Peyer's patch to the surrounding mucosa. This mechanism implies so far unrecognized regional specification of Peyer's-patch-primed T cells. Our findings may impact treatment strategies to avoid intestinal inflammation or foster immunity after oral vaccination.

IX. Zusammenfassung

T-Zell Infiltration in den Darm erfolgt nach Primen und Aktivierung in den mesenterialen Lymphknoten und Peyerschen Plaques durch Rezirkulation über die Blutbahn. Wir stellten die Hypothese auf, dass zusätzlich zur vaskulären Route ein Teil der T-Zellen im Peyerschen Plaque direkt in die angrenzende *Lamina propria* des Dünndarms wandert. Um diese Hypothese zu testen, setzten wir ein Mausmodell für eine akute Graft-*versus*-Host Reaktion ein, um die direkte Migration von T Zellen aus den Peyerschen Plaques in die angrenzende L*amina propria* zu untersuchen.

Zuerst analysierten wir die Randzonen um die Peyerschen Plaques mit histologischen Schnitten und konnten bestätigen, dass der Peyersche Plaque von keiner Kapsel oder Basalmembran umschlossen ist, sodass die Gewebearchitektur den direkten Zugang des umliegenden Gewebes zulässt. Mithilfe der Lichtblatt-Fluoreszenzmikroskopie von Dünndarm-Komplettpräparaten quantifizierten wir einen dreidimensionalen T-Zell Gradienten um Peyersche Plaques an den Tagen 2,5 und 3 nach allogener Stammzelltransplantation. Dieser Gradient verschwand zwischen an Tag 4 und Tag 6, als eine hohe Anzahl an T-Zellen begann, den Darm gleichmäßig über die Blutbahn zu infiltrieren. Wir bestätigten, dass die Gradienten-bildenden T-Zellen im Gewebe der *Lamina propria* und nicht in lymphatischen Gefäßen saßen, um zirkulierende Zellen von der Gradientenbildung auszuschließen.

Um direkt zu beweisen, dass die T-Zellen um dem Peyerschen Plaque unmittelbar aus diesem Plaque ausgewandert sind, haben wir ein Protokoll für intravitale Photokonversion von T-Zellen im Peyerschen Plaque etabliert. 12 h nach der Photokonversion in einem einzelnen Peyerschen Plaque befanden sich die T-Zellen nur um diesen bestimmten Plaque herum. Dies zeigt, dass die T-Zellen das Gewebe nicht über die Blutbahn infiltrierten, sondern direkt in die angrenzende *Lamina propria* des Dünndarms gewandert waren. Dynamische intravitale Zweiphotonenmikrokopie offenbarte, dass diese T-Zellen um den Peyerschen Plaque nach zufälligem Schema wanderten. Dies legte nahe, dass diese T-Zellen keinem positiven Chemokingradienten folgten, sobald sie die Lamina propria erreicht hatten. Laser-Mikrodissektion kombiniert mit RNA-Sequenzierung der Mukosa nahe des Peyerschen Plaques identifizierte eine große Auswahl an migrationsfördernden Faktoren. Hierunter waren Chemokine, kostimulatorische Rezeptoren und intrazelluläre migrationsassoziierte Moleküle, welche Kandidaten sind, diese direkte Migration aus den Peyerschen Plaques zu fördern.

In dieser Arbeit zeigen wir erstmalig, dass zusätzlich zur vaskulären Route ein Teil der T-Zellen direkt vom Peyerschen Plaque in die umliegende Mukosa wandert. Dieser Mechanismus impliziert bislang unerkannte regionale Spezialisierung von T Zellen,

welche in Peyerschen Plaques aktiviert wurden. Diese neuen Befunde können zukünftige Behandlungsstrategien gegen intestinale Entzündungserkrankungen oder für Immunreaktionen nach oraler Impfung beeinflussen.

1 Introduction

1.1 The intestinal immune system

The organs of the immune system are divided into lymphopoietic or primary lymphoid organs (bone marrow and thymus) and secondary lymphoid organs, where immune responses unravel. The secondary lymphoid organs include the spleen, lymph nodes, and mucosa-associated lymphoid tissues (MALT) in the gastrointestinal tract, the nasal and respiratory tract, the urogenital tract and other mucosa. The MALT of the intestine consist of the multifollicular Peyer's patches, isolated lymphoid follicles, and cryptopatches. Furthermore, the intestinal *lamina propria* harboring lamina propria lymphocytes represents the largest reservoir of T cells in the body together with the intraepithelial lymphocytes in the intestinal epithelium (Mowat and Agace, 2014). The mucosal surfaces mount up to an estimated total size of 400 m² (Murphy and Weaver, 2016), and are separated from the outside only by a single layer of epithelial cells covered by mucus. Therefore, this delicate tissue requires extensive immunological surveillance to ensure proper barrier function. Furthermore, these surfaces play a major role in educating the immune system to distinguish between harmful and innocuous antigens of the environment that need to be tolerated by the immune system, such as food antigens or the commensal microbiota (Kuhn and Stappenbeck, 2013; Qiu *et al.*, 2016).

1.1.1 Lymphoid organs in the small intestine

Peyer's patches are visible with the naked eye and are embedded in the mucosa on the antimesenterial side of the small intestine. In man, there are about 60 Peyer's patches in newborn and up to 240 at puberty (Cornes, 1965), and their frequency and size increases from duodenum to ileum. In mice, there are 6-12 Peyer's patches that are distributed throughout the intestine (Pospischil, 1989; Reboldi and Cyster, 2016), and are regarded to be distributed evenly, although personal observation suggested that some locations along the murine intestine were more likely to have Peyer's patches than others. Each Peyer's patch consists on average of 100 follicles in man (Cornes, 1965) and 3-12 in mice. These B cell follicles, which lie below the dome region covered by the follicle-associated epithelium containing microfold cells (M-cells), are surrounded by the T cell zones, also called interfollicular regions (Figure 1-1) (Jung *et al.*, 2010). M cells are not covered by mucus and serve as sampling shuttles of the luminal contents for presentation to T and B cells by antigen-presenting cells in the Peyer's patches. In contrast to lymph nodes,

Peyer's patches lack afferent lymphatic vessels, but bear efferent lymphatic sinuses towards the serosal side (Schmidt *et al.*, 2013).

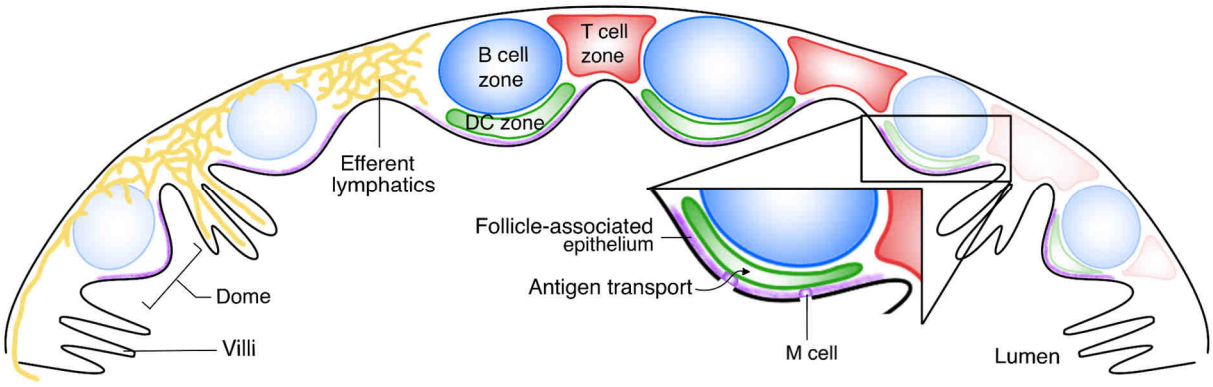

Figure 1-1 Organization of a Peyer's patch. Each dome region contains one B cell follicle covered by an area of dendritic cells (DC). The B cell follicles are surrounded by T cell areas, which are suffused by the efferent lymphatic sinus. Antigens are transported into the Peyer's patch through the M cells inside the follicle-associated epithelium.

Isolated lymphoid follicles (ILF) are single B cell follicles inside the mucosal tissue of the small intestine, which contain mostly B cells, and T cells at low frequencies. They do not contain clear T cell zones like the Peyer's patch (Hamada *et al.*, 2002), and are a site of T-cell-independent B cell responses against pattern-carrying antigens (Tsuji *et al.*, 2008). Mice have an estimated 1000-1500 ILF in their small intestine, and humans are believed to have around 30,000 ILF (Mowat and Agace, 2014). Like Peyer's patches, the frequency of ILFs increases from duodenum to ileum in man. ILF may arise from cryptopatches, which are progenitor cell-rich accumulations of immune cells near the crypts of the small and large intestine (Pabst *et al.*, 2005). Unlike ILF, cryptopatches are less organized accumulations of fewer numbers of immune cells.

Together, the intestinal lymphoid structures combine to an efficient sampling and surveillance system in mucosal immunity.

1.1.2 Immune cell populations in the *lamina propria*

Outside of organized lymphatic structures in the intestine, the *lamina propria* and epithelial layer harbor a high number of interspersed immune cells (Figure 1-2). These consist of T cells, B cells, type 1-3 innate lymphoid cells and myeloid cells, which are mostly macrophages, but contain also dendritic cells, eosinophils and mast cells (Gross *et al.*, 2015; Mowat and Agace, 2014).

Lamina propria B cells are mostly IgA-secreting plasma cells. They produce large amounts of IgA that is transported across the epithelium and integrated into the mucus layer. The commensal microbiota are largely non-motile and cannot penetrate the mucus layer, whereas pathogenic bacteria attempting to penetrate this barrier are then

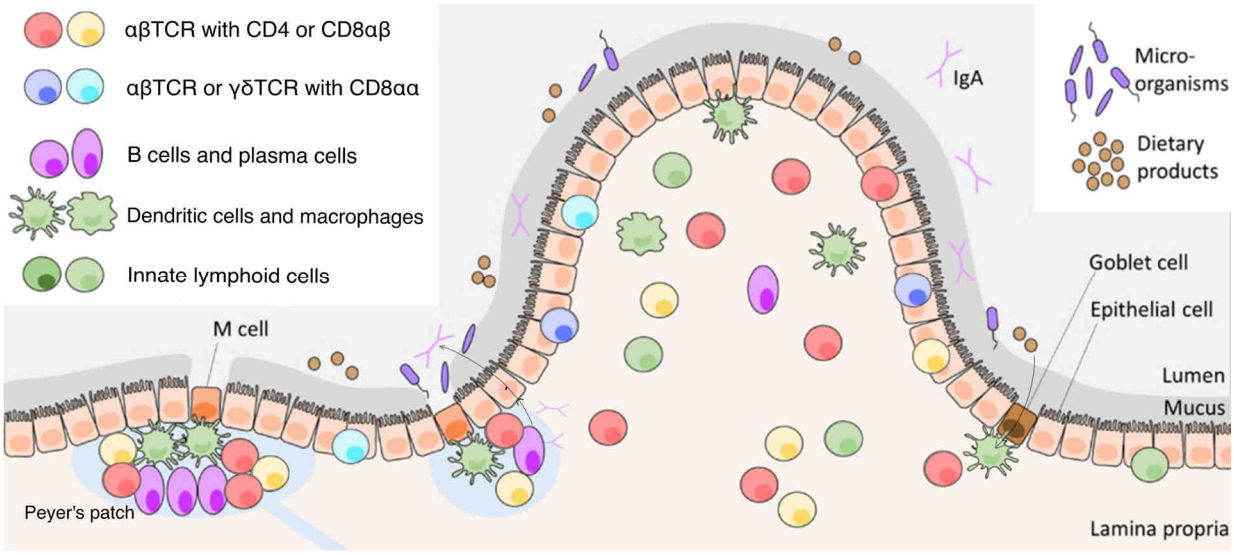

Figure 1-2 Immune cell populations in the intestine. Conventional T cells (αβTCR co-expressing CD4 or CD8αβ) are located in the lamina propria of the small intestine. They also populate the epithelium, where additionally unconventional T cell subsets (CD8αα co-expressing αβTCR or γδTCR) are situated. M cells and Goblet cells both transport antigens to antigen-presenting cells in the intestine, which are mostly macrophages but also dendritic cells. Plasma cells in the lamina propria produce IgA, which is transported across the epithelium to protect the mucosal surface from invading pathogens. Modified from Brucklacher-Waldert *et al.*, 2014.

opsonized with IgA antibodies (Hansson, 2012). Intruders can thus easily be detected by the complement system or phagocytes upon entry to the mucosa. The T cells inside the intestine are much more diverse than in the average lymphoid organ.

In the *lamina propria*, 2/3 of the T cells express CD4 and 1/3 expresses CD8αβ. Both are similar in phenotype to T cells in other organs, and have a memory phenotype. They are thought to develop from conventional T cells primed in the secondary lymphoid organs (Mowat and Agace, 2014). Apart from the dominating αβTCR T cells in the *lamina propria*, γδ T cells are also reported, from flow cytometric experiments, to reside in the intestinal *lamina propria* (Kadivar *et al.*, 2016).

In combination, these cell types interact inside the lamina propria to enforce the mucosal barrier function and to communicate on the commensal microbiota or potential threats to intestinal integrity.

1.1.3 Immune cells in the intestinal epithelium

T cells are the only type of immune cells that also populates the intestinal epithelium, and their frequency in the intestinal epithelium is high (10-15% of epithelial cells) (Mowat and Agace, 2014). There, they represent the first line of defense against intruders. Apart from the intraepithelial T cells, myeloid cells in the *lamina propria* have direct access to the lumen by reaching across the basal membrane and the epithelium with long protrusions, but their cell bodies remain in the *lamina propria* and the antigens

presented are shuttled by goblet cells in healthy tissue (McDole *et al.*, 2012). Eosinophils are even reported to exit the tissue into the lumen and attack helminths (Hällgren *et al.*, 1989).

Intraepithelial lymphocytes include the conventional αβTCR T cells carrying either CD4 or CD8αβ, but consist to a large extent of unconventional T cells. These include αβTCR T cells or γδTCR T cells carrying no co-receptor or the CD8αα homodimer. These unconventional T cell subsets originate from the thymus and are positively selected on self-antigens (Leishman *et al.*, 2002). They are currently believed to exit the thymus in a $CD4^{-}CD8^{-}$ double-negative state and undergo further differentiation in the intestine (Cheroutre *et al.*, 2011). Intraepithelial lymphocytes usually express CD69 on their surface and depend on the integrin α_E (CD103) to localize to the epithelial layer expressing E-cadherin (Cheroutre *et al.*, 2011). Recently, the migration of this cell type inside the epithelium and to the *lamina propria* has been associated with G-protein coupled receptor 55 (GPR55), a receptor for lysophosphatidyl inositols. Engagement of this receptor inhibits the migration of γδ T cells in the intestine (Sumida *et al.*, 2017). Their positioning at the very surface of the intestinal barrier make intraepithelial lymphocytes important actors of mucosal surveillance and tolerance.

1.1.4 Intestinal immune tolerance

The intestine is a major site of immune tolerance induction and maintenance (Harrison and Powrie, 2013). Tolerogenic antigen-presenting cells secreting transforming growth factor β (TGFβ), IL-10 and retinoic acid induce a regulatory phenotype in T cells (induced regulatory T cells, iTregs) that express Foxp3 and secrete IL-10 (Coombes *et al.*, 2007; Sun *et al.*, 2007). Together with natural Tregs (nTregs) from the thymus, they provide a tolerogenic milieu towards the intestinal microbiota and food antigens locally and systemically.

Apart from the interactions between the cells of the immune system, the immune cell populations in the intestine are greatly influenced by cell contacts and soluble mediators from stromal cells including epithelial and endothelial cells, fibroblasts and pericytes (Nowarski *et al.*, 2017). Regulation by the enteric nervous system adds another layer of complexity to the regulation of intestinal immunity (Yoo and Mazmanian, 2017).

In summary, the intestinal immune system in its diversity and complexity can efficiently protect this delicate barrier from damage. Intestinal lymphoid structures such as the Peyer's patches are important inductive sites of mucosal immune responses. T cells play a major role in the first-line protection of this large surface, immune tolerance and long-term memory.

1.2 T cell migration and trafficking

T cells are an important arm of the adaptive immunity, and serve the individual by getting educated in the thymus to afterwards selectively protect against an antigen that a particular T cell is specific for. As a collective, T cells effectively patrol the body to eradicate threats to the health of the individual, such as invading pathogens or other harmful substances. However, in order for one single naïve T cell clone to find its cognate antigen, it has to efficiently patrol strategically positioned hubs of antigen presentation: the secondary lymphoid organs including the lymph nodes. Regarding the minute size of a T cell in comparison to the vast body surfaces of skin, lung and intestine, it is remarkable how efficiently antigen-specific T cells find their antigen (Beilhack and Rockson, 2003). After detecting its cognate antigen, the T cell can interact with other cell types to receive additional information about the type of immune response required. As antigen-specific responder cells, T cells can help other immune cells to effectively exert their effector functions, or directly attack the threat upon MHC-mediated cognate antigen recognition. The phenomenon of immune cell trafficking will be introduced in more detail during this chapter.

1.2.1 Use of the terms trafficking, homing and migration

T cells need to travel through the body in different situations and by different modalities. In case of motion through blood and lymph vessels, this is called trafficking. In this thesis, the term trafficking will be used as opposed to migration inside a tissue, which partly uses similar mechanisms and molecules but does not involve the intravascular route. A specialized kind of trafficking comprises vascular trafficking to the primary and secondary lymphoid organs, and is termed homing. Nevertheless, the term 'homing receptors' has been coined also for trafficking to peripheral tissues other than secondary lymphoid organs and will be used here accordingly.

1.2.2 Vascular trafficking and homing receptors

Immune cells and cells outside the immune system, such as endothelial or epithelial cells, produce guidance cues aimed at recruiting or repelling immune cells. For recruitment of lymphocytes from the blood, this includes the homing receptors of the three classes of selectins, integrins and chemokines, which in their combination provide an 'address' for the immune cells to enter different tissues. To extravasate into a tissue, immune cells perform three steps: rolling, tight adherence and transmigration (Figure 1-3). T cells can make the first contact with the vessel wall with the help of selectins binding to glycoproteins on the endothelium, such as L-selectin on naïve T cells to peripheral node addressin (PNAd) on the Glycosylation-dependent cell adhesion

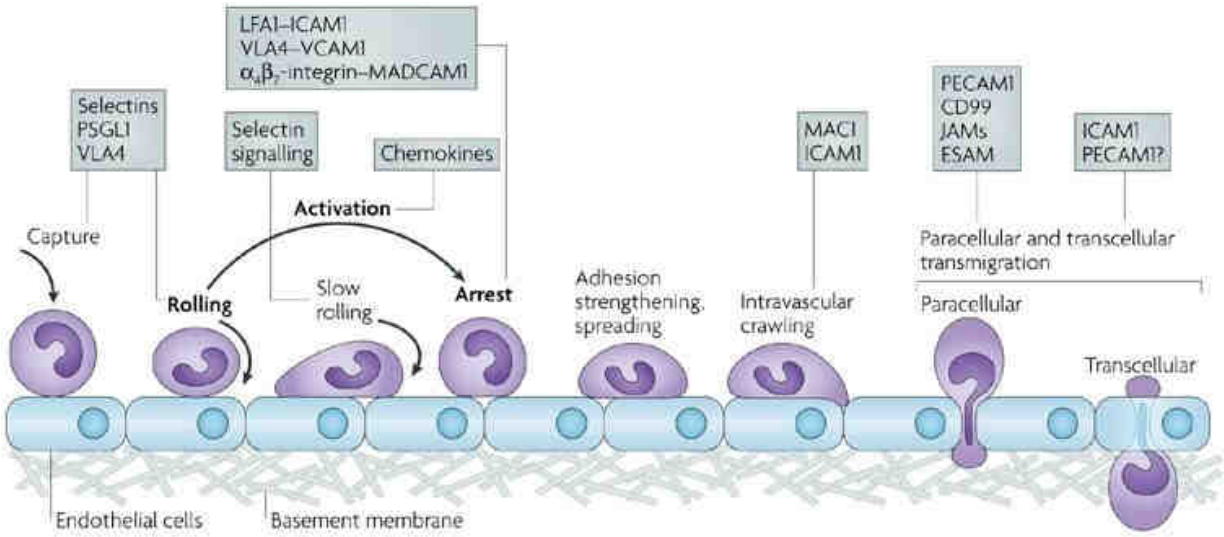

Figure 1-3 Leukocyte extravasation. Leukocytes are captured at the vascular surface and roll along the endothelium using selectins. With the help of chemokines, integrins acquire their high-affinity conformation and lead to arrest of the cell on the endothelium. Subsequently, the leukocyte can enter the tissue between two endothelial cells or directly through it via the transcellular route. Image modified from Ley *et al.*, 2007.

molecule-1 (GlyCAM-1) or CD34 expressed by endothelial cells of lymph nodes (Streeter *et al.*, 1988). This event triggers rolling of the T cell along the vessel wall, and the speed of rolling depends on the molecule engaged in this process (Jung *et al.*, 1996; Zarbock and Ley, 2009). Much of the early work on leukocyte rolling was performed using neutrophils, but this mechanism is common for all leukocytes. Next, chemokines transcytosed and presented on the luminal surface of endothelial cells (Middleton *et al.*, 1997) are detected, if the cells carry the appropriate receptors. For T cells, the major homing receptor for recruitment of naïve and central memory cells into lymph nodes at steady state is the C-C Motif Chemokine Receptor type 7 (CCR7) recognizing the C-C Motif Chemokine Ligand 19 (CCL19) and CCL21 (Förster *et al.*, 1999; Gunn *et al.*, 1998). CCL19 and CCL21 are presented on the endothelium of the T cell zones (Baekkevold *et al.*, 2001), and detection with CCR7 on T cells induces inside-out signaling towards integrins inside the lymphocyte. On naïve T cells, this is typically the Lymphocyte function-associated antigen 1 (LFA-1), which then acquires an extended, high-affinity conformation (Shamri *et al.*, 2005). Binding of the high-affinity form of LFA-1 to the Intracellular Adhesion Molecule 1 (ICAM-1) induces firm arrest of the cell on the vessel wall and enables transmigration of the cells into the tissue.

The access of T cells to different tissues is regulated by selectins, chemokines and integrins expressed in different tissues, and the sets of receptors differ between steady-state and inflammation. On the T cell side, the priming site and differentiation state determine the set of homing receptors that the cell expresses. Naïve T cells express L-Selectin (CD62L), CCR7, CXCR4 and LFA-1, which grant them access to the secondary lymphoid organs (Fu *et al.*, 2016), although CXCR4 plays only a minor role in lymph

node homing compared to CCR7 (Okada *et al.*, 2002). This way, the T cells can carry out their prime task of searching the lymph nodes for antigen.

Once a T cell becomes activated, the effector cell downregulates L-Selectin and CCR7, and starts to express homing receptors which enable the specific entry into the target site (von Andrian and Mempel, 2003). This depends on the region that the lymph node drains: in skin-draining lymph nodes, T cells upregulate P-Selectin glycoprotein ligand 1 (PSGL-1, CD162), CCR4, CCR10, the Cutaneous Lymphoid Cell Antigen 4 (CLA4) and Integrin $\alpha_4\beta_7$; liver-draining lymph nodes induce CCR1, CCR5 and Integrin $\alpha_4\beta_1$ (Fu *et al.*, 2016); and the mesenteric lymph nodes and Peyer's patches induce expression of CCR9 and $\alpha_4\beta_7$ (Beilhack *et al.*, 2008; Hammerschmidt *et al.*, 2008). The different homing receptors are induced as a response to local additional information provided by fibroblastic reticular cells and dendritic cells. For instance, fibroblastic reticular cells produce the Vitamin-A-metabolite retinoic acid to induce CCR9 and $\alpha_4\beta_7$ expression in gut-homing T cells (Iwata *et al.*, 2004), and dendritic cells in skin-draining lymph nodes produce Vitamin D to induce CCR10 expression after priming (Sigmundsdottir *et al.*, 2007). Equipped with the homing receptors specific for the target tissue, the T cells can specifically extravasate into the target organ where the ligands are expressed.

In addition to the priming site, each T cell differentiation state is associated with characteristic homing receptors. Effector and central memory T cells differ by their expression of L-Selectin and CCR7 (Sallusto *et al.*, 1999), which enable central memory T cells to enter the lymph nodes and Peyer's patches whereas the effector memory T cells are excluded from the secondary lymphoid organs. Tissue-resident $CD8^+$ cells often express CD69 and CD103, the Integrin α_E, which can for instance pair with β_7 to induce T cells resident in the intestinal epithelium (Annunziato *et al.*, 2006; Gorfu *et al.*, 2009; Higgins *et al.*, 1998). $CD4^+$ T cells that have differentiated into specialized effector T helper lineages carry distinctive receptor sets: Type 1 T helper cells (Th1) carry the receptors CXCR3 recognizing CXCL9-11, CXCR6 recognizing CXCL16, and CCR5 recognizing CCL3-5. IN contrast, Th17 cells are characterized by CCR4 and prominently CCR6 which binds to CCL20. The Th2 and Th9 subsets express even different sets of receptors, which are reviewed in Fu et al., 2016.

Important intestine-specific migrational cues in the steady state are CCL25 and CCL28 expressed by the epithelial cells in the small and large intestine, respectively (Habtezion *et al.*, 2016). They are recognized by CCR9 on T cells and CCR10 on B cells, whereas T cells are directed to the colon via G Protein-Coupled Receptor 15 (GPR15), an orphan receptor homologous to chemokine receptors (Kim *et al.*, 2013; Nguyen *et al.*, 2015).

Furthermore, the postcapillary venules of the intestine express the Mucosal-associated cell adhesion molecule 1 (MAdCAM-1), which can be bound by lymphocytes expressing $\alpha_4\beta_7$.

Upon inflammation, the endothelial cells inside the tissue upregulate further recruitment factors. They increase their expression of E-and P-selectin, upregulate CXCL8 and CXCL16 to recruit neutrophils, or the early Th1 inflammatory cytokines CCL3-5 and CXCL9-11 (Bouazzaoui *et al.*, 2009). Through inflammatory mediators, immune cells can be recruited to tissues that they would not access during steady-state conditions and are then able to initiate an immune reaction.

In summary, T cells can specifically traffic to secondary lymphoid organs and peripheral tissues using specific homing receptors depending on their current phenotype and differentiation status. After tight adherence to the vessel wall, T cells are able to transmigrate on the basolateral side of the endothelium or even through the cell body of endothelial cells into the tissue, where they will migrate to find their cognate antigen (Muller, 2011).

1.2.3 Modes of T cell migration

Once inside the tissue, T cells can perform different modes of migration, classified by their adherence to the substrate, their search strategies and interactions with other cell types. Which mode of migration a cell displays depends on its cell type-intrinsic features, its differentiation status, the mechanic properties of the environment and the receptors and chemotactic cues that the cell detects and the environment expresses (Mrass *et al.*, 2010).

1.2.3.1 Necessity of substrate interactions for migration

To achieve forward motion, cells protrude a lamellipodium or pseudopodium at the leading edge of the direction of motion (Figure 1-4 A). With the help of biochemical interactions with the substrate, usually via integrins or chemokine receptors, the cell generates the traction force to push forward. Contraction of the uropod at the tailing edge completes the motion cycle, and requires loosening of the interactions made with the substrate. These mechanisms requires an intrinsic cell polarity, and are regulated by cell-type-intrinsic actin polymerization rates, cell membrane and nucleus rigidity. The described mode of migration is termed haptokinesis referring to the haptic interaction of the cell with the substrate (Krummel *et al.*, 2016).

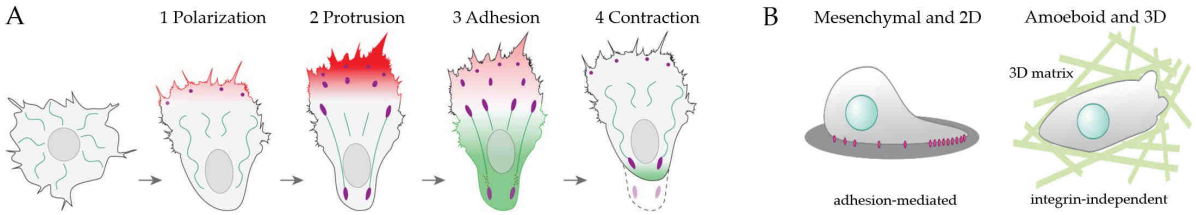

Figure 1-4 Migration cycle and modes. **A** Haptokinetic movement involves four steps: it requires cell polarization (1), and is initiated by protrusion of a lamellipodium (2). Tight adhesion is necessary (3) to generate forward motion during contraction (4). Modified from Reig *et al.*, 2014. **B** Mesenchymal cells and T cells in 2D migrate adhesion-mediated, whereas T cells in a confined 3D environment migrate integrin-independently in an amoeboid fashion. Modified from Paluch *et al.*, 2016.

Haptokinesis is realized by interactions of integrins with components of the extracellular matrix, such as collagen and fibronectin. This mode of migration is used mostly by mesenchymal cells. In contrast, immune cells including T cells rather migrate in an amoeboid fashion (Figure 1-4 B). Especially in a confined 3D environment, T cells do not firmly adhere to the substrate. They mediate forward motion through squeezing and pushing inside the dense environment, where integrins play a less important role than for mesenchymal cells (Jacobelli *et al.*, 2009; Lammermann *et al.*, 2008). Additionally to integrins, chemokines bound to extracellular glucosaminoglycans can also induce haptotactic movement of T cells (Woolf *et al.*, 2007). Integrin-independent migration can be faster because overly strong adhesion to the substrate decreases cell speed (Liu *et al.*, 2015; Toyjanova *et al.*, 2015), but in environments with limited contact points, integrins provide additional traction forces that speed up T cells. For instance, T cells perform jumps when contacting dendritic cells in the lymph nodes (Katakai *et al.*, 2013), and in many settings, T cell migration velocities are reduced after inhibition of integrin contacts (Katakai and Kinashi, 2016). Recently, the role of chemokines and integrins was studied in greater detail for naïve T cells, yielding that sensing of soluble chemokines induced retrograde actin flow. The cells were only able to translate this actin flow into migration speed in the presence of the integrin ligand ICAM-1. This experimentally substantiated that chemokines stimulate cell migration speed, whereas integrins enable the traction forces for efficient forward motion (Hons *et al.*, 2018).

Likely, the large variety of possible contacts via different integrins and chemokine receptors are redundant at promoting efficient movement of T cells *in vivo*. Furthermore, the different requirements for traction forces depend on the mechanical and spatial properties of different tissues, and the different modes of migration may in part explain the differences observed in the importance for adhesion for T cell migration.

To conclude, T cells generally migrate using amoeboid migration. Stronger adhesion and haptokinesis is important for mesenchymal cell migration, but can also apply to T cells in steady-state and inflammatory situations.

1.2.3.2 T cell search strategies

The search strategies that T cells employ differ slightly between the differentiation states and whether the T cell is in the lymphoid organs or at effector sites. The common goal in both situations is to find the cognate antigen in complex environments – whether it is presented to a naïve T cell in a lymph node, or an effector cell that seeks to eliminate its target. However, these situations differ in the assumptions on the likelihood of success: A naïve T cell is much less likely to find its cognate antigen than a T cell that has been positively selected in an immune reaction. Next, after successfully localizing the antigen, the persistence and type of interaction with the cell carrying the antigen differs vastly in the two circumstances.

Naïve T cells enter the lymph node via the high endothelial venules in the T cell zone and migrate on the network of fibroblastic reticular cells, which express CCL19 and CCL21 and carry immobilized CCL21 on their surface. CCR7 on naïve T cells and activated dendritic cells sequesters these two cell types on this network (Bajénoff *et al.*, 2006; Cyster, 1999; Katakai *et al.*, 2004; Sixt *et al.*, 2005). This increases the likelihood of a productive encounter: cognate antigen recognition. Naïve T cells migrate randomly in lymph nodes (Miller *et al.*, 2002), and scan the antigen presenting cells for only short times. Such behavior has been interpreted to equalize the possibility of antigen detection for a wide variety of clones bearing cells specific for an antigen at very low frequencies (Figure 1-5 A) (Krummel *et al.*, 2016). Once a T cell encounters its antigen, it starts to swarm around the antigen-presenting cell, before it switches to prolonged interactions (Mempel *et al.*, 2004). After this encounter, the search strategy of the T cell differs (Figure 1-5 B). Now, the likelihood that this cell is needed for the immune response is high, and the likelihood of antigen encounter in the vicinity increases dramatically. During encounters with antigen-presenting cells, the T cells change their transcriptional program. They upregulate chemokine receptors that enable them to detect and aim for the antigen-presenting cells, and can preferentially interact with them in comparison to the non-specific naïve T cells also present. Dendritic cells that have interacted with $CD4^+$ T cells secrete CCL3/4 and attract CCR5-expressing $CD8^+$ T cells (Castellino *et al.*, 2006). $CD4^+$ T cells secrete XCL1 after activation to recruit dendritic cells to provide help for $CD8^+$ T cells (Eickhoff *et al.*, 2015). T cells destined to give help to B cells upregulate CXCR5 and migrate towards CXCL13 produced by follicular dendritic cells, where they interact with B cells (Campbell *et al.*, 2001). This 'informed motion' pattern is also

inherent to memory cells inside lymph nodes, which locate near B cell follicles (Kastenmuller *et al.*, 2013). However, in this thesis we focus on recently activated effector T cells, which is why migration patterns of memory T cells will not be described in more detail.

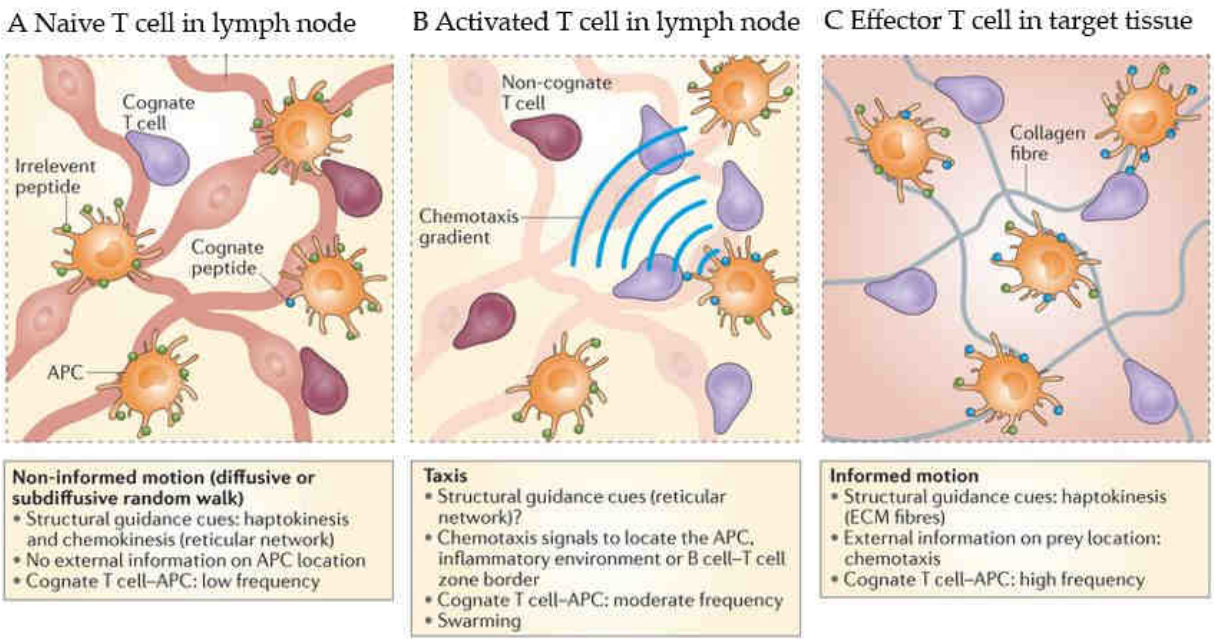

Figure 1-5 T cell migration inside tissues. **A** Naïve T cells migrate randomly to equalize chance for all different T cell clones to encounter antigen-presenting cells. **B** Activated T cells follow chemotactic cues from antigen-presenting cells and preferably interact with them in comparison to naïve T cells. **C** Effector T cells in peripheral inflamed tissues often migrate on the extracellular matrix in a haptokinetic fashion and are able to follow chemotactic cues towards inflammatory sites or antigen-presenting cells. Image taken from Krummel et al., 2016.

After scanning a lymph node for antigen, T cells must also find their way out of the lymph node. Currently, it is assumed that T cell exit is achieved by random encounter with cortical lymphatic vessels that densely suffuse the T cell zone (Cyster and Schwab, 2012; Grigorova *et al.*, 2010; Grigorova *et al.*, 2009). The requirement for T cells to transmigrate and exit via these portals is expression of the receptor for the small lipid sphingosine-1-phosphate (S1P). T cells carry the isoform Sphingosine-1-phosphate receptor 1 (S1PR1), which induces transmigration of the T cell upon probing of the lymphatic sinus (Matloubian *et al.*, 2004). However, more recent studies have pointed towards a gradient of S1P inside lymph nodes, which may nevertheless attract T cells towards the lymphatics (Fang *et al.*, 2016). Whether this mechanism only plays a role for T cells close to the medullary region of the lymph node, or whether these gradients also attract T cells towards the lymphatics inside the T cell area, has not been conclusively answered yet.

The concentration of S1P is high in lymph and blood, so that the receptor S1PR1 is constantly down-modulated by desensitization in circulating T cells. Upon lymph node

entry, naïve T cells recycle the receptor to the cell surface and exit the lymph node after 6-12 h (Tomura *et al.*, 2008). In presence of interferon gamma, T cells upregulate CD69, which intracellularly sequesters S1PR1 and targets it for degradation (Shiow *et al.*, 2006).Thus, T cells remain longer in lymph nodes bearing an ongoing immune reaction. Cognate antigen recognition additionally represses the transcription of S1PR1 for three days (Matloubian *et al.*, 2004). This leaves time for proliferation and selection of highly specific clones.

The decision whether a T cell leaves the lymph node depends on the fine-tuning of the two opposing signals of CCR7-mediated retention and S1PR1-initiated egress. Modulation of these two receptors delicately balances the decision of staying inside or leaving the lymph node (Pham *et al.*, 2008).

Once an activated T cell has entered the site of inflammation, it faces a different structural environment. Depending on the organ, the sometimes stiff environment rich in extracellular fibers such as collagen promotes haptokinesis (Figure 1-5 C) (Overstreet *et al.*, 2013). T cells sensitive for chemokines such as CXCL9-11 can perform chemotaxis towards antigen-presenting cells in the tissue, enhancing the probability of antigen encounter (Krummel *et al.*, 2016). Furthermore, danger signals such as extracellular release of ATP from necrotic cells can attract neutrophils (Chen *et al.*, 2006), and may have also effects on other cell types. β-defensins activate CCR2 to induce chemotaxis (Röhrl *et al.*, 2010). The often cited Lévy-walk was so far only observed in the brain for T cells, but not in other non-lymphatic tissues (Harris *et al.*, 2012).

To conclude, naïve T cells largely migrate randomly inside secondary lymphoid organs in search for their cognate antigen. Once they become activated, they upregulate chemokine receptors and integrins that make them sensitive to migratory cues produced in the immediate environment. On one hand, this enables them to leave the lymphoid tissue after a few rounds of proliferation. On the other hand, it renders them more efficient in detecting antigen-presenting cells and arms them for efficient target organ infiltration.

1.2.4 Measuring T cell migration

T cell migration can be measured in different meaningful ways (reviewed in Beltman et al., 2009). One of the most intuitive measurements of cell migration is the migration speed, defined by the distance that a cell travels in a certain amount of time. The mean and degree of fluctuation is dependent on the cell type. For instance, fibroblasts migrate very consistently with an average speed of less than 1 μm/min (Lo *et al.*, 2000), dendritic cells migrate slightly faster at 2-6 μm/min *in vivo* (Lindquist *et al.*, 2004; Ng *et al.*, 2008),

B cells move at a steady pace of 6-11 µm/min (Coelho *et al.*, 2013; Okada *et al.*, 2005), and T cells characteristically move at a speed of 10-12 µm/min (Miller *et al.*, 2002). The migration of T cells differs from that of the previously mentioned cell types because the T cell migration speed fluctuates frequently, with peak velocities of up to 25 µm/min (Katakai *et al.*, 2013; Miller *et al.*, 2002). The stiffness of the substrate that the cells migrate in and the presence or absence of migration-stimulating factors such as chemokines influences the speed of cell migration. For example, naïve T cells migrate faster in lymph nodes with a speed of 15 µm/min due to the presence of CCL19 and CCL21 (Worbs *et al.*, 2007) whereas T cells in tumors migrate at a much reduced speed of 5-8 µm/min (Boissonnas *et al.*, 2007). The overall speed of a cell is furthermore affected by how often and for how long the T cells pause in the tissue to interact with other cells. This can be quantified as arrest rate, which is commonly measured as the percentage of time that individual T cells migrate slower than 2-3 µm/min (Boissonnas *et al.*, 2007).

Apart from the speed, directionality is an important feature of cell motility. It measures how straight and thus efficiently a cell moves and approaches its potential target. The most easily comprehensible measure for this is the turning angle, which is the angle between the direction that a cell moves before and after turning (Figure 1-6 C). Small turning angles indicate ballistic migration in almost a straight line, and large turning angles indicate random movement with frequent changes of direction. To some extent, this parameter is influenced by cell intrinsic mechanisms (Gérard *et al.*, 2014).

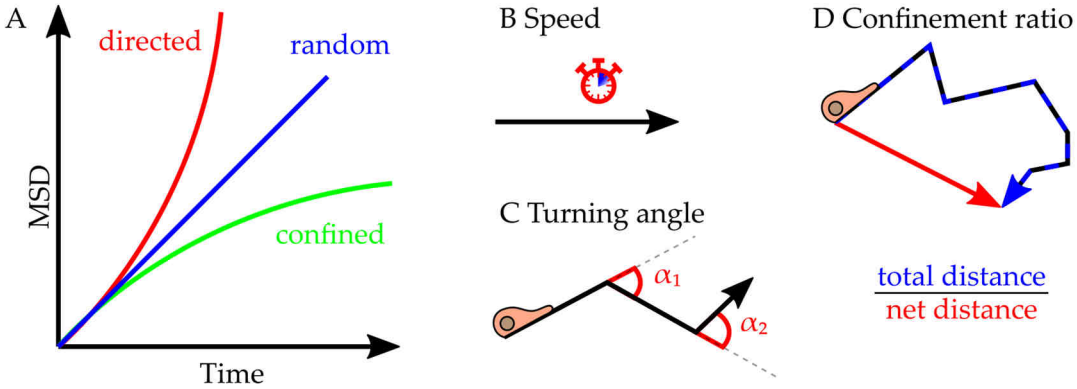

Figure 1-6 Measurement of T cell migration. **A** Plotting the mean squared displacement (MSD) against time, directed, random and confined migration can be discriminated. **B** Migration speed is the distance that a cell has traveled within a given time. **C** Turning angles measure the angle between the directions of movement in one step compared to the next step. **D** Confinement ratio is calculated from the total distance a cell has traveled divided by the direct line from start to end (net distance).

Another very meaningful measurement of directionality is the confinement ratio, which is calculated by the net distance that the cell has reached at a certain time point (shortest distance from start to end) divided by the distance of the total track that a cell has

migrated along up to this time point (Figure 1-6 D). The ratio can lie between 0 and 1: in highly confined cells, this number is small because the cells migrate and turn without reaching far from the start point. In directionally migrating cells, the values approach 1 because the distance traveled is similar to the net distance reached after this time (Beltman *et al.*, 2009).

The overall propensity to migrate, independent of whether it is random or directional, can be measured by the mean squared displacement (Beauchemin *et al.*, 2007). Highly motile cells have a higher mean squared displacement than cells whole migration tracks cover less area in the same amount of time. Plotting the mean squared displacement against the square root of time, the curve gives information about the migration mode, that is, whether the cell moves randomly, directed or super-diffusively, or is constrained in space (Figure 1-6 A) (Krummel *et al.*, 2016). Furthermore, the persistence time can be deviated from the plot, which is the period that a cell intrinsically migrates in one direction before turning (Fürth, 1920). This is cell type-specific and depends on intracellular factors such as actin polymerization rate and polarity (Bosgraaf and Van Haastert, 2009; Li *et al.*, 2008; Maiuri *et al.*, 2015).

Although *in vivo* analyses of T cell migration are undoubtedly more representative for a physiological situation than migration in a two-dimensional *in vitro* scenario, there are a few caveats when analyzing cell migration in *in vivo* microscopy data. First, sufficient and uninterrupted perfusion of the tissue of interest by blood and lymph is pivotal to maintain physiological conditions. Second, the imaging parameters can greatly skew the following migration analysis: The time steps between the acquisition frames should be shorter or equal to the cell-intrinsic persistence time, whereas the overall track duration should be significantly longer than the persistence time. Also, the size of the acquired volume should be chosen wisely, because the anisotropic shape influences the conclusions drawn from the data (Textor *et al.*, 2011). Therefore, the finite image volume should be large enough in the direction that the cells are expected to travel in order not to miss a potential directionality. Third, the analysis of cell tracks needs to ensure the comparability of two different sets of data in terms of time step interval, overall track duration and size of image window. Because some migration parameters depend on each other, such as track duration and displacement, quality checkups or normalization need to ensure that this is comparable for the sets of data analyzed.

Most of the cell track analyses focus on cell populations or complete cell tracks. This method risks not to pick up directional movement of cells that switch between directional and non-directional movement. Alternatively, staggered cell track analyses can be performed; this more detailed analysis is able to represent also directional

movements within cell tracks of cells that switch between directional and random migration (Mokhtari *et al.*, 2013).

In summary, T cell migration analysis is a powerful tool to derive information about their sensitivity to environmental stimuli, and to infer their differentiation status and current effector mechanism.

1.2.5 Microscopy techniques and their applicability

Microscopy techniques are useful and valuable to study the interaction of immune cells inside organs, because apart from the information about the cells of interest, they give information about their localization in respect to other cell types, organs and extracellular structures. This information is lost upon extraction of the cells from the tissue. Different types of microscopy are more suitable for certain questions asked. Large-scale imaging of whole small animals such as mice can be accomplished with positron-emission tomography or bioluminescence imaging. It is possible to non-invasively image living anesthetized animals to for instance repetitively monitor metabolic parameters using tracers, or to observe over a time course of weeks and months the trafficking of cell populations expressing luciferase that produces bioluminescence.

To gain higher resolution, organs can be extracted and imaged in whole-mount light sheet fluorescence microscopy. For this technique, organs are fixed, permeabilized and can be stained with antibodies coupled to fluorescent dyes. Afterwards, the tissue is made transparent by replacing the water inside the cells with a solution that matches the refractive index of the tissue, thus light can pass through the organ without being scattered. The organs can then be acquired in a microscope by illuminating optical sections of the organ with a sheet of light and acquisition in a rectangular angle. This technique enables subcellular resolution in a comparably large volume, which can be reconstructed to a three-dimensional model afterwards (Brede *et al.*, 2012). Unfortunately, todate this technique is limited to transparent organisms for *in vivo* imaging, and murine or human tissues cannot be observed with this technique yet *in vivo*.

Light of long wavelengths is scattered less in living tissues, which make it suitable for imaging live opaque tissue. The scattering modality inside biological specimens is called Mie scattering, which decreases linearly with longer wavelengths (Johnsen and Widder, 1999). Two-photon microscopy employs long wavelengths of light for fluorophore excitation and is based on the principle of two-photon absorption by fluorescent dyes (Göppert-Mayer, 1931). Instead of classical one-photon excitation at the suitable

wavelength, the same fluorophore can be excited with two photons of approximately twice the wavelength (Figure 1-7). This greatly enhances the efficiency of fluorophore excitation inside scattering tissues and makes two-photon microscopy a useful technique to observe biological processes in live tissues.

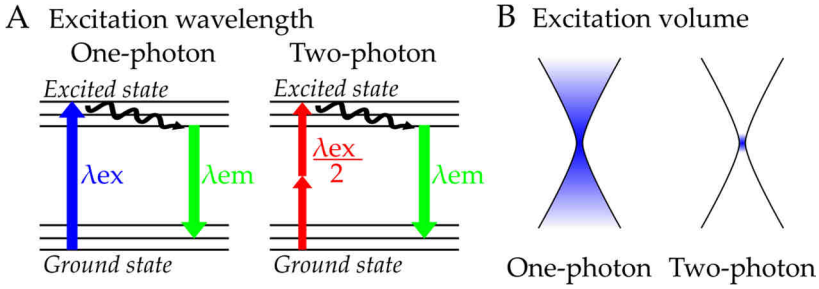

Figure 1-7 Advantages of two-photon microscopy. **A** Excitation wavelengths in two-photon microscopy are half the wavelengths of one-photon microscopy. **B** In one photon microscopy, fluorochromes are excited along the light path, whereas in two-photon microscopy, the high photon density required to elicit emission is only reached in the focal spot.

The resolution of two-photon microscopy is higher than in light sheet fluorescence microscopy, because it is inherently confocal: Sufficient excitation photon densities are only reached at the confocal spot. Although in deep tissues, the resolution is not as good as in confocal microscopy, two-photon excitation can be combined with a pinhole setup to get true confocal images. This is particularly efficient close to the tissue surface, where strong fluorescence emission can be detected. More recently, there are efforts to combine two-photon excitation with light sheet microscopy, a promising approach to image fast processes in living organisms (Lavagnino *et al.*, 2016).

To sum up, bioluminescence imaging is suitable for repetitive and whole-body imaging of small animals, and gives a good overview of localization of cell populations within a whole organism. For more detailed analysis of single cells, light-sheet fluorescence microscopy is a useful tool to analyze the localization of single cells inside whole organs. To observe biological processes dynamically *in vivo*, two-photon microscopy is the superior technique enabling visualization of deep live tissue areas.

In summary, T cell trafficking and migration is a specific and efficient mechanism tailored to the type of tissue (secondary lymphoid organ or effector tissue), situation (steady state or inflammation), and T cell differentiation. The versatility and flexibility of this system enables efficient distribution of an effective T cell mediated immune response to maintain bodily integrity and health.

1.3 Acute Graft-versus-Host Disease

Acute Graft-*versus*-Host Disease (aGvHD) occurs as a complication in 30-80% of all patients undergoing allogenic hematopoietic stem cell transplantation (Gooley *et al.*, 2010; MacMillan *et al.*, 2002). Next to disease relapse, it is the major cause or morbidity and mortality after this most successful curative therapy for blood-borne diseases such as leukemia. aGvHD is characterized by skin rashes, nausea and heavy diarrhea, lung obstruction and liver pathologies such as bilirubinaemia (Ferrara *et al.*, 2009). In contrast to chronic GvHD, aGVHD occurs early after transplantation, which in a clinical setting means within the first 100 days after transplantation. Pathophysiologically, aGvHD is a T cell mediated reaction and dominated by Th1 polarization and cytotoxicity, whereas the mechanism of cGvHD is rather antibody-mediated and affects additionally the eyes, salivary glands, more frequently the lung than in aGvHD, and is characterized by fibrosis rather than cell death.

1.3.1 MHC mismatch and alloreactivity against tumors

Allogenic hematopoietic cell transplantation is a successful treatment against blood-borne malignancies. After chemotherapy or irradiation, allogenic (*allo* is greek for 'other') donor cells from a healthy donor bone marrow cells are infused into the patient and replace the recipient's immune system. The transplant is always contaminated with few mature T cells (5×10^4 per kg body weight is considered the threshold for induction of GvHD), which are not selected in the patient's thymus. Through allorecognition the donor T cells can be effective surveyors eradicating remnant tumor cells. Some T cells can directly recognize host major histocompatibility complexes (MHC) independently of the peptide presented. This occurs at a much higher frequency than normal cognate MHC-peptide recognition. In a major mismatch setting, an estimated 5-10% of allogenic T cells become alloreactive (Suchin *et al.*, 2001). Additionally, in fully MHC-matched transplantations, donor T cells may recognize presented host peptides, which is called minor mismatch and occurs in 40% of MHC-matched transplants (Ferrara *et al.*, 2009). Common antigens recognized by allogenic T cells are the minor histocompatibility antigens such as HA-1 or y-chromosomal proteins in sex-mismatched transplantations (Bleakley and Riddell, 2004).

Allorecognition of MHC molecules or presented peptides is central to residual tumor surveillance and the mechanism with which this therapy is so successful. However, these allogenic T cells can also become reactive to non-malignant tissues of the recipient and cause GvHD. Thus, clinicians need to establish a fine balance between enough

alloreactivity to fight against the tumor, and enough tolerance or immune suppression to prevent GvHD destroying healthy host tissues.

1.3.2 Clinical relevance of GvHD

GvHD is the cause of death in 20-30% of all patients undergoing hematopoietic cell transplantation (Gooley *et al.*, 2010). Without immunosuppressive treatment, 100% of allogenic transplant recipients develop GvHD. The severity of GvHD is graded into four categories, but differences exist between different scoring criteria (Glucksberg, Minnesota, Consensus or International Bone Marrow Transplant Registry, IBMTR) (Glucksberg *et al.*, 1974; Przepiorka *et al.*, 1995). Based on these differences, different incidences of GvHD are registered in different transplantation centers. According to the Glucksberg criteria, mild grade I GvHD includes only the skin, this is often the first obvious symptom of GvHD. Moderate Grade II GvHD includes moderate skin and mild to moderate liver and intestinal damage. Grade III GvHD is characterized by severe damage in all three target organs, and grade IV is very severe GvHD. Severe and very severe GvHD have poor survival prognoses with 25% and 5%, respectively. Intestinal grading of GvHD is performed clinically according to the volume of diarrhea and morphologically according to crypt- and epithelial cell apoptosis, immune cell infiltrates and villus blunting (Washington and Jagasia, 2009). The first-line treatment against GvHD is, and has been for a long time now, steroids aiming at limiting alloreactive T cell expansion. Unfortunately, around 50% of the patients develop steroid-refractory GvHD and require alternative treatments, which are to date limited in success and lead to mortality rates of 70-80% (Hill *et al.*, 2018).

In summary, GvHD frequently complicates allogenic hematopoietic cell transplantation. It poses a major hindrance to therapy success and causes severe morbidity and mortality. Because a high percentage of patients become resistant to the standard therapy, it is important to develop new strategies to more efficiently tailor the immune response for patients to benefit from this treatment.

1.3.3 GvHD pathophysiology and target organs

GvHD pathophysiology occurs in three stages: tissue destruction due to the conditioning regimen (phase I), activation of antigen-presenting cells and subsequent alloreactive T cell expansion (phase II), and finally tissue destruction and cytokine storm (phase III) (Ferrara *et al.*, 2009). Despite expression of allo-antigens in all host tissues, not all host tissues are affected by GvHD to the same extent. In aGvHD, the skin, intestine, liver and lung are target organs, whereas others such as the kidney or the heart are not affected. Factors that may contribute to allo-immune responses against these organs are

their high cellular turnover rates, which leads to more extensive damage than in organs with a higher percentage of non-dividing cells. This affects the extent of tissue damage in phase I. Secondly, the skin, intestine, lung and the liver via the portal vein are exposed to a large variety of microbiota and fungi, which make them rich in immunostimulatory molecules recognized by the innate immune system. This affects the activation of antigen-presenting cells in phase II. Third, intestine, liver and skin are organs rich in resident immune cell populations, which partly survive the conditioning regimen and therefore provide a large reservoir for cells producing large amounts of cytokines (phase III).

Additionally to the three classical aGVHD target organs gut, liver and skin, other organs can also be affected: The lung, mouth, eye and vaginal mucosa can be attacked in acute and chronic GvHD (Teshima *et al.*, 2016). There are also reports of central nervous system infiltrates (Hartrampf *et al.*, 2013; Ruggiu *et al.*, 2017).

1.3.4 Cytokines and chemokines in aGvHD

During GvHD, the damage resulting from the conditioning regimen induces production of IFNγ, which activates macrophages to produce large amounts of TNFα and IL-12 (Nestel *et al.*, 1992). This affects endothelial cells to increase the vascular permeability, and polarizes T cells to a Th1 phenotype, which subsequently produce IL-2 and IFNγ. This in turn renders macrophages more sensitive to LPS and creates a vicious cycle leading to a fulminant immune reaction. However, IFNγ in GvHD is a double-edged sword since it is not only not required for the development of GvHD, but it has been shown in multiple studies to play a partly protective role (Yang *et al.*, 1998). This is likely due to pro-apoptotic properties, partly during the contraction phase of an immune response. Nevertheless, IFNγ is an important mediator particularly of gastrointestinal GvHD, as discussed below.

IFNγ induces the expression of further inflammatory mediators including the cytokines CXCL9-11. This recruits alloreactive CXCR3$^+$ T cells into the target organs, where they subsequently produce CCL2-5 (Bouazzaoui *et al.*, 2009). Furthermore, CXCL16 recruits CXCR6$^+$ T cells, and XCL1 is produced, mostly in the intestine. Under steady state conditions, intestinal T cells may produce XCL1 to recruit cross-presenting dendritic cells, which might be important to in turn maintain intraepithelial lymphocytes (Ohta *et al.*, 2016).

The classical gut-homing chemokine is CCL25 produced by intestinal epithelial cells. Although its ligand CCR9 is upregulated on alloreactive T cells infiltrating the intestine, deletion of CCR9 does not ameliorate GvHD (Schreder *et al.*, 2015). The CCR9

antagonist CCX282 has shown some positive trends in treatment of Crohn's disease, but the phase III clinical trial did not substantiate this trend (Wendt and Keshav, 2015). In contrast, blockade or deletion of the gut homing integrin $\alpha_4\beta_7$ in GvHD ameliorated GvHD (Gorfu *et al.*, 2009; Schreder *et al.*, 2015). Furthermore, a phase 1 and 2 clinical trial showed efficacy of the CCR5 blocker Maraviroc (Moy *et al.*, 2017).

In summary, the strong IFNγ response induces strong T cell activation alongside with early inflammatory chemokines attracting alloreactive T cells to the target tissues. Attempts to interfere with this process are in development, but not yet broadly applied.

1.3.5 The intestine as an early GvHD target organ

Due to the extensive damage from the conditioning regimen in the intestinal tract and the large amount of microbiota at this surface, gastrointestinal GvHD develops frequently. Translocation of microbes from the lumen further fuels systemic GvHD, and intestinal GvHD symptoms quickly become life-threatening when diarrhea leads to extensive water loss and hampers proper nutrient uptake. These factors can contribute to the early infiltration of T cells into the intestine in the mouse model employed. The intestine is infiltrated before other organs are affected (Beilhack *et al.*, 2005).

Intestinal GvHD is induced in the mesenteric lymph nodes and the Peyer's patches, where the primed T cells upregulate the homing receptors $\alpha_4\beta_7$ and subsequently infiltrate the small intestine and colon. Although early reports demonstrated a pivotal role of Peyer's patches in GvHD (Murai *et al.*, 2003), the mesenteric lymph nodes also significantly contribute to intestinal homing T cells in GvHD. Later, it became evident that also other peripheral lymph nodes and even the spleen can give rise to gut homing T cells in GvHD, particularly in combination with a stronger conditioning regimen (Beilhack *et al.*, 2008; Masopust *et al.*, 2010).

Currently there are many attempts at characterizing and manipulating the microbiota to ameliorate GvHD. High diversity and the occurrence of bacterial species such as *Lactobacillus* or *Blautia* producing short-chain fatty acids have been associated with better GvHD outcomes (Jenq *et al.*, 2015; Shallis *et al.*, 2018). In contrast, low diversity, *Clostridium difficile* and dominating enterococci have a worse prognosis. Despite a protective role of certain bacterial species, prophylactic antibiotics are effective in reducing GvHD after transplantation (Beelen *et al.*, 1992). The efficacy of this treatment seems to depend on the degree of depletion of selective bacterial species, since some broad-spectrum antibiotics can also exacerbate GvHD via expansion of mucus-degrading commensals (Shono *et al.*, 2016). Fecal transplantations are a promising

approach to overcome the sparse microbial diversity after antibiotic treatment (DeFilipp *et al.*, 2018).

Since early infiltration of T cells into the intestine leads to increased GvHD in other target organs, it is desirable to interfere in this process as early as possible. Depletion of allogenic T cells would impede surveillance of residual tumor cells, therefore blocking T cell entry into the GvHD target organs is a promising alternative strategy. However, since infiltration of allogenic T cells is mediated by more than four different redundant homing molecules, a complete block of intestinal T cell homing is challenging (Beilhack *et al.*, 2008). We hypothesize that additionally to vascular recruitment of T cells, direct migration from the Peyer's patches may be a route of T cell infiltration that possibly underlies completely different regulatory mechanisms than vascular trafficking.

In summary, the microbe-rich environment contributes to activation of T cells in the Peyer's patches and mesenteric lymph nodes and to early infiltration of the intestine as compared to other target organs. However, the peripheral lymph nodes and the spleen also contribute to intestinal T cell homing. Manipulation of the intestinal microbiota may be a promising strategy to ameliorate gut GvHD pathology. However, to completely block intestinal infiltration, we propose that direct access from the Peyer's patches to the surrounding tissue may be a heretofore unknown source of intestine-infiltrating T cells.

1.3.6 GvHD mouse model

Immune cell populations are comparably easy to extract from tissues, because particularly most types of lymphocytes sustain only weak cell contacts with neighboring cells. This enables easy and rapid extraction of these cells for detailed analyses *in vitro*. However, there are many biological processes that are to date too complex to be reproduced fully *in vitro*, which is why it is important to study these processes in a living organism.

There are a number of different well-established mouse models for GvHD (Schroeder and DiPersio, 2011). In our study, we employed the C57BL/6 to BALB/c model, where bone marrow cells and T cells from B6 (H-2K^b) are transplanted into fully MHC-mismatched BALB/c recipients (H-2K^d). Both CD4$^+$ and CD8$^+$ T cells contribute to GvHD pathology in this model by producing IFNγ or by directly lysing target cells via perforin, granzyme and Fas ligand (Graubert *et al.*, 1997; Maeda *et al.*, 2005; Via *et al.*, 1996). In our study, we use this model to study the wave of intestinal infiltration by activated T cells after synchronized expansion of the population in different activation sites. This model was very useful because the time course of infiltration was quite well

characterized at the beginning of this thesis. The strong orchestrated infiltration wave proved to enable detailed and reproducible observation of different infiltration steps while enabling time-efficient experiments. These characteristics made the model suitable to study the infiltration of T cells from Peyer's patches to the *lamina propria*.

1.4 Knowledge gap

Peyer's patches are embedded inside the target organ, which T cells are induced to migrate into after activation: the intestinal mucosa. To date, this is thought to occur via T cell egress via the lymphatics, recirculation through blood vessels and extravasation into the *lamina propria* of the small intestine. It is not known whether the location and architecture of Peyer's patch inside the target organ allows for direct infiltration from priming site to effector site without lymphatic and circulatory trafficking. Furthermore, it is unclear whether T cells can migrate from the Peyer's patch directly to the surrounding tissue.

2 Specific Aims

The overall aim of this thesis was to determine whether allogenic T cells can migrate from the Peyer's patches directly to the adjacent *lamina propria* of the small intestine. The specific aims to test this hypothesis were to

1. Study whether border of Peyer's patches is permissive for direct cell migration.
2. Test whether a T cell gradient establishes around the Peyer's patch.
3. Prove direct T cell migration from Peyer's patch to the adjacent *lamina propria*.
4. Determine the driving forces of direct migration by analyzing
    a. the migration mode of egressed cells.
    b. the role of S1P for egress.
    c. a screen for other migration-promoting factors.

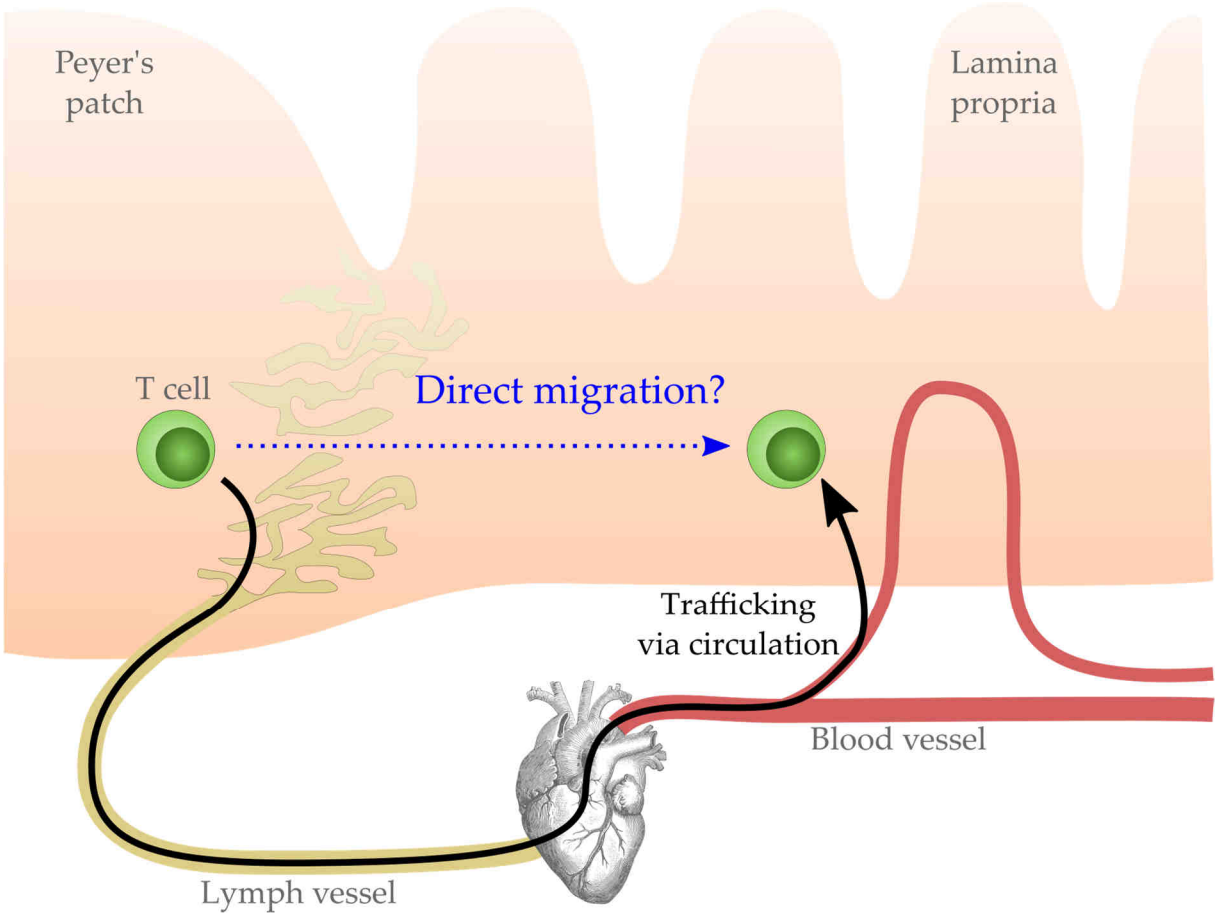

Figure 2-1 Hypothesis. To reach from Peyer's patches as T cell priming site to the target organ small intestine, T cells egress via the lymphatics and enter the small intestinal *lamina propria* from blood circulation. We hypothesize that a fraction of T cells accesses the lamina propria surrounding the Peyer's patch by migrating directly from the Peyer's patch without vascular trafficking.

3 Materials and Methods

3.1 Materials

Material	Catalog #	Company
Chemical reagents		
Acetone	33201	Sigma-Aldrich
Albumin from chicken egg white	A5378	Sigma-Aldrich
Avidin/Biotin blocking kit	SP-2001	Vector Laboratories
Benzyl alcohol	4478.2	Carl Roth
Benzyl Benzoate	B6630	Sigma-Aldrich
Entellan new	1.07961	Merck
Cresyl violet	7651.2	Carl Roth
Ethanol absolute	2246	Chemsolute
Liquid blocker super PAP pen	N71310	Science services
0.9% NaCl, sterile		Fresenius
n-Hexane	1.04367	Merck
O.C.T. Tissue tek	4583	Sakura
Paraformaldehyde	P6148	Sigma-Aldrich
TritonX-100	2051.3	Carl Roth
Trypan blue	A0668,0025	Applichem
Vectashield embedding medium	H-1200	Vector Laboratories
Dispensables		
General		
Syringe, 1 ml insulin (30Gx×1/2″ (0,3mm × 12mm), Omnican® 100	9151141	Braun
Syringe, 1 ml 26GA×3/8″ (0,45 × 10 mm), BD Plastipak™	300015	Becton Dickinson
Flat bottom glass containers (Rollrandgläser)	RR02	Hartenstein
Microscopy cover slips 21×26	01 01092	Marienfeld
SuperFrost® Plus Objektträger	03-0060	R. Langenbrinck
Syringe, 5 ml BD Discardit™ II	300850	Becton Dickinson
Accu-jet® pro	26300	Brandt
Cell strainer, 100 μm	130-110-917	Miltenyi Biotec

Material	Catalog #	Company
(MACS® Smart Strainers)		
Cell strainer, 70 µm EASYstrainer™	542070	Greiner Bio-one
serological pipettes, disposable	760180, 607180, 606180	Greiner Bio-one
MembraneSlides PEN 2.0 µm	11505189	Leica
Micropipettes	042760930, 642752433, 942741768, 342733754, 042720454, 942711302	VWR
Microtubes 1.5 ml	72.706	Sarstedt
Pasteur pipettes	2600111	NeoLab
Scalpel blades, feather #10, sterile	BB510	B. Braun
Tube 50 ml	227261	Greiner Bio-one
Tube 15 ml	188271	Greiner Bio-one
U-bottom 96-well plates	83.3922.500	Sarstedt
Kits		
Cell counting chamber (Neubauer)	ZK03	Hartenstein
Cell Trace™ Violet Cell Proliferation Kit	C34557	Thermo Fisher Scientific
LIVE/DEAD™ Fixable Violet Dead Cell Stain Kit, for 405 nm excitation	L34955	Thermo Fisher Scientific
PBS without Ca^{2+}/Mg^{2+}	P04-36500	Pan Biotech
RNeasy MicroKit	74004	Qiagen
T cell enrichment kit ($CD11b^-$, $CD16/32^-$, $CD45R^-$ and $Ter\text{-}119^-$, Dynabeads Untouched Mouse T cells Kit)	11413D	Thermo Fisher
Zombie Aqua Fixable Viability Kit	423101	Biolegend
Operation equipment		
Eye ointment (Bepanthen®)		Bayer
Analgetic (Novalgin®)		Sanofi

Material	Catalog #	Company
Razors	704028	Body products, Relax Pharma u. Kosmetik GmbH
Sterile Dissecting swab (Setpack® Size 2)	12780	Lohmann & Rauscher
Sterile Gauze swab (Gazin® 5×5 cm)	13695	Lohmann& Rauscher
Sterile Cotton swab (Rotilabo®)	EH12.1	Carl Roth
Operation towel	800430	BARRIER, Mölnlicke healthcare
70% Ethanol	T931.3	Carl Roth
Quickpad® 70% 2-Propanol		Holtsch Medizinprodukte GmbH
Povidone iodine (Braunol® 7,5% solution)	3864065	BRAUN
Suture, 6-0 with beveled needle	V301G	Ethicon
Cell culture		
RPMI Medium1640	21875-034	Gibco®
Penicillin, Streptamycin	15140-122	Gibco®
L-Glutamine	25030081	Gibco®
Fetal bovine serum	10270-106	Gibco®
Recombinant human IL-2	589106	Biolegend
Equipment		
Centrifuge (Megafuge 40R)		Thermo Fisher Scientific
CO_2 incubators	150i	Thermo Fisher Scientific
Collimator, 405 nm, f= 4,02 mm, numerical aperture=0,6 SMA Fiber Collimation	F671SMA-405	THORLABS
Cryostat	CM1950	Leica
Glass fibre, 1500 μm, NA=0,5		Prizmatix
heating mats (20 × 30 cm)	76085	Trixie heimtierbedarf GmbH
High-Power UV LED lamp, fibre-coupled	Silver LED-405 nm	Prizmatix
Hot bead sterilizer FST250	18000-45	Fine Science Tools
Infrared lamp	BF 27	Beurer
Laboratory stand with bosshead and ring clamp		VWR

Material	Catalog #	Company
Laminar flow hood Hera safe	KS 18	Thermo Fisher Scientific
Orbital shaker	PSU-10i	Grant Instruments
Powermeter PM100	discontinued	Thorlabs
Rectal probe for mice	RET-3	Physitemp
Rhodent thermometer	BIO-TK8851	Bioseb Lab
Surgery tools: 2 fine forceps, 1 pair of small scissors, 1 pair of large scissors, 2 thread holders, 1 needle holder		Karl hammacher GmbH and megro
Tubing Tygon		Cole-Parmer GmbH
Tubing pump ISMATEC Reglo Analog MS 2/12	ISM795C	Cole-Parmer GmbH
Thermometer (Dual Thermo Max/Min)	E609790	Amarell Electronic
UV protection glasses	F18P1L051001	Laservision
Water bath	WNB 14	Memmert
X-Ray irradiation source	CP-160	Faxitron
FACS Canto II equipped with 405 nm, 488 nm and 633 nm lasers and a high-throughput sampler (HTS)		Becton Dickinson
Filter sets for FACS 488 channel: 735 LP+780/60, 655LP+760LP, 610LP, 556LP+585/42, 520LP+530/30, 488/10; 405 channel: 502 LP+510/50, 450/50; 633 laser: 735LP+780/60, 685LP, 660/20		Becton Dickinson
FACS Attune equipped with 405 nm, 488 nm, 561 nm and 633 nm lasers and a high-throughput sampler		ThermoFisher Scientific
Filter sets for 405 nm laser: Pacific blue: 440/50; 488 laser: FITC 530/30, PerCP-Cy5.5 695/40; 561 laser: PE 574/26, PE-Cy7 870/60; 633 laser: APC 670/14, APC-Cy7 870/60.		ThermoFisher Scientific

Material	Catalog #	Company
Laser capture microdissection microscope	AS-LMD and LMD6000B	Leica
Illumina NextSeq500		Illumina
2-Photonenmikroskop DM6000 CFS, equipped with Objective HC Fluotar L 25x/1.0 Imm mot Corr, 2 PMTs: Hamamatsu R9624, 2 HyD-RLD 2 detectors, Chameleon Vision II TiSa laser, Beam splitters: RSP 620 + BP440/20 + 675/50, RSP 455, RSP 560 + 525/50 + 585/40, RSP 495+ BP 440/20		Leica
Software		
Imspector	Version 380	LaVision Biotec
Leica Application Suite X	Version 3.1.5.16308	Leica
ZEN pro	Version 11.0	Zeiss
Imaris	Versions 7.7.2 to 9	Bitplane
Matlab	Version R2016a	Mathworks
INGENUITY Pathway Analysis	Version 01-08	Quiagen
Fiji Is Just ImageJ	Version 1.52e	Wayne Rasband, NIH, USA
FigureJ	Version 1.10b	Jerome Mutterer, CNRS, France; Edda Zinck HTW, Germany
Ingenuity Pathway Analysis (IPA)	Version 45868156	Quiagen
Graphpad Prism	Version 6	GraphPad Software
Office	Version 2010 to 2016	Microsoft
Mice		
B6;129S-Gt(ROSA)26Sor$^{tm1.1(CAG-COX8A/Dendra2)Dcc}$/J	018397	Jackson Laboratories
B6;129S4-*Gt(ROSA)26Sor*$^{tm1(rtTA*M2)Jae}$ *Col1a1*$^{tm7(tetO-HIST1H2BJ/GFP)Jae}$/J	016836	Jackson Laboratories
B6.Cg-Tg(CAG-DsRed*MST)1Nagy/J	006051	Jackson Laboratories
B6.TyrC$^{-/-}$ Tg(Itgax-DTR/OVA/EGFP)1Garbi/J	-	Bred in the Beilhack Laboratory

Material	Catalog #	Company
C57BL/6. *Tg(CAG-luc,-GFP)L2G85Chco Ptprc^a*/J	-	Bred in the Beilhack Laboratory
C57BL/6. *Tg(CAG-luc,-GFP)L2G85Chco Thy1^a*/J	-	Bred in the Beilhack Laboratory
BALB/c (BALB/cAnNCrl)	Strain Code 028	Charles River
C57BL/6 (C57BL/6NCrl)	Strain Code 027	Charles River

3.1.1 Antibodies

Table 3-1 Antibodies

Reactivity	Coupled to	Host species	Clone/order ID	Manufacturer
Primary antibodies				
CD3	-	Armenian hamster	145-2C11	BD Pharmingen
CD4	AF488	Rat	RM4-5	Biolegend
CD4	PerCP-Cy5.5	Rat	RM4-5	Biolegend
CD4	APC-Cy7	Rat	RM4-5	Biolegend
CD8	APC	Rat	53-6.7	Biolegend
CD8	PE-Cy7	Rat	53-6.7	Biolegend
CD44	PerCP-Cy5.5	Rat	IM7	Biolegend
CD90.1	APC	Mouse	HIS51	eBioscience
CD45.1	AF647	Mouse	A20	Biolegend
CD45.1	AF700	Mouse	A20	Biolegend
MAdCAM-1	Biotin	Rat	MECA-367	Biolegend
Lyve-1	eFluor660	Rat	ALY-7	eBioscience
Laminin	-	Rat	AL-4	Biolegend
Secondary antibodies/ reagents				
Rat IgG	Cy3	Donkey F(ab')$_2$	712-166-153	Dianova
(Biotin)	AF546	Streptavidin	S11225	Invitrogen

3.1.2 Preparation of reagents

- Anesthetic: 2 ml of Ursotamin® (100 mg/ml, Serumwerk) and 2 ml of Xylavet® (20mg/ml, CP-pharma) were added to 21 ml DPBS. 10 µl per g body weight was injected to reach desired concentrations (Ketamin 80 mg/kg, Xylazin 16 mg/kg).
- Analgetics: Metamizol (Novalgin®): 266 µl of Novalgin® were added to 100 ml of drinking water (1.33 mg/ml). Additionally, mice received 200 mg/kg of Novalgin injection solution. 10 µl of Novalgin injection solution was injected per g body weight, prepared from 8 µl of Novalgin mixed with 192 µl of NaCl, subcutaneously at recovery from anesthesia.

- Erythrocyte lysis buffer: 89.9 g NH_4Cl, 10 g $KHCO_3$ and 0.37 g EDTA were dissolved in 1L of deionized water.
- Trypan blue solution: 1 g of trypan blue was dissolved in 100 ml of PBS. To receive the working solution, the Stock was diluted 1:10 in PBS to mix at equal volumes or diluted 9:10 with cell suspension.
- Enrichment buffer: 0.5 g BSA and 0.375 g EDTA were dissolved in 500 ml DPBS and sterile-filtered.
- Dissociation buffer: per mouse, 70 ml was prepared. 55.836 mg of EDTA was dissolved in 66.5 ml HBSS without Ca^{2+}/ Mg^{2+}. 3.5 ml FCS was added to receive HBSS with 5% FCS, 2 mM EDTA.
- Proliferation medium: RPMI medium1640 with 10% FCS, 1% PenStrep solution, 30 ng/ml anti-CD3 antibody, 50 IU/ml IL-2.

3.2 Methods

This study was carried out in accordance with the recommendations and regulations of the Regierung von Unterfranken. The procedures were approved under the protocol numbers 55.2-2531.01-82/14 and 55.2 2532-2-48.

3.2.1 Transplantation

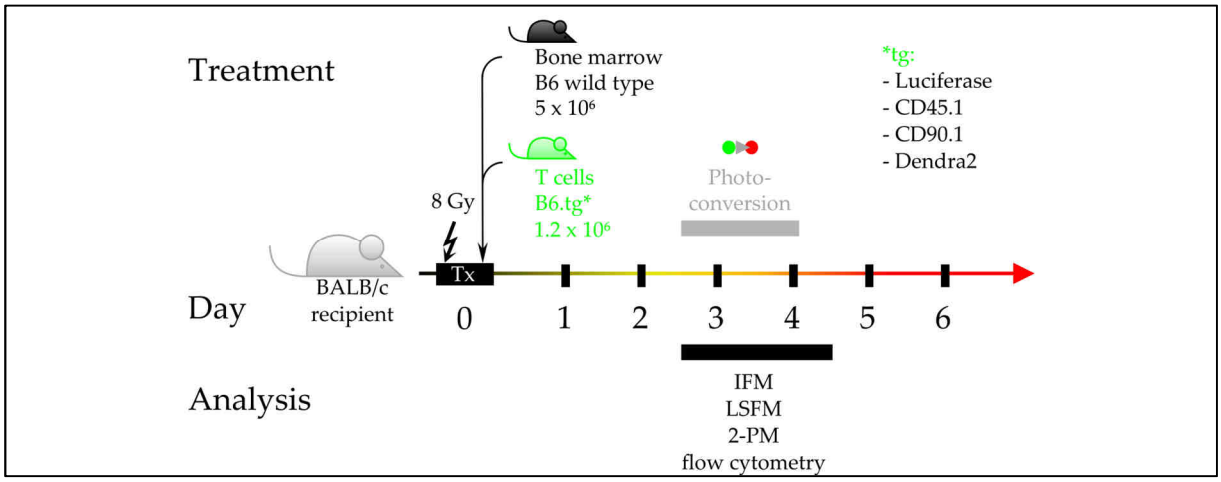

Figure 3-1 Transplantation scheme. BALB/c recipients were irradiated with 8 Gray and transplanted with 5×10^6 B6 wild type bone marrow cells and 1.2×10^6 T cells. The T cells were congenically marked and/or carry a transgene depending on type of subsequent analysis.

3.2.1.1 Donor T cell enrichment

T cells were isolated from the spleen of donor mice at the age of 8-14 weeks. Splenocyte suspensions were enriched for T cells using the Dynabeads Untouched Mouse T Cells Kit according to the manufacturer's protocol, counted by trypan blue exclusion and

adjusted to a density of 12×10^6 cells per ml in PBS. Typical T cell yields lay between 15 and 30% of the splenocyte input with a final T cell purity of 85-95%.

3.2.1.2 Donor bone marrow isolation

Bone marrow cells were isolated from hind legs (femura and tibiae) of 8-12 week old C57BL/6 mice. Cell numbers were determined by trypan blue exclusion, and the cell concentration was adjusted to 50×10^6 cells per ml. Typical bone marrow cell yields were $1 – 1.5 \times 10^8$ cells per mouse.

3.2.1.3 Transplantation

BALB/c mice at the age of 8-14 week were myeloablatively irradiated (8 Gray), and 1.2×10^6 donor T cells were intravenously injected via the retro-orbital venous plexus together with 5×10^6 bone marrow cells (Figure 3-1) in a total volume of 200 µl PBS. The T cells were isolated from mice expressing the CD45.1 allele for LSFM processing, or CD90.1 for cryosections. Dendra2$^+$ cells were transplanted for photoconversion studies, and Luciferase-expressing T cells for bioluminescence imaging. The drinking water was supplied with Baytril (Enrofloxacin, 0.05%) for 7 days after transplantation to avoid infections. GvHD was scored clinically according to Table 3-2 and Table 3-3 daily.

Table 3-2 Clinical score to assess GvHD severity.

	Score 0	Score 1	Score 2
Weight loss	< 10%	>10% <20%	Score 2+: >20% longer than 2 days
Posture	normal	Hunchback at rest	Hunchback limits mobility
Behavior	normal	Reduced slightly to moderately	absent, only after provocation
Ruffled fur	normal	slightly to moderately	Strong, no grooming
Skin	normal	Dandruff on paws and tail	Strong fur defects
Eyes	normal	Conjunctivitis of one eye or slightly of both eyes	Strong conjunctivitis of both eyes
Licking and scratching of inflamed skin	none	<1x/min	>1x/min
Stool	normal	Slight diarrhea, anus swollen	Strong diarrhea, melena
Anemia	normal	Paleness visible on skin without fur	Paleness visible on whole body

Table 3-3 Criteria to define the humane endpoint.

	Intestinal aGvHD	Skin aGvHD	Anemia
Weight loss	1-2+	0-1	1-2+
Posture	2	0-1	2
Behavior	1-2	0	1-2
Ruffled fur	1-2	2	0-1
Skin	0	2	0
Eyes	0-1	1-2	0-1
Licking and scratching of inflamed skin	0	2	0
Stool	1-2	0	0
Anemia	0	0	1-2
Score sum	6-11	7-10	5-10
Humane endpoint		≥ 8	

3.2.2 *In vitro* photoconversion

A few drops of peripheral blood was isolated from a Dendra2$^+$ mouse and erythrocytes were lysed in 4 ml of Erythrocyte lysis buffer for 10 min. The cells were pelleted at 330×*g* for 5 min at 4 °C and washed with 3 ml of PBS. After another centrifugation step at 330×*g* for 5 min at 4 °C, the cells were resuspended in the remaining supernatant. 10 µl of the cell suspension was transferred onto a glass slide and covered with a cover slip. The cells were imaged and photoconverted in a confocal microscope. Individual cells were scanned using the 405 laser at 4% power in 34 Z sections using a 63×/1.2W immersion objective with a voxel size of 0.09 µm × 0.09 µm × 0.52 µm (X×Y×Z) and a pixel dwell time of 5.06 µs. Photoconversion was validated by imaging the same cell before and after conversion.

3.2.3 *In vivo* photoconversion

The operation for photoconversion is described in detail in (Jarick *et al.*, 2018). Briefly, mice were anesthetized with 100 µg/kg Ketamine and 20 µg/kg Xylazine and remained

on heating pads during anesthesia. After 10 min, anesthetic depth was ensured to be stadium III.2 (surgical tolerance) by pinching the hind paw. If anesthesia was insufficient, further anesthetic was provided retro-orbitally. Not more than 20-50 µl was injected at a time, because the fast pharmacodynamics of intravenously delivered anesthetics can quickly lead to over-dosage.

The shaved and sterilized abdomen was opened with a 1.5 cm incision in the skin and peritoneum, and one or more Peyer's patches were gently externalized for photoconversion using PBS-soaked cotton swabs. The intestine is extremely sensitive to mechanical stress, because this can cause a postoperative ileus (Luckey *et al.*, 2003). In this condition, tissue-resident macrophages become activated and the neuronal activity of the enteric nervous system is disturbed. As a result, the intestinal muscles are paralyzed and no longer perform a propulsive movement. Gas and fluids accumulate in the lumen and cause abdominal pain, in mice this situation can become lethal. Therefore, the intestines were handled very carefully. UV illumination was applied using a sterile tin foil stencil, exposing the Peyer's patch through a hole with the diameter of approximately 2 mm for 2 min at maximum power. A collimator was connected to the UV lamp via a glass fiber and fixed on a laboratory stand. UV protection glasses were worn whenever the lamp was in operation.

The abdomen was closed with interrupted suture of both the peritoneum and the skin, and mice were provided with one dose of subcutaneous analgesia as well as in the drinking water until the final analysis 12 h later.

A clean recovery cage was placed under an infrared lamp or on a heating pad, and the temperature of the recovering animals was monitored not to rise above 37 °C using a thermometer with a rectal probe.

3.2.4 Isolation of T cells for flow-cytometric analyses

At different time points after photoconversion (0 h, 4 h, 12 h, 24 h), mice were sacrificed and the blood, mesenteric lymph nodes, Peyer's patches and small intestine were harvested as described in Jarick et al., 2018. One spleen was isolated for control stainings.

Briefly, up to 700 µl of peripheral blood was collected from the vena cava inferior with an insulin syringe (Figure 3-2) and lysed in 30 ml of Erythrocyte lysis buffer for 15 min at room temperature.

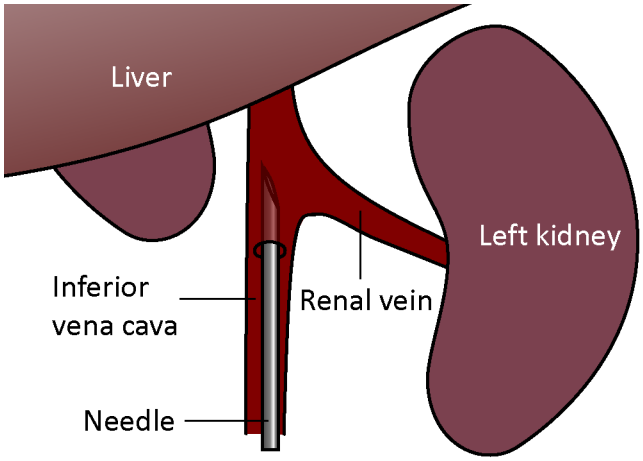

Figure 3-2 Collection of blood from the vena cava.

To isolate T cells from Peyer's patches, the patches were excised from the intestine generously and trimmed afterwards. Peyer's patches surrounded by intestinal tissue were spread out on PBS-moistened paper towels, and all surrounding tissue was precisely cut off using a scalpel.

Mesenteric lymph nodes and Peyer's patches were thoroughly minced through a PBS-pre-wet 70 µm strainer using the sterile plunger of a 5 ml syringe, and rinsed through with 5 ml of ice-cold PBS. Cells were pelleted at 330×*g* for 5 min at 4 °C, and the supernatant was removed. Lymph node cells were resuspended in the residual volume and directly transferred completely onto a 96-well plate for staining. Cells from the Peyer's patch were washed once with 5 ml of ice-cold PBS, centrifuged and then transferred onto the 96-well plate in the residual volume.

3.2.5 Intestine

Cells were isolated from the intestine using a protocol modified from Geem and colleagues (Geem *et al.*, 2012). The small intestinal tube was opened longitudinally and vigorously dragged through 300 ml PBS to remove fecal contents. It was cut into 2 cm segments and transferred into a 50 ml tube containing 30 ml of dissociation buffer. The tube was horizontally fixed on an orbital shaker set to 250 rpm for 20 min at 37 °C. The solution was passed through a 100 µm strainer into a 50 ml tube. The incubation and filter step were repeated with another 30 ml of dissociation buffer. The first dissociation fraction was centrifuged at 330×*g* for 5 min at 4 °C and the pellet was washed in 30 ml of PBS. The two filtered cell suspensions were united and the PBS washing step was repeated. In initial experiments, the *lamina propria* fraction was additionally processed according to (Geem *et al.*, 2012), but all donor T cells were found in the epithelial wash fraction. Although histological analyses clearly show that most donor T cells are located in the *lamina propria*, these highly migratory cells may be only loosely attached to the

extracellular matrix and are thus easily washed out during the separation of the epithelium from the *lamina propria*.

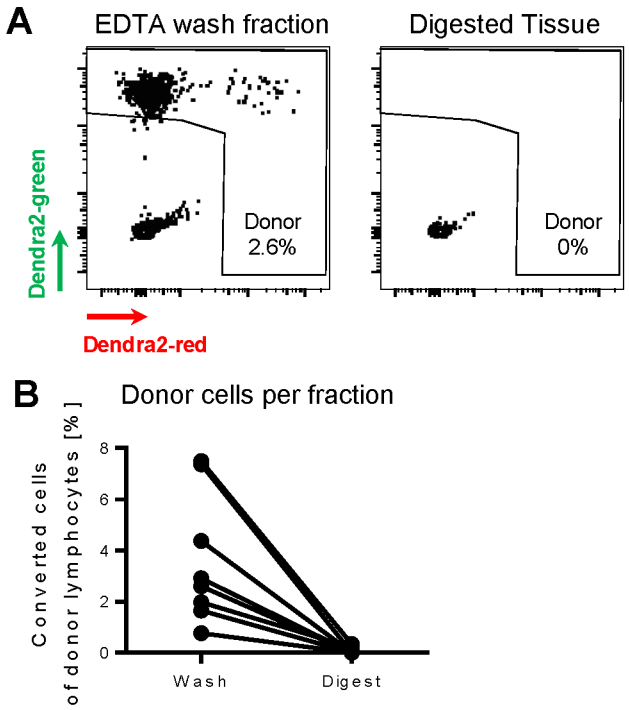

Figure 3-3 Donor T cells are isolated from the epithelial wash fraction.

3.2.6 Spleen

A 70 µm cell strainer on a 50 ml Falcon was pre-wet with 2 ml of Erythrocyte lysis buffer. The organ was placed on the strainer, incised crosswise a few times, minced with the plunger of a 5 ml syringe and passed through the strainer by rinsing with 8 ml of Erythrocyte lysis buffer. Erythrocytes lysis was stopped after 2 min by adding 10 ml of PBS through the strainer. Cells were pelleted for 5 min at 330×*g* at 4 °C and resuspended in 5 ml of PBS.

3.2.7 Flow cytometry

Up to 1 × 10^6 cells were stained per well. Cells were resuspended in 100 µl blocking buffer and incubated for 5 min at 4 °C. 100 µl of antibody mix was added, and cells were stained for 30 min at 4 °C in the dark. Cells were pelleted at 330×*g* for 5 min at 4 °C and resuspended in 200 µl of PBS.

Fluorescence signal was acquired at 1,000 – 3,000 events per second, and washing wells were measured between different sample groups to exclude cross-contamination. The Dendra2 signal is extremely bright, especially in the FITC/GFP channel, and care was taken not to saturate any PMT. Supplementary Table 1 contains a representative

compensation matrix. Donor T cells were identified by gating on lymphocytes - live cells - singlets - Dendra2-green and/or Dendra2-red positive cells (Supplementary Figure 3).

3.2.8 Proliferation assay

Splenocytes were isolated from Dendra2$^+$ mice as described in section 3.2.6. Half of the cells were photoconverted in a black 24-well dish for 2 min with a rotating motion of the glass fiber and without the collimator. 5 × 10^6 cells per ml were stained with 1 µl of cell trace violet (CTV) for 6 min at room temperature. 500 µl of FBS and 5 ml of RPMI were added successively, and samples were incubated at 37 °C in a water bath for 5 min. The samples were centrifuged pelleted at 330×*g* for 5 min at room temperature and resuspended in 5 ml of PBS. Cells were seeded on a 96 well round bottom plate at 200,000 cells per well in 200 µl of proliferation medium and left to proliferate for three to four days.

3.2.9 Cyotoxicity assay

Lymph node and spleen cells were isolated from untreated B6:Dendra2$^+$ mice, and the containing T cells were stimulated in a mixed lymphocyte reaction with allogenic BALB/c splenocytes to generate cytotoxic T cells. The BALB/c splenocytes were either T-cell-depleted or irradiated with 30 Gray. 8 × 10^6 B6:Dendra2 responder cells were incubated for 4-5 days in culture with 4 × 10^6 BALB/c splenocytes in 2 ml RPMI with 10% FCS, 1% PenStrep and 1 mM sodium pyruvate in 24-well plates. Cytotoxic killing was performed in round-bottom 96-well plates with 50,000 Luciferase$^+$ MOPC-315.BMP.FUGLW target cells and 50,000 to 5 × 10^6 MLR effector cells containing cytotoxic T cells. Target cells only were used as a negative control, and 0.1% Triton-X-100 lysed all cells in the positive control. Bioluminescence from the target cells indicated target cell numbers, and percentage of specific lysis was calculated from the formula (experimental signal - background signal) / (maximal signal - background signal) × 100.

3.2.10 Immunofluorescence microscopy of histological sections

Organs were harvested, embedded in O.C.T Tissue-Tek medium and frozen on dry ice. The samples were sectioned at a thickness of 5 µm in a cryostat onto microscopy slides. After thawing, the sections were dried for 5 min and fixed for 7 min in acetone at room temperature, and circumscribed with a hydrophobic PAP pen to restrict added liquids to the sample area. The sections were washed three times for 2 min at room temperature in a cuvette, then blocked with 150 µl 2% normal rat serum in PBS. If necessary, the samples were additionally blocked with avidin in the first blocking step and after another three washing steps with biotin. The samples were washed three times with

PBS and the primary antibodies were added in 150 µl blocking solution, and incubated for 1 h at room temperature in the dark. Three washing steps preceded incubation with the secondary antibodies or streptavidin incubation for 30 min at room temperature in the dark. The sections were washed five times, embedded in Vectashield mounting medium with DAPI, and sealed with a cover slip and entellan. Images were acquired on a confocal microscope using the 20× Objective with a zoom of 0.6 and a tiling function to record large areas with a high resolution.

3.2.11 Light-sheet fluorescence microscopy

Mice were intracardially perfused with 40 ml of ice-cold PBS to remove all red blood cells, and subsequently with 40 ml of ice-cold 4% paraformaldehyde in PBS to fix the tissues. The tissues were excised and fixed for 2 h at 4 °C in 4% paraformaldehyde. After three washing steps in PBS at 4 °C, the tissues were blocked and permeabilized in 2% FBS and 0.01% TritonX-100 in PBS at 4 °C overnight. All following incubations were carried out at 4 °C. The primary antibodies were added in 800 µl of PBS at a dilution of 1:100, except for α-MAdCAM-1 coupled to biotin, which was incubated at a dilution of 1:200. The samples were incubated in flat-bottom glass containers on an orbital shaker for 24 h, and after three 30 min washing steps in PBS, Streptavidin incubation was performed for another 24 h on the shaker. After three more washing steps in PBS, the samples were dehydrated in ascending concentrations of ethanol in water (30%, 50%, 70%, 80%, 90%) for 1.5 h at room temperature, and incubated in 100% ethanol overnight at 4 °C. Final dehydration with n-hexane was performed for 2h at room temperature, which was afterwards gradually replaced with the clearing solution BABB (2 parts benzyl alcohol: 1 part benzyl benzoate). This solution has a refractive index of 1.56, which matches that of soft tissues. Because this abolishes light scattering at water/ tissue interfaces with different refractive indices inside the tissue, it makes them transparent. Clearing solution was added three times for 30 min, and air contact of the samples was strictly avoided to prevent a tissue-darkening reaction. The images were acquired in a home-built light sheet microscope equipped with a 20× objective (Stegner *et al.*, 2017). The principle of light sheet microscopy is illumination of one plane inside the sample and acquisition from a rectangular angle (Figure 3-4). The whole-mount sample is optically sectioned, and the slices are afterwards reconstructed to a three-dimensional image.

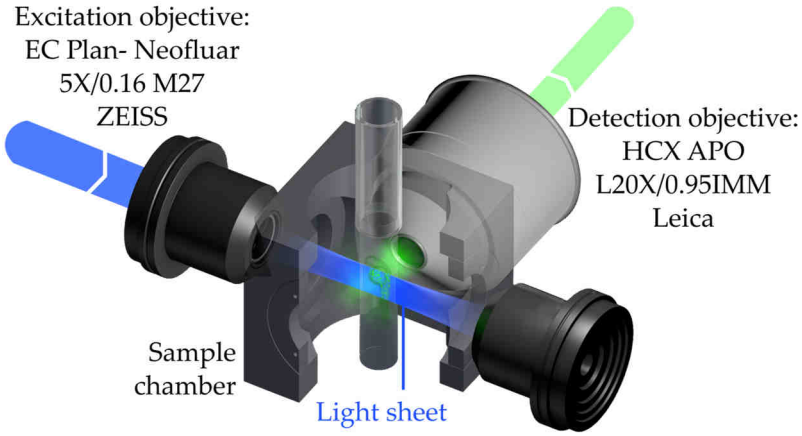

Figure 3-4 Geometrical setup for light sheet microscopy. The excitation light is focused to a thin light sheet using a 5× objective. The cleared and thus transparent sample is positioned inside the sample chamber filled with clearing solution. One optical section of the sample is illuminated by the light sheet. The 20× detection objective is arranged perpendicular to the light sheet. It projects the fluorescence emitted from the sample towards a photomultiplier tube (not displayed). Graph under creative commons license from Zeiss, modified.

3.2.12 Intravital cell migration

Mice were anesthetized and an intestinal loop was exposed as described in the photoconversion operation procedure (3.2.2). Instead of wetted gauze and operation towels, cling foil was used to avoid lint sources in the microscope. The mouse was anesthetized using isoflurane or with Ketamine+ Xylazine injection anesthetic and positioned on a heating pad. The intestinal loop was positioned under a glass cover slip using two custom-made holders. The tissue was kept moist using sterile 0.9% NaCl solution, and pressure on the tissue was minimized to preserve physiological blood flow. Good perfusion was checked immediately after mounting the sample under the objective by inspection through the ocular. Fluorophores were excited at a wavelength of 840 nm- 880 nm. The excitation light intensity was increased as the square of penetration depth between 5 - 30% of full laser power. Images were acquired every 30 seconds in a field of view of 495 × 495 µm with a resolution of 256 × 256 pixels and a distance of 3 µm between two Z-planes.

3.2.13 Image Analysis

Light sheet and 2-PM images were analyzed using the IMARIS software.

3.2.13.1 T cell gradient quantification

For the T cell gradient quantification, the T cells were segmented from the images based on pixel intensity in the stained- and autofluorescence channel, as well as shape characteristics (Figure 3-5). The T cell channel was smoothed (1 µm) and the background was subtracted using a rolling ball diameter of 6 µm. The threshold was manually set depending on the sample, and the spots were selected upon the number of

voxels (e.g. 100-1500), the sphericity (e.g. 0.747), the minimal max-Intensity in the T cell channel (e.g. >350) and the maximal med-intensity in the autofluorescence channel (e.g. <300). The Peyer's patch was detected using the intensity values of the CD45.1 or the CD45.1 and MAdCAM-1 stainings. The channels were smoothed to 20 µm without background subtraction. A distance transformation map was produced where each voxel of a newly created channel was set to the value of its smallest distance to the Peyer's patch surface.

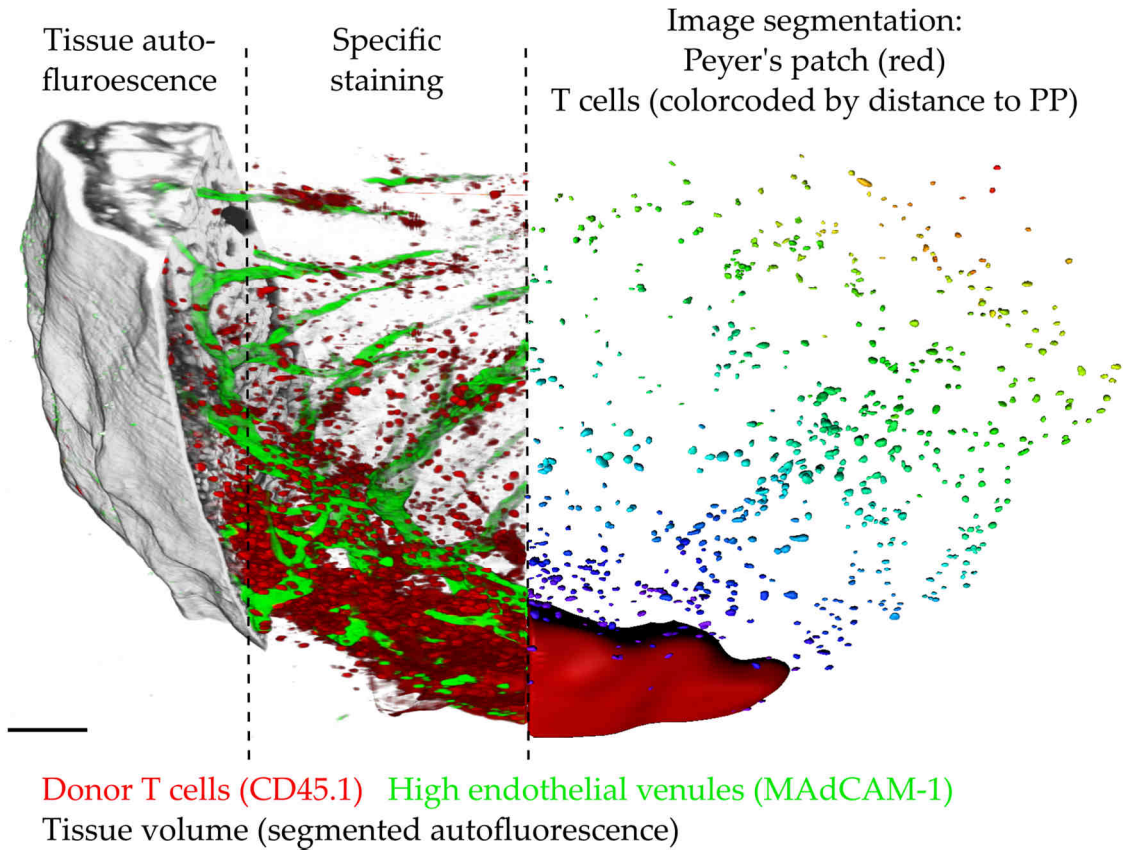

Figure 3-5 Analysis of T cell gradient. Light sheet fluorescence microscopy image of a Peyer's patch and the surrounding intestinal tissue. The autofluorescence signal of the tissue (left) is used to measure the volume of the tissue. The Peyer's patch surface is generated from the T cell signal, sometimes taking into the account the signal from the high endothelial venules (middle). The T cells were segmented and are displayed in color-code respective to their distance from the Peyer's patch surface (right), as measured from a distance transformation map generated from the Peyer's patch.

Subsequently, the median value of this transformation channel was exported for each segmented T cell, yielding the distance of the center of each T cell to the Peyer's patch surface. The volume of the tissue was measured from surfaces generated from the autofluorescence signal and the transformation channel. The tissue volume surface was generated and the transformation channel was masked by this surface, setting all values outside to zero. Then, two new surfaces were generated with the thresholds of 50-200 (area 1, close to the Peyer's patch) and above 200 (area 2, far from the Peyer's patch). The T cells were then quantified in these volumes, and additionally in another complete

Z stack that was acquired with a lateral distance of 2 FOV away from the Peyer's patch (ca. 1000 μm, area 3, periphery).

3.2.13.2 Quantification of converted T cells around Peyer's patches

A vessel on the border of the Peyer's patch was identified and all cells further away in the tissue were counted manually. Cell accumulations that obviously belonged to the Peyer's patch were omitted. All green cells that only had the low background level of red fluorescence were counted as green cells, whereas all cells that had varying higher levels of red fluorescent signal were counted as red cells.

3.2.13.3 T cell migration analysis

The T cells were tracked using the spots function of the program IMARIS. Where photoconverted cells were tracked, a subtraction channel (Ch4) was generated by subtracting the unconverted signal from the converted signal in a ratio, that the value of photoconverted signal in cells negative for photoconverted signal was zero. This lead to reduction of background fluorescence in the photoconverted channel due to bleed through and autofluorescence. The photoconverted cells were then detected in the photoconverted channel with background subtraction using the rolling ball method with a diameter of 12 μm. The spots were then selected based on their signal in the subtraction channel (Ch4). For tracking, the maximal distance between two time points to be accepted for tracking was set to 20-25 μm, with a maximal gap of two and a spot distance to the xyz borders of more than zero. Afterwards, each track was manually corrected and all gaps were filled.

The tracks were then corrected for drift or shaking artefacts using the drift correction function. One to four non-motile spots in the tissue, such as a collagen bifurcation or an autofluorescent spot was tracked over the time of the acquisition and the image with all contained objects was corrected for translational drift. Care was taken to include correction spots from differently moving areas in the field of view in cases where the tissue was moving unevenly.

The tracks were then exported to an Excel file and subsequently analyzed for their migration characteristics by Dr. Zeinab Mokhtari using Matlab.

Results are represented as box plots (Figure 3-6), indicating several descriptive values of the data.

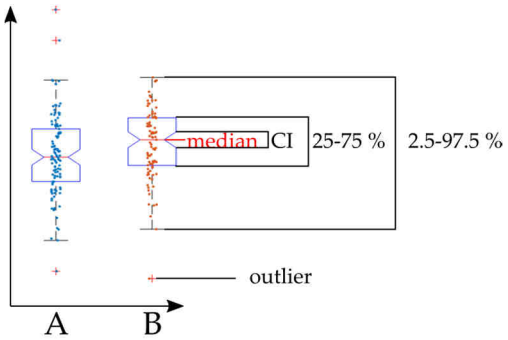

Figure 3-6 Data presentation of migration analysis. Each dot represents one cell track. The median is indicated by a red line, and the confidence interval (CI) is displayed by the height of the indent of the boxplot. The box encloses the values that lie in the central 50% of the data, and the whiskers reach to 2.5% from the edge of the dataset (central 95%). Outliers are indicated by a plus.

3.2.14 RNAseq analysis

The experimental procedures for the RNAseq analysis were carried out by Lukas Scheller and supervised by myself. Extended experimental details are expected to be stated in the medical thesis of Lukas Scheller. Briefly, BALB/c mice were transplanted with 5 ×10^6 bone marrow cells and 1.2 × 10^6 T cells from B6. On day 4, Peyer's patches with surrounding tissue were embedded in tissue-tek, cryosectioned onto RNase-free slides covered with a polyethylene naphtalate membrane and stained with cresyl violet. Areas of mucosa near the Peyer's patch (approximately within 500 µm from the edge) and far away from the Peyer's patch (>1000 µm from the edge) were excised with a laser-capture microdissection microscope and the RNA was isolated using the RNeasy Micro Kit. Further sample processing was performed by the laboratory of the Core Unit Systemmedizin of the University of Würzburg, including the library preparation (SMARTer Stranded Total RNAseq-Pico Input Kit v2), running of the sequencing flow cell (Illumina) and bioinformatic processing of the readouts (using STAR software V2.5.2b) yielding a table with the raw reads and the fold changes and adjusted p-values of selected comparisons. The raw reads from these tables were uploaded to heatmapper.ca (Babicki *et al.*, 2016) to generate heatmaps clustered by complete linkage and the distance measurement 'Kendall's Tau'. This method uses pairwise comparisons of the genes between the samples to be compared, and then orders the genes by their difference. The data was scaled by rows to visualize the change in gene expression over the different samples, yielding the Z-score. Afterwards, some of the major clusters were selected for display and the genes were manually reordered within the cluster according to their function.

4 Results

4.1 The Peyer's patch is not enclosed by a capsule or basement membrane

The aim of this thesis was to investigate whether T cells can migrate directly from the Peyer's patch to the adjacent *lamina propria*. The complex tissue microenvironment greatly influences the migration behavior of cells: the architecture may support this migration by a loose extracellular matrix and adhesion molecules, or hinder it by compact capsular structures such as in the lymph node. Therefore, we stained sections of Peyer's patches with and antibody against laminin, an integral component of basement membranes, to see whether the Peyer's patch is separated from the *lamina propria* by a capsule or a basement membrane. Laminin staining revealed a dense border towards the serosal side of the Peyer's patch, but no enclosing basement membrane towards the *lamina propria* (Figure 4-1). This means that in terms of basement membranes, the edge of the Peyer's patch leaves room for direct exit routes to the surrounding tissue, which is in favor of our hypothesis of direct T cell migration.

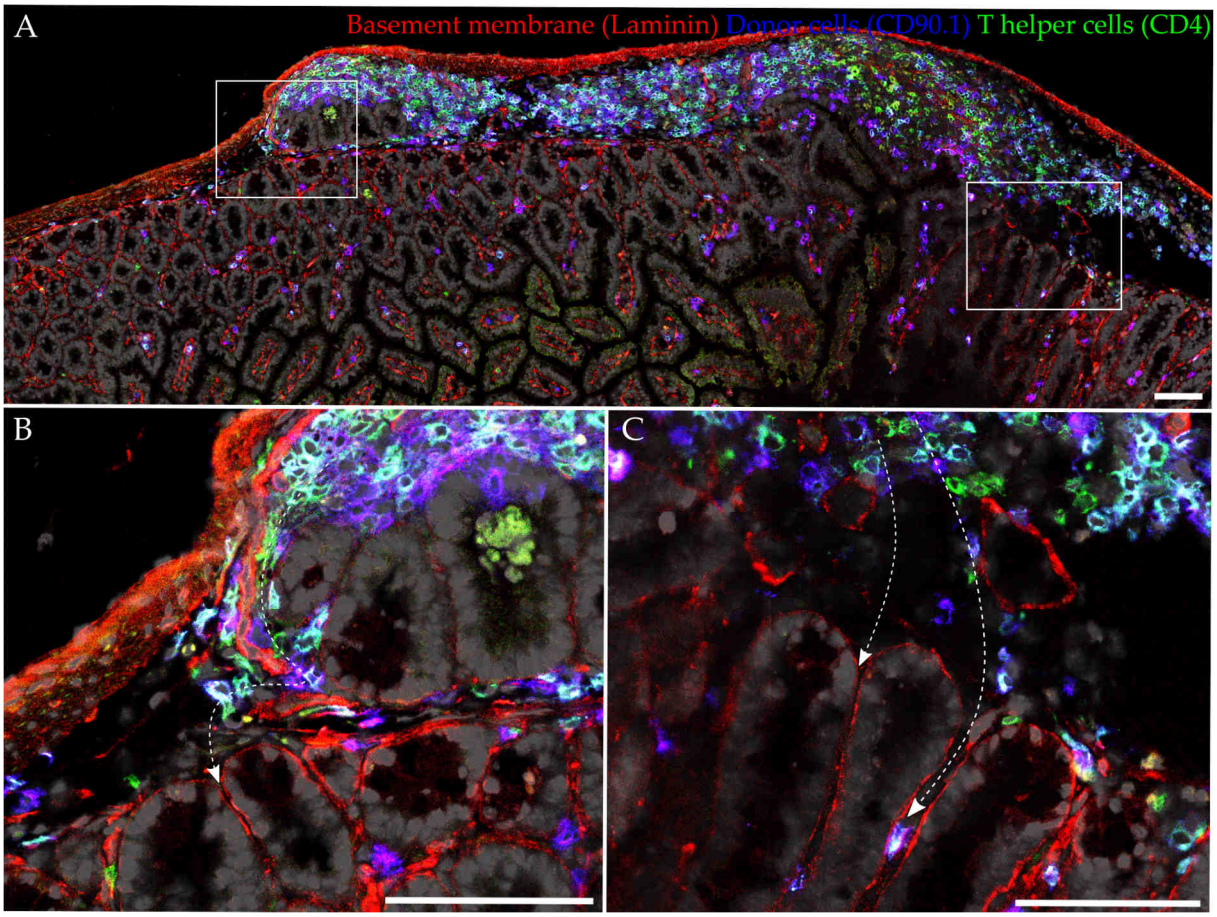

Figure 4-1 Peyer's patches are not enclosed by a capsule or membrane. **A** Confocal immunofluorescence microscopy of a section of a Peyer's patch and the surrounding intestinal tissue 4 days after transplantation. **B** Magnification of the left Peyer's patch edge. The arrow indicates potential migration routes from the Peyer's patch to the adjacent *lamina propria*. **C** Magnification of the Peyer's patch edge near a T cell zone in immediate proximity to the underlying crypts of adjacent villi. Arrows indicate potential migrational access routes. Scale bar 100 μm.

4.2 T cells form a gradient around the Peyer's patch in GvHD

4.2.1 Introduction to transplantation model

To study the egress wave of T cells from the Peyer's patches, we employed a GvHD transplantation model. In this study, BALB/c mice were transplanted with T cells and bone marrow from B6 mice or from mice which had been backcrossed two to seven generations from 129.S to B6. The B6 and the 129.S strains share the same MHC haplotype H2-K^b, but to confirm that the GvHD models are comparable, we performed survival experiments. As expected, the bone marrow controls were successfully reconstituted and survived for the 30 day observation period of the experiment. The irradiation controls died due to anemia resulting from the myeloablative treatment. Both B6 and 129;B6 donor cells caused acute GvHD, which was lethal within 8 days, there was no significant difference between the survival or the weight change of these two groups (Figure 4-2 A). Ex vivo bioluminescence imaging during the initiation phase of GvHD revealed infiltration of luciferase$^+$ donor T cells into the secondary lymphoid organs on day 2.5 after transplantation (Figure 3-1 B). The spleen, mesenteric lymph nodes and Peyer's patches and some colonic cryptopatches showed signal on day 2.5, which increased up to day 3 due to cell proliferation. On day 4, the first T cells entered the small intestine. Intestinal tissue near the Peyer's patch emitted stronger signal than areas further away. This indicated that the ideal time point to study the egress from the Peyer's patches to the adjacent tissue was between day 3 and day 4. On day 4, the first T cells were detected in areas far away from the Peyer's patch, which have likely infiltrated the tissue from circulation. To focus on the cells that did not come from circulation, we therefore focused the analysis of T cells around the Peyer's patches on early time points before day 4 after transplantation.

4.2.2 T cell gradient around Peyer's patch

To investigate the T cell distribution around Peyer's patches in more detail, we employed light sheet fluorescence microscopy (LSFM) to quantify the T cell density around the Peyer's patches during the initiation phase of GvHD. On day 2.5 and day 3 after transplantation, the first T cells were detected close to the Peyer's patches (Figure 4-3 A, A', B). On day 4, the time point when the first activated T cells circulate in the blood, the infiltration near the Peyer's patch but also further away increased more (Figure 4-3 A''). On day 6 after transplantation, alloreactive T cells had massively infiltrated the intestine in all locations (Figure 4-3 A''').

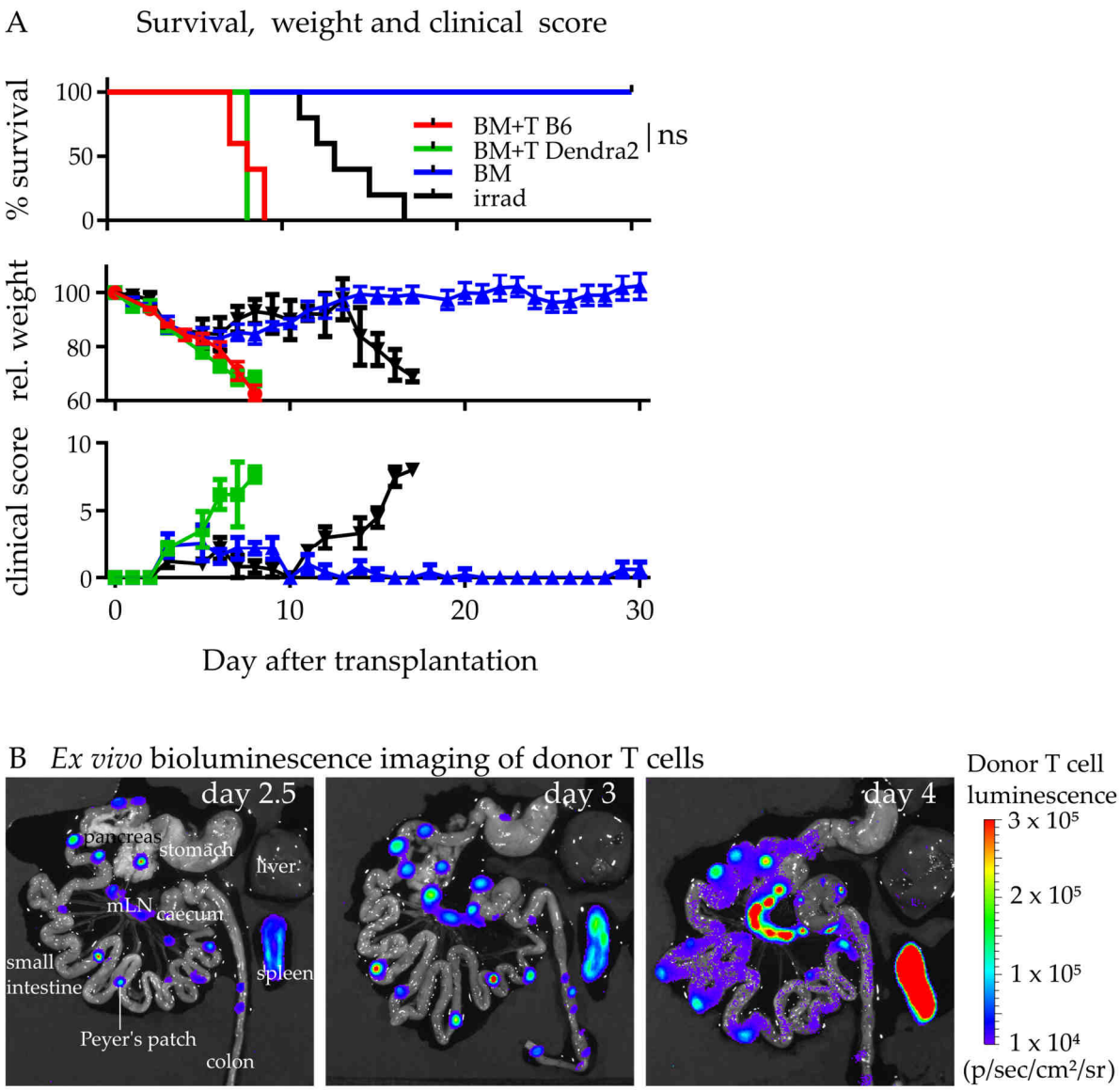

Figure 4-2 GvHD model B6→ BALB/c. **A** Survival, weight changes and clinical score of BALB/c (H2-K^{d}) recipients transplanted with bone marrow and T cells of congenic B6 wt (H2-K^{b}) strain (red) and B6;129S.Dendra2 mixed background (both H2-K^{b}) (green) are comparable. The mice succumbed to GvHD on day 8 after transplantation, irradiation controls survived until day 12 to 15, whereas all bone marrow controls survived. After the irradiation-induced weight loss, only the GvHD groups lost further weight and had an increased clinical score until the humane endpoint was reached. n=5 animals/group, Log-rank (Mantel-Cox) test and paired Student's t-test. Data from B6 donors courtesy of Musga Qureischi. **B** Bioluminescence images of congenic B6 T cells in explanted organs of recipient mice on day 2.5 to day 4 after transplantation. Luciferase-expressing T cells were detected in the secondary lymphoid organs, where they proliferate on day 2.5 and day 3 after transplantation. First T cells infiltrated the small intestine on day 4 after transplantation.

The T cells formed a gradient around the Peyer's patch early during the initiation phase on day 2.5 and 3, which evened out on day 4 to day 6 after transplantation (Figure 4-3 C). This gradient supported the hypothesis that recently activated alloreactive T cells directly migrate from Peyer's patch to the adjacent intestinal *lamina propria*.

This gradient supported the hypothesis that the T cells directly migrate out of the Peyer's patch to the adjacent *lamina propria*.

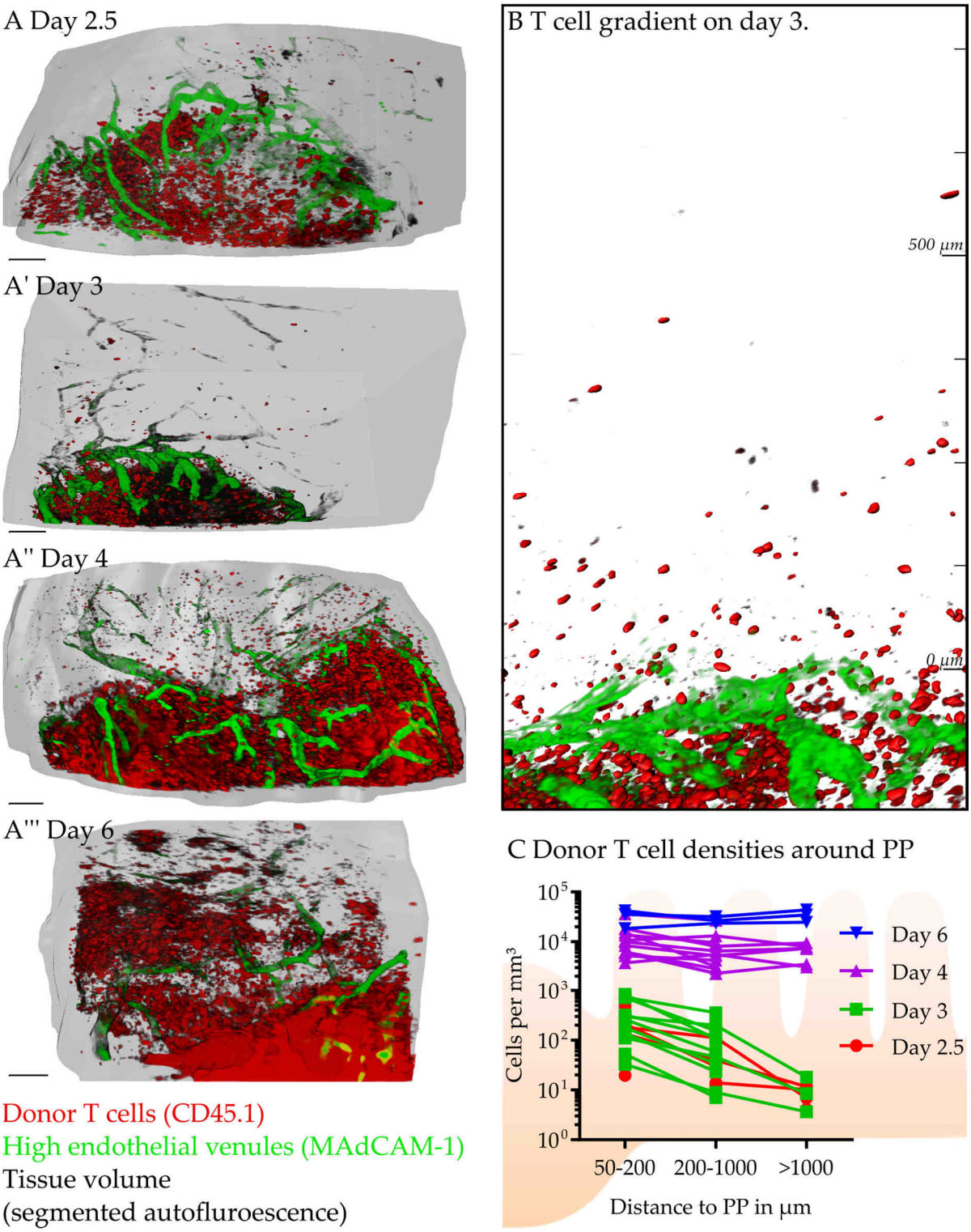

Figure 4-3 Recently activated alloreactive T cells form a gradient around the Peyer's patch early after allogenic hematopoietic cell transplantation. **A** Light sheet fluorescence microscopy of Peyer's patches after aGvHD induction. Donor T cells accumulated around a Peyer's patch as soon as after day 2. Fluorescence data of T cells and high endothelial venules are displayed alongside with the segmented tissue surface. **B** Higher magnification of tissue block shown in A'. Fluorescence data of high endothelial venules and T cells are displayed with segmented T cells. **C** Donor T cell densities around Peyer's patches as quantified from LSFM data. T cells formed a gradient around the Peyer's patch on day 2.5 and 3, some samples still displayed a gradient on day 4. On day 6, the gradient had evened out. One triplet of points connected by a line indicates the densities around one Peyer's patch. Scale bars 100 µm.

4.2.3 T cells are in the extracellular matrix and not inside lymphatic vessels

We hypothesized that the T cells directly migrate from the Peyer's patch to the surrounding *lamina propria*. Because the intestine is densely suffused by a network of blood and lymph vessels (Figure 4-4), there was a chance that the T cells quantified around the Peyer's patches may reside inside those vessels.

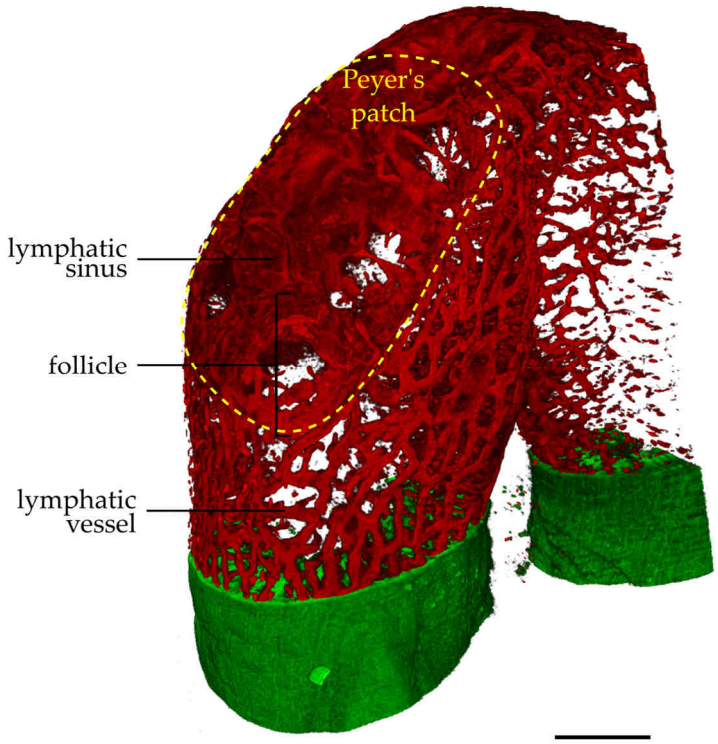

Figure 4-4 Lymph vessels densely suffuse the small intestine. Lyve-1 (red) staining of lymphatics in a Peyer's patch and the surrounding intestinal loop. The tissue volume is displayed from the autofluorescence signal in green at the base of the intestinal loop. Scale bar: 500 μm.

Localization of recently activated donor T cells within lymphatic vessels appeared as a possible explanation of the observed T cells gradient around Peyer's patches as this could represent trafficking T cells within these vessels en route to distant target sites. To exclude that the quantified T cells resided inside those vessels, we co-stained T cells around the Peyer's patch with Lyve-1, a marker for lymphatic vasculature, and MAdCAM-1, a marker for high endothelial venules in the Peyer's patches. The analysis revealed that the T cells were situated outside the vasculature and hence inside the mucosal tissue (Figure 4-5, white arrows). Only single donor T cells outside the Peyer's patch were detected inside lymphatic vessels (yellow arrow). These results confirmed that the T cells forming the gradient around the Peyer's patch were located inside the mucosal tissue.

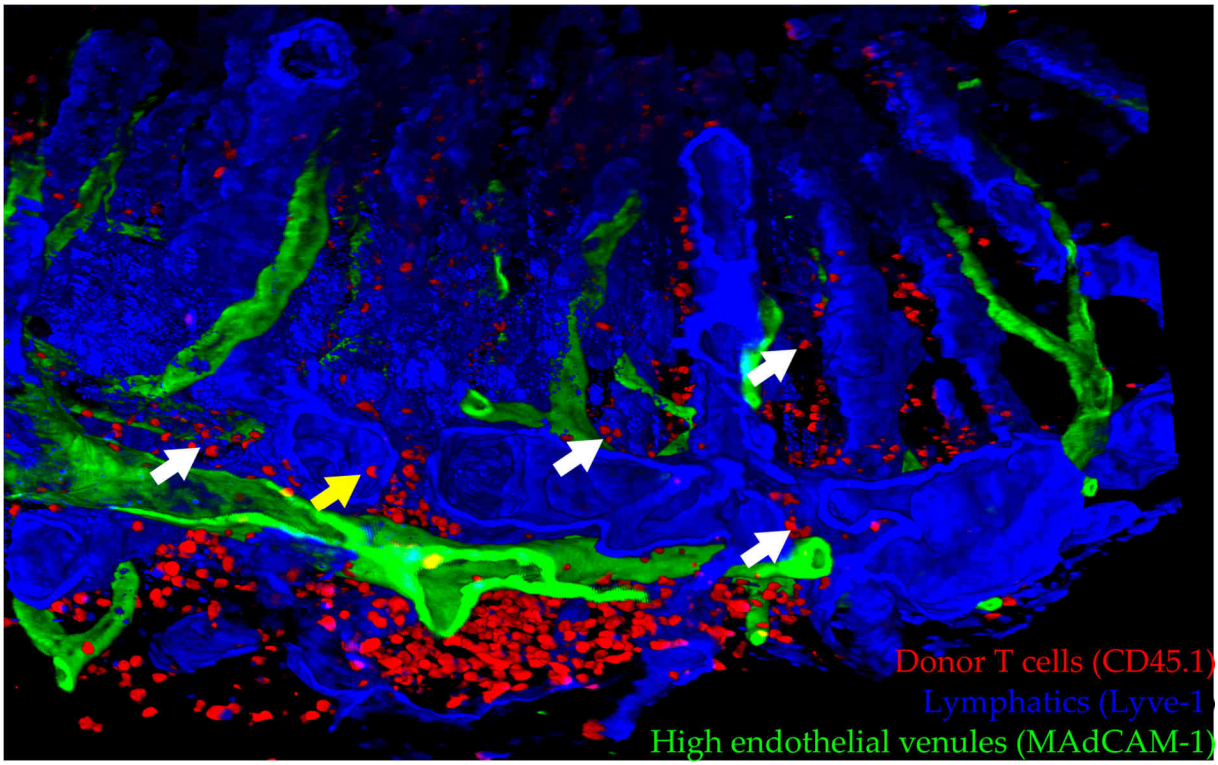

Figure 4-5 T cells around the Peyer's patch are not located inside lymphatic vessels. LSFM image of lymphatics (blue) and high endothelial venules (green) alongside with segmented T cells (red) at the border of a Peyer's patch 4 days after transplantation. White arrows indicate T cells outside of lymphatic vessels, the yellow arrow indicates a cell sticking to the inside of a lymphatic vessel wall.

4.3 T cells egress from the Peyer's patch directly into the adjacent *lamina propria*

The T cell gradient around the Peyer's patch confirmed the underlying hypothesis of direct egress to the surrounding tissue, but other mechanisms may also lead to this phenomenon (see chapter 5 Discussion). To positively prove that the T cells around the Peyer's patch originate directly from that patch, we established a protocol using photoconversion of the Peyer's patch-residing T cells.

4.3.1 Photoconversion technique and setup

The technique was validated in detail and published (Jarick *et al.*, 2018). We transplanted T cells expressing the photoconvertible protein Dendra2, and photoconverted five to seven Peyer's patches at the end of the initiation phase of GvHD (between day 3 and day 4, depending on the subsequent analysis) (Figure 4-6).

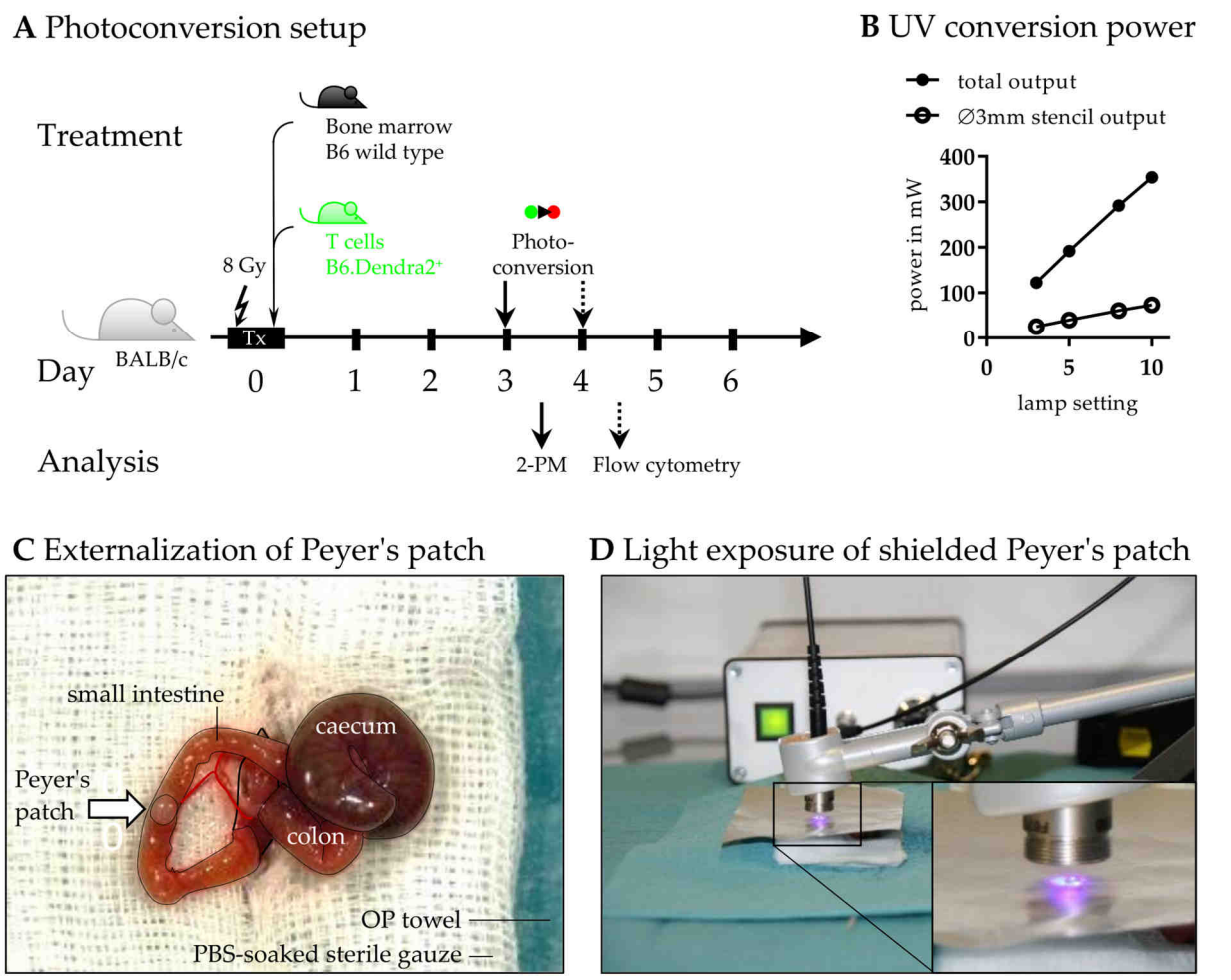

Figure 4-6 Photoconversion timeline and setup. **A** BALB/c recipient mice were transplanted with 5×10^6 bone marrow cells and 1.2×10^6 T cells from B6 to induce GvHD. 12 h before the time point of analysis, the Peyer's patches were photoconverted by exposing them to UV light for 2 min during laparotomy. **B** Total UV power output of the conversion lamp and UV power output through the Peyer's patch stencil. **C** Externalization of Peyer's patch during laparotomy. **D** UV light exposure of Peyer's patch shielded by aluminum stencil.

4.3.2 T cells are efficiently photoconverted

Directly after photoconversion, the photoconverted cells were quantified in different organs to validate the photoconversion efficiency. Using flow cytometry, the donor lymphocyte population was analyzed (Figure 4-7 A). Photoconverted Peyer's patches contained a high purity of photoconverted T cells (on average 89.3%), whereas no photoconverted cells were detected in the blood or intestine (Figure 4-7 B, C). Only single converted cells were found in the mesenteric lymph nodes immediately after photoconversion. Furthermore, the photoconversion can be clearly detected using two-photon microscopy (Figure 4-7 D), despite the spotty appearance of the Dendra2 protein expressed in the mitochondria (inset).

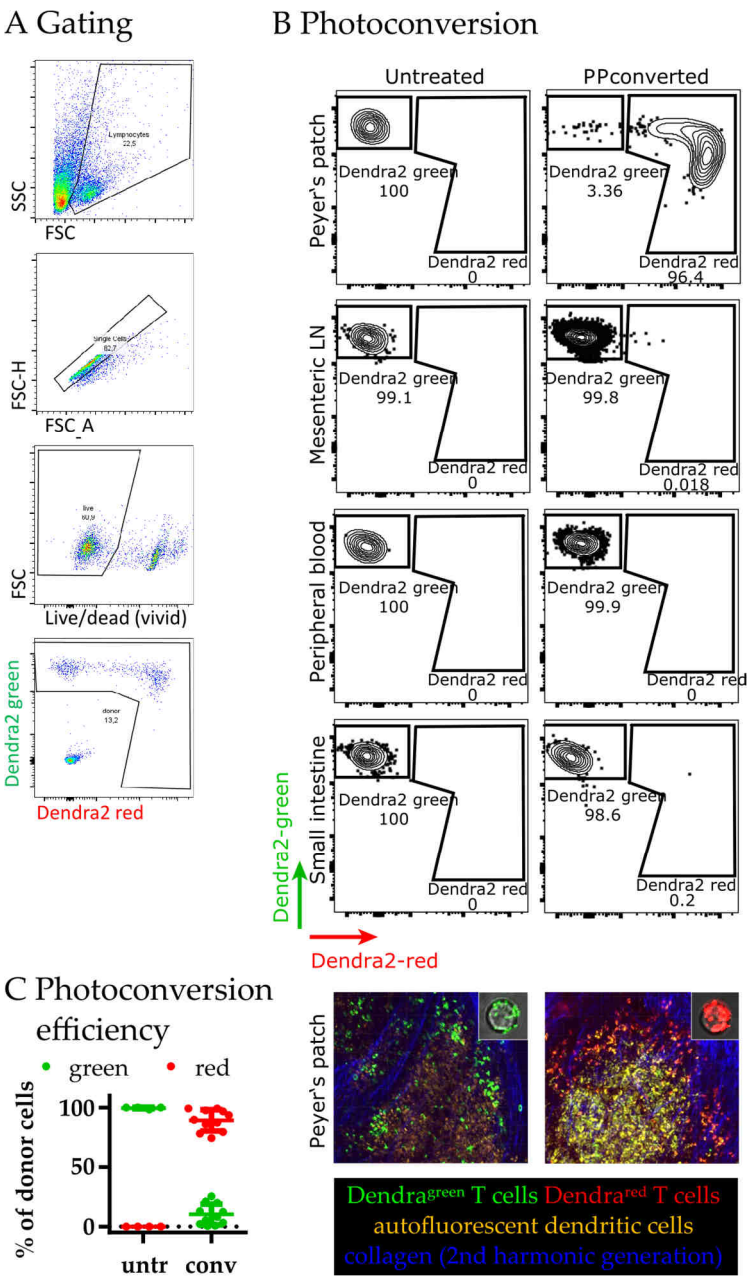

Figure 4-7 T cells are efficiently photoconverted *in vivo*. **A** Gating strategy to identify total donor T cells. **B** Flow cytometric analysis of Peyer's patches, mesenteric lymph nodes, peripheral blood and small intestine before and after photoconversion on day 4 after transplantation (top panels). Two-photon microscopy images of Dendra2$^+$ donor T cells in a Peyer's patch with and without photoconversion (bottom). Inset: confocal micrograph of an individually photoconverted Dendra2$^+$ cell *in vitro* before and after photoconversion. Dendra2 expression is localized to the mitochondria. **C** Photoconversion efficiency of the Peyer's patches reaches an average of 89.3%, one dot represents 5-7 pooled Peyer's patch of one mouse, untreated n=4 (untr), converted n=11 (conv).

4.3.3 T cells proliferate after photoconversion

Using ultraviolet light for the photoconversion may potentially be harmful to cells. Due to its high energy content, it may damage the DNA via fusion of adjacent pyrimidine base pairs, or indirectly damage cellular molecules via oxidative stress. This hinders replication and cell division, and may eventually lead to apoptosis of the damaged cell (Rastogi *et al.*, 2010).

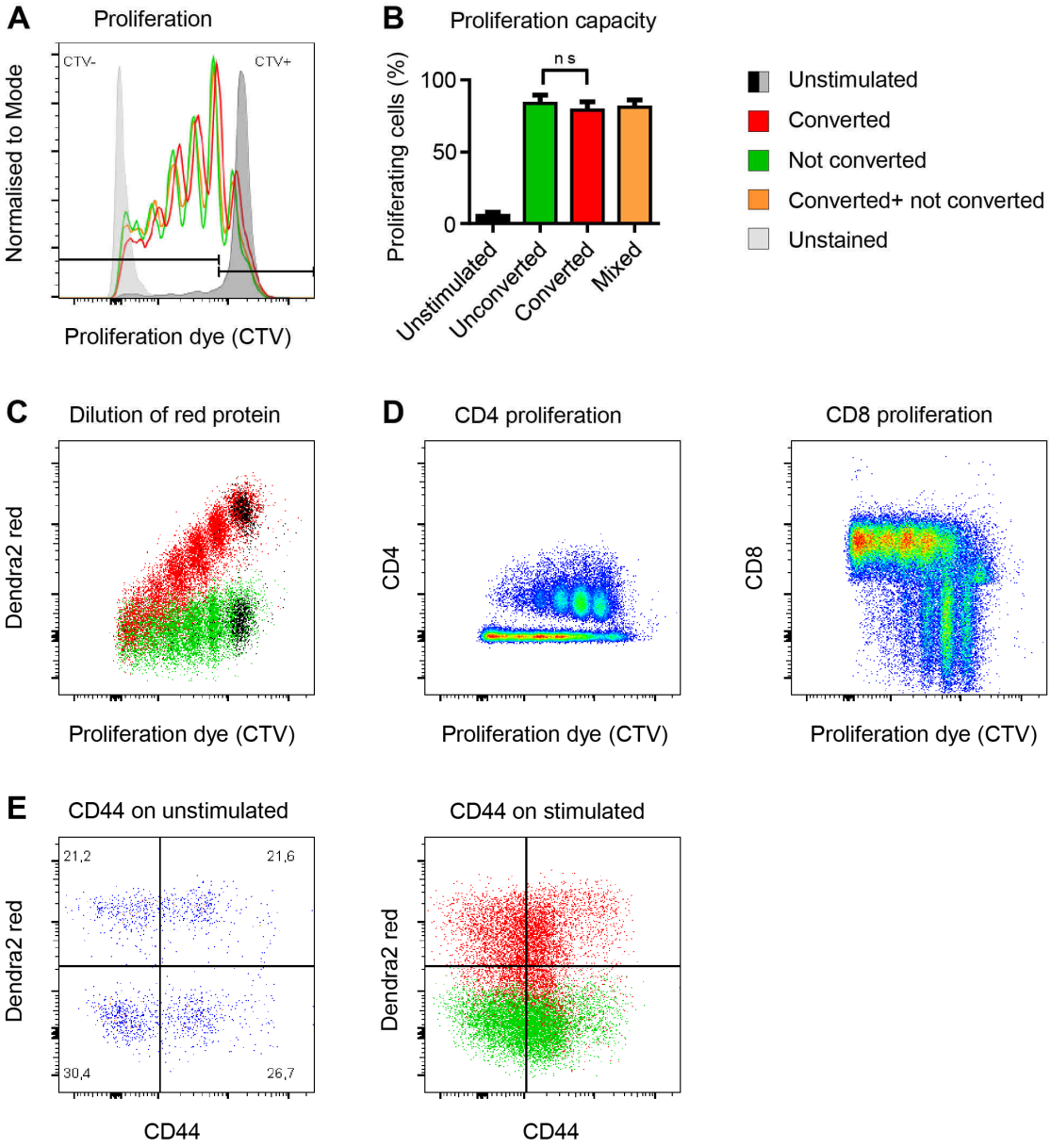

Figure 4-8 T cells proliferate after photoconversion. **A, B** Proliferation of T cells stimulated in culture with and without prior photoconversion. Converted cells, unconverted cells and cells which were co-incubated in one well proliferated to the same extent. Unstimulated cells were kept in culture for the respective time, and unstained cells were stimulated but not stained with the cell division tracer. Unpaired non-parametric Mann-Whitney test. n=3 mice, displayed here are 3 technical replicates from one mouse. **C** The photoconverted red form of the protein was diluted by half with every cell division cycle. Photoconverted unstimulated cells remained positive during the four days in culture (black). **D** $CD8^+$ cells proliferated more vigorously in this setting and had divided 2-6 times, whereas the majority of the $CD4^+$ T cells had divided 1-4 times. **E** CD44 expression as a marker of T cell activation was not altered after photoconversion. Photoconverted and unconverted cells expressed the same level of CD44 in the stimulated or unstimulated condition.

The viability and expansion of the donor T cells is crucial for the development of GvHD. Since it is highly undesirable for the photoconversion to diminish T cell viability or expansion in these experiments, we tested whether T cell proliferation was altered after photoconversion. T cells isolated from the spleen of $Dendra2^+$ mice were photoconverted

and stimulated with IL-2 and an antibody against CD3 *in vitro*. Unconverted, converted, and mixed cells proliferated to the same extent (Figure 4-8 A, B). This indicates that the dose of ultraviolet light needed to induce strong photoconversion was not sufficient to damage the cells such that they would induce senescence.

The red, converted form of Dendra2 remained detectable in high amounts in photoconverted cells that were kept in culture for 4 days without stimulation (Figure 4-8 C). With every cell division, the amount of red protein was diluted by half, whereas the green protein was continuously synthesized anew. This lead to a shift from red over orange and yellow to green fluorescence of the cells. In this *in vitro* setting, both $CD4^+$ and $CD8^+$ T cells proliferated. $CD8^+$ T cells completed more division cycles (2-6 divisions) than $CD4^+$ T cells (1-4 divisions), which had divided less vigorously within the 4 days of incubation (Figure 4-8 D). Furthermore, photoconversion did not alter the activation state of the T cells as measured by expression of the activation marker CD44, which is upregulated on antigen-experienced cells (Figure 4-8 E). In summary, photoconversion did not impact cell proliferation or activation and therefore was considered suitable for the study of T cell homing and migration behavior in the inflammatory setting of GvHD.

4.3.4 T cells traffic, migrate and kill after photoconversion

The rationale to establish the photoconversion technique was to visualize direct T cell migration from the Peyer's patch to the surrounding tissue. To be able to prove this convincingly, it is important to verify that the photoconverted cells were still able to traffic properly via the lymphatic and blood circulation, and that for instance a block in lymphatic trafficking would not skew the migration profile of the T cells leaving the Peyer's patch. Therefore, we tested whether the photoconverted cells were still able to traffic from the Peyer's patches through the mesenteric lymph nodes and the peripheral blood to the intestine. Flow cytometric analysis of these organs at different time points after photoconversion revealed trafficking converted T cells at all tested sites. The majority of the T cells in the Peyer's patches remained positive for the red fluorescent protein within the 24 h observed (Figure 4-9 A). The first converted cells appeared within 4 h in the mesenteric lymph nodes and the blood (Figure 4-9 B, C), and accumulated over time as more and more cells left the photoconverted Peyer's patches. The photoconverted cells also accumulated in the intestinal tissue distant from the Peyer's patches within 24 h (Figure 4-9 D), indicating that the cells were able to enter the target organ.

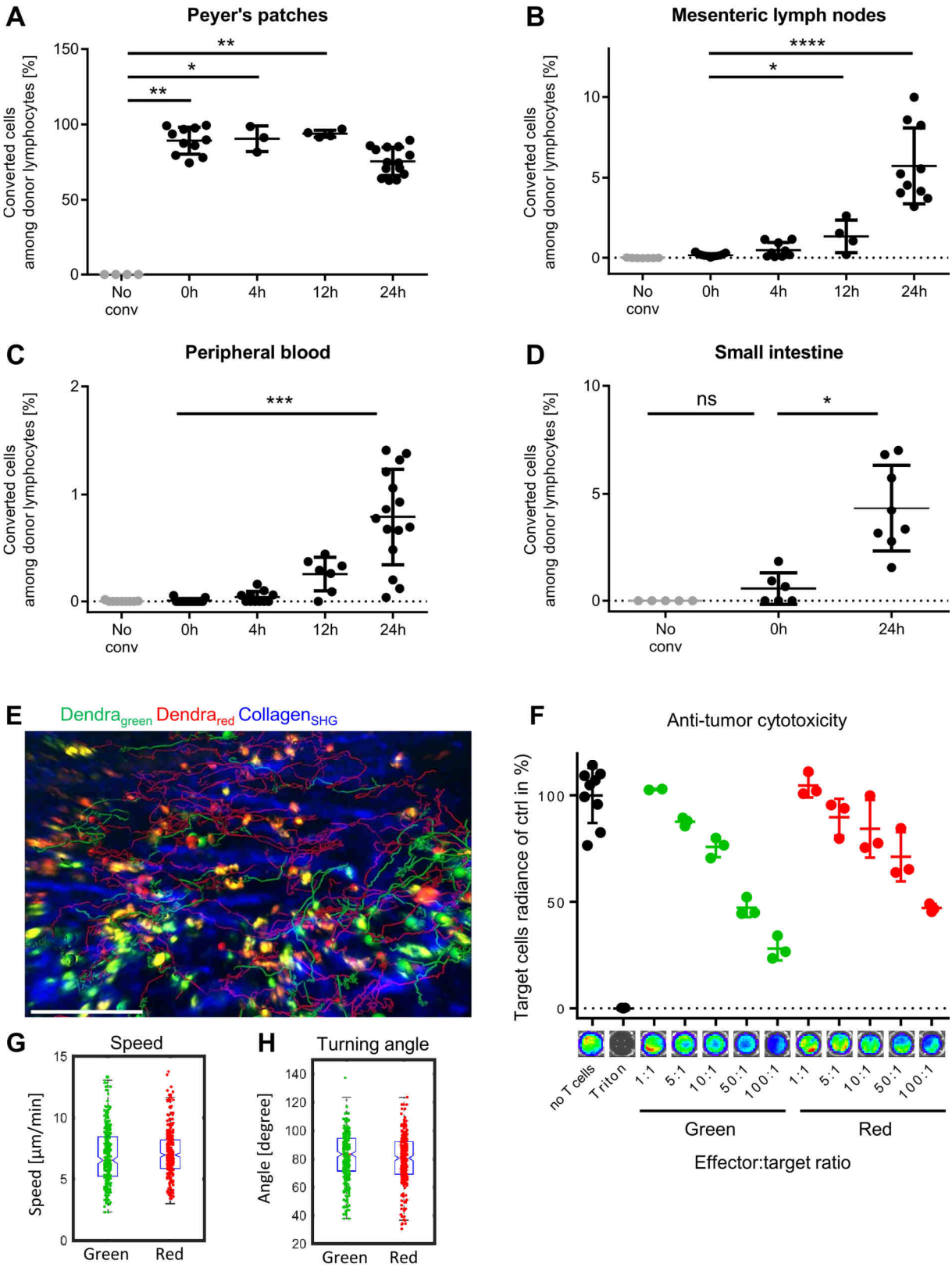

Figure 4-9 Photoconversion does not impair key functions of T cells, such a T cells trafficking, migration and killing capacity. **A-D** Photoconverted T cells trafficked from the Peyer's patch to the mesenteric lymph nodes and via the peripheral blood to the small intestine. One dot represents one mouse, unpaired non-parametric Kruskal-Wallis test. **E** Photoconverted and unconverted T cells migrated in the small intestine. **G, H** Speed and Turning angle as simple measurements for cell motility were comparable in green and red cells. One dot represents one cell track. **F** Photoconverted and unconverted T cells performed cytotoxic killing of MOPC tumor cells in culture. One dot represents one well, n=2 mice.

The converted cells represented approximately 6% of donor cells in the mesenteric lymph nodes, 1% in the peripheral blood and 5% in the small intestine 24 h after photoconversion. In the intestine, they migrated with comparable migration characteristics, as measured by the speed and turning angle as basic measures of their ability of migration and directionality (Figure 4-9 E, G, H). Lastly, the cytotoxic potential of the T cells after photoconversion was assessed. Splenic B6.Dendra2$^+$ T cells were stimulated with allogenic BALB/c stimulator splenocytes in culture, which selects for and enriches alloreactive cytotoxic B6.Dendra2$^+$ T lymphocytes. After photoconversion, the cytotoxic T lymphocytes (effector cells) were incubated with the BALB/c tumor cell line MOPC expressing luciferase (target cells). The killing capacity of photoconverted and not converted T cells was measured by the decrease in luciferase signal with increasing effector- to target cell ratios. The mean signal of target cells without effector cells served as a negative control and was set to 100%, and Triton-X-100-lysed cells were used as a positive control. Photoconverted cells showed a trend towards reduced lysis (47.9% vs. 28.1% at a 1:100 E:T ratio) , which was however not significant (Figure 4-9 F, non-parametric Kruskal-Wallis test). This means that the T cells were still able to lyse target tumor cells after photoconversion. In summary, photoconverted T cells were still able to traffic via the lymphatics and blood, proliferated and performed effector functions. Therefore, photoconversion did not block T cell egress from the Peyer's patches to the lymph. We concluded that the direct egress of T cells from the Peyer's patch to the adjacent *lamina propria* can be observed using this technique without hindering the cells' lymphatic trafficking route.

4.3.5 T cells egress directly into the adjacent *lamina propria*

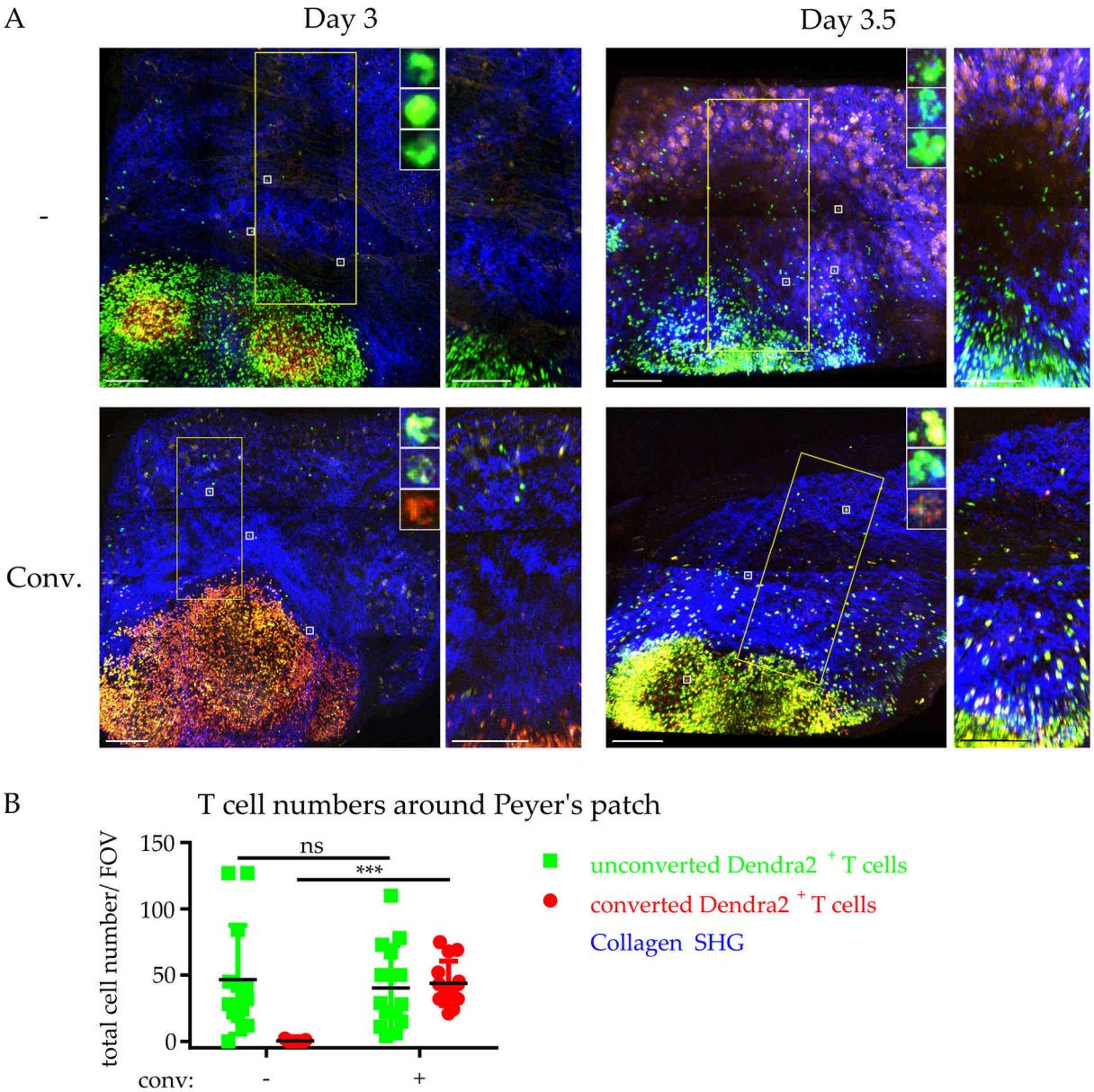

Figure 4-10 T cells egress directly into the adjacent *lamina propria*. **A** Stitched two-photon images of explanted Peyer's patches directly after photoconversion (day 3 after transplantation) and 12 h later (day 3.5). Unconverted Peyer's patches were surrounded by only unconverted cells, whereas converted Peyer's patches were surrounded by both unconverted and converted cells. Images of day 3 converted and both day 3.5 images represent Fingolimod-treated animals. Scale bar 200 µm. **B** Quantification of T cells around the Peyer's patches. Photoconverted T cells were found only around previously converted Peyer's patches. The size of one field of view (FOV) was 500 x 500 µm (x/y). Combined total T cell numbers (converted+ unconverted) did not change significantly after photoconversion (not displayed). One dot represents one FOV, n=4 mice per group. *** $p < 0.001$, unpaired non-parametric Kruskal-Wallis test.

Since our established photoconversion technique was suitable to study the migration and trafficking of alloreactive T cells in GvHD, we employed this technique to test the hypothesis of direct egress of alloreactive T cells from Peyer's patches into the *lamina propria*. Photoconversion on day 3 of transplanted Dendra2$^+$ T cells was restricted to the

Peyer's patch (Figure 4-10 A). The unconverted Peyer's patches of the respective mouse served as a negative control and harbored only unconverted green cells, whereas the converted Peyer's patch harbored only converted red cells. Except for single cells very close to the Peyer's patch, the scarce cells in the surrounding mucosa remained negative for the Dendra2-red signal. 12 h later, a high number of converted cells resided around converted Peyer's patches but not around Peyer's patches that were not converted (Figure 4-10 B). This means that the converted cells were enriched in the *lamina propria* only around converted Peyer's patches. This result rules out the possibility that the T cells only accumulated around the Peyer's patches due to enhanced vascular trafficking to this region. As mentioned in more detail in the discussion, enhanced vascular T cell trafficking may occur predominantly near the Peyer's patches because of early upregulation of trafficking molecules such as MAdCAM-1 in the intestinal vasculature around Peyer's patches. If the Dendra2-red cells were found equivalently around converted and non-converted Peyer's patches, this would mean that the cells must have reached this site via vascular trafficking. The fact that Dendra2-red cells are not found around non-converted Peyer's patches speaks for the hypothesis that the T cells migrate to the area around the respective Peyer's patch and do not get there via vascular trafficking.

4.4 T cell migrate non-directionally to the adjacent *lamina propria*

After confirming the local emigration from the Peyer's patch to the *lamina propria*, we wanted to explore the migration mechanism of T cell egress. Potentially, the T cells may be attracted by a chemotactic gradient leading them out of the Peyer's patch, which is possibly detectable by directional migration from the Peyer's patch to the *lamina propria*. Alternatively, there might be a loss of sequestration of the T cells inside the Peyer's patch, which is usually accomplished by CCL19/21 expression by fibroblastic reticular cells in the T cell zones of the Peyer's patch. We hypothesized that loss of this sequestration would lead to a more diffusive, random migration pattern of the egressing T cells. To differentiate between these two options, the T cell migration was analyzed adjacent to Peyer's patches on day 3 and day 4 after transplantation (Figure 4-11 A-A'').

The T cell migration speed was lower on day 4 than on day 3, and slightly elevated in the *lamina propria* when compared to the Peyer's patch (Figure 4-11 C). On day 3 after transplantation, the cells migrated with a mean speed of 9.7 μm/min inside the Peyer's patch and 11.2 μm/min in the *lamina propria*. On day 4, the cells migrated slower at 6.5 μm/min and 7.2 μm/min in the Peyer's patch and the *lamina propria*, respectively.

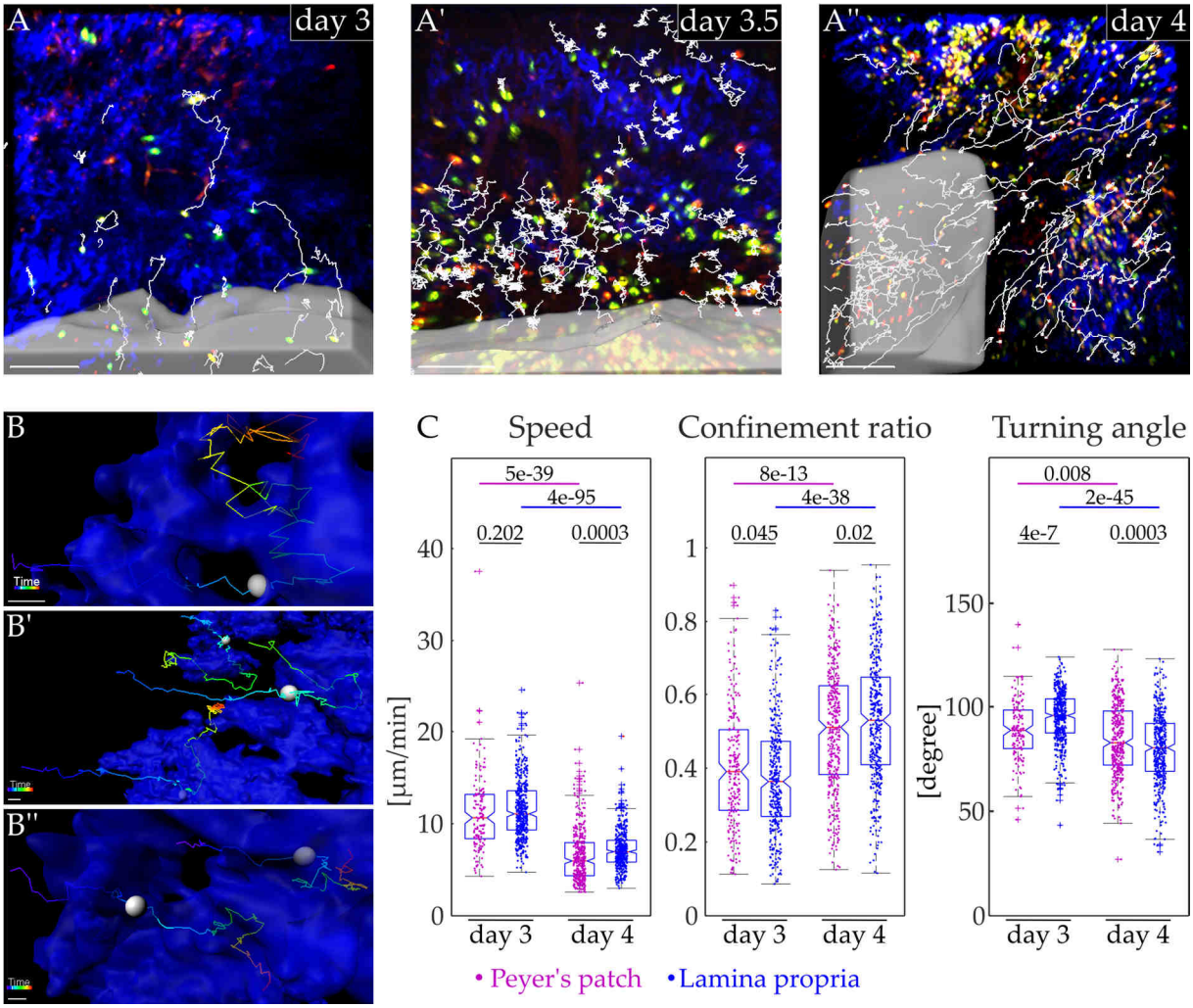

Figure 4-11 Egressing T cells migrate non- directionally in the *lamina propria*. Intravital two-photon microscopy of allogenic Dendra2+ T cells in the *lamina propria* adjacent to a Peyer's patch. **A** Migration tracks within a 30-minute time frame are displayed in white. The Peyer's patch is outlined by a semi-transparent white surface. Scale bar 100 µm. **B** Tracks of T cells egressing from the Peyer's patch on day 3 or day 3.5, color-coded by the time. The collagen network segmented from the second harmonic generation signal is displayed in blue. The T cells often approached the edge of the Peyer's patch highly directedly and then switched to a less straight migration mode. Scale bar 10 µm. **C** Analysis of the cell migration tracks inside and adjacent to Peyer's patches. Cells migrated faster on day 3 than on day 4. The confinement ratio was higher on day 3 *vs.* day 4, and the turning angle was inverse-proportionally altered. Data for day 3 and day 3.5 were pooled. One dot represents one cell track n=5/ 13/ 2/ 2 mice (left to right), outliers are indicated by a plus. P-values are generated from Student's t-test.

The degree of straightness as measured from the confinement ratio was higher on day 4 than on day 3. Three days after transplantation, the confinement ratio was slightly lower in the *lamina propria* (0.44, mean) than in the Peyer's patch (0.47), whereas on day 4, it was slightly higher in the *lamina propria* (0.50 *vs.* 0.53). The degree of straightness as measured by the confinement ratio was confirmed by inversely proportional values of turning angles. The turning angles were generally lower on day 4 than on day 3. On day 3, the cells turned less sharply in the *lamina propria*, as indicated by higher values of turning angles (87.6° *vs.* 91.5°). Lower turning angles were measured in the *lamina propria* on day 4 when compared to the cells inside the Peyer's patch (80.2° *vs.* 84.5°).

Among the cells tracked on the border of the Peyer's patch, a few tracks led from the Peyer's patch directly to the surrounding mucosa (Figure 4-11 B). Although this behavior has not yet been quantified, it appears that the cells approached the border of the Peyer's patch in a highly directed fashion. Upon contact with the collagen, which was visualized from the second harmonic generation signal, the T cells followed this structure and performed less straight migration. These cells directly migrating from the Peyer's patch to the surrounding tissue were most prominent on day 3 and 3.5, despite a much higher cell number on day 4 in the *lamina propria*.

In summary, the migration patterns between T cells around Peyer's patches differ more between day 4 and day 3 than between the Peyer's patch and the *lamina propria*. There was no overall directionality within the T cell population after the time point of egress. This hints to a mechanism not involving attraction of the T cells into the *lamina propria*, but rather to a loss of sequestration within the Peyer's patches. Nevertheless, we show that the donor T cells left the Peyer's patch to the adjacent *lamina propria* around day 3 after transplantation.

4.5 T cell egress to the *lamina propria* does not depend on S1PR1

Sphingosine-1-phosphate mediates the egress of lymphocytes including T cells from the secondary lymphoid organs including Peyer's patches. Although this attraction is not exerted in form of gradients leading the cells towards the lymphatic exit, it plays an important role for transmigration into the lymphatics. The current literature assumes that the T cells approach the lymphatic vessels either with random motion or due to desensitization of CCR7 (Cyster and Schwab, 2012; Grigorova *et al.*, 2009). This loss of gradient may potentially be sufficient to allow egress of the T cells towards the lymphatics. S1PR1-mediated egress plays a role in the lymph nodes, Peyer's patches, the spleen and the thymus.

To address whether this widespread mechanism is also involved in the sideways migration of the T cells to the adjacent *lamina propria*, we blocked the S1PR1 by treatment with fingolimod, which mimics the receptor's natural ligand Sphingosine-1-phosphate (S1P) (Figure 4-12 A). Subsequent down modulation of the receptor leads to inhibition of lymphatic egress of the lymphocytes. CD90.1+ donor T cells were quantified in the blood, lymph nodes and spleen of fingolimod-treated transplant recipient mice to verify that the donor T cells were trapped in the lymph nodes and disappeared from circulation (Figure 4-12 B, C). Fingolimod-untreated mice transplanted with bone marrow cells only did not have circulating donor T cells.

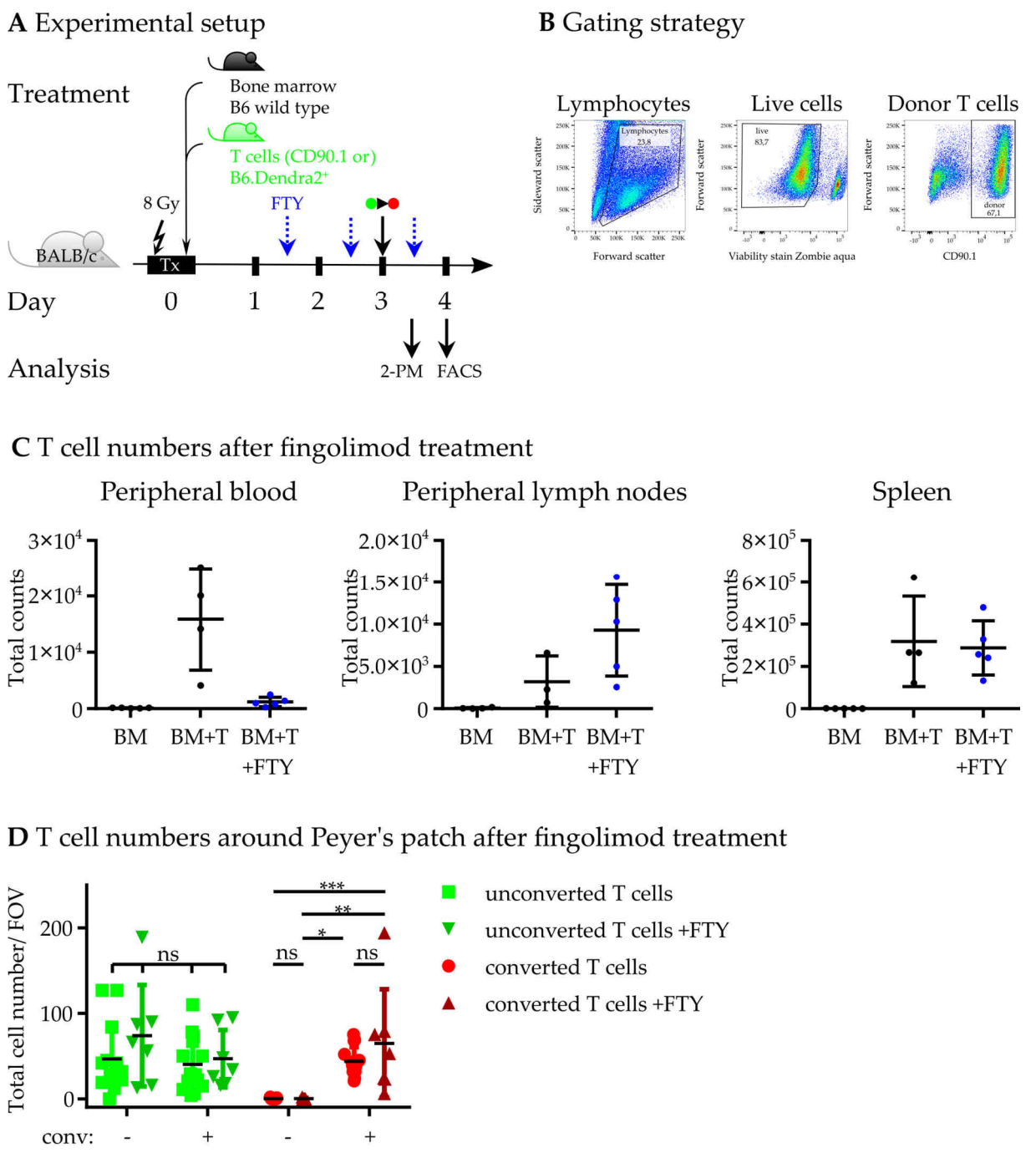

Figure 4-12 Direct T cell egress does not depend on S1P gradient sensing. **A** Experimental time line of transplantation and fingolimod (FTY) treatment. Mice were transplanted with T cells from CD90.1+ or Dendra2+ donors and were photoconverted three days later. One group of mice received fingolimod treatment on days 1.5, 2.5 and 3.5 after transplantation. The results were obtained on day 3.5 for two-photon imaging or on day 4 for flow cytometry. **B** Gating strategy to identify CD90.1+ donor T cells. **C** T cell numbers in the peripheral blood, peripheral lymph nodes excluding mesenteric lymph nodes and the spleen four days after transplantation with and without fingolimod treatment. Bone marrow controls were used as a negative control. Fingolimod treatment abolished circulating lymphocytes because they were trapped inside the lymph nodes, where the numbers increased after treatment. n=10 from two separate experiments, displayed here are the results from experiment 2. **D** T cell numbers of photoconverted around Peyer's patches were not affected by fingolimod treatment. Data from mice not treated with fingolimod are the same as from Figure 4-10. Fingolimod treated mice were observed in multiple experiments but quantified from n= 9 or 10 FOV of 2 or 3 Peyer's patch of 2 mice from 1 experiment, Kruskal-Wallis Test.

In contrast, mice to which T cells were transplanted to induce GvHD had varying numbers of T cells in circulation. This was abrogated by fingolimod treatment, which trapped the T cells inside the lymph nodes. There were more T cells in lymph nodes of fingolimod treated mice than in the GvHD control (on average 3192 *vs.* 9275 cells measured in flow cytometry), and the T cells disappeared from circulation as expected (on average 15876 *vs.* 1191 cells). The T cell numbers in the spleen were not altered upon fingolimod treatment. Hence, the fingolimod treatment effectively blocked the lymphatic egress of the T cells from the secondary lymphoid organs in this model.

On the basis of this finding, we performed photoconversion experiments as in 4.3.5 and analyzed whether T cells were still able to leave the Peyer's patch into the *lamina propria* despite the block of lymphatic egress. There was a comparable number of unconverted T cells around Peyer's patches that were converted or not converted, both in mice with and without fingolimod treatment (Figure 4-12 D). There were no converted T cells around unconverted Peyer's patches, but untreated and fingolimod-treated mice both had converted T cells around the Peyer's patches. This indicates that despite fingolimod treatment, the T cells are still able to leave the Peyer's patch to the adjacent *lamina propria* and that the S1PR1 does not play a significant role in this process.

4.6 RNAseq reveals candidates potentially fostering the egress to the *lamina propria*

To identify molecules that may be involved in attraction or random migration of the T cells to the *lamina propria*, we screened for molecules upregulated in the *lamina propria* near the Peyer's patch. We employed laser-capture microdissection of cryosections to excise specific regions near the Peyer's patch (<500 μm) and further away (>1500 μm) in the *lamina propria* of GvHD-bearing mice. Mice transplanted with bone marrow and untreated mice were used as controls. The samples were subsequently analyzed with RNAseq and mass spectrometry. This strategy allowed us to identify molecules upregulated in the tissue and on the T cells according to their location respective to the Peyer's patch.

The mass spectrometry results were largely inconclusive and yielded no significantly changed proteins, likely because the complexity of the sample was too high for the small amount of protein gathered with this sampling method. Therefore, an overview of the results of the RNAseq only is presented here.

4.6.1 Genes upregulated in GvHD

First, bioinformatic analysis of transcripts in GvHD *vs.* the BM control was performed to screen for migration-promoting factors upregulated in the tissue during GvHD in general. The rationale was that migration promoting factors do not essentially have to be enriched near the Peyer's patch, as long as there is an overall difference between the Peyer's patch and the *lamina propria*. When comparing the overall mucosa of GvHD bearing mice with bone marrow controls, 7261 genes were differentially expressed. Significantly upregulated genes were clustered in a heatmap, of which selected genes of three clusters are displayed in Table 4-1.

The top five upregulated genes in GvHD were Pla2g4c (6.71), Socs1 (5.18), Retnlb (5.18), Ifng (5.16) and Gsdmcl-ps (5.02). They have very different roles in cell physiology and immunity and will be evaluated upon in the discussion.

As expected, Th1 inflammatory signature genes were upregulated (Tnf, Ifng, Stat1, Stat4), which validated that this method was able to represent the overall immunological status known for GvHD. Co-stimulatory molecules (Gitr, Ox40, 4-1BB) were upregulated as well as activation markers of antigen-presenting cells (Cd40, Baff, Tlr-2). Many of the upregulated genes play a role in cell migration. Among those are chemokines (Cxcl2, 5, 9-11, CCL 3, 4, 7, 8, 11, 17, 22 and Ccrl2), chemokine receptors (Ccr7 and 9, Cxcr6), integrins (Itgβ7, Ceacam12) and the P-selectin ligand Selplg. Also, transcripts involved in the cytoskeleton or the remodeling thereof (Tubα3, Tubβ3, Coro1α, Rac2) were increased. Furthermore, gene products involved in mucosal integrity were upregulated (TWEAK, Reg3β and Reg3γ). Counter-regulatory immunological mechanisms were also detected, such as Il10, Ido1+2, Socs1+3. Lastly, several genes from the Ly6 family were upregulated, which are not well studied yet and of which the function of many proteins remain unknown. However, murine Ly6B, Ly6C and Ly6G play a role in neutrophil migration, although these proteins have no homologs in humans.

As can be seen from the heat map in Table 4-1, most of these genes displayed were upregulated in the GvHD condition only, both near the Peyer's patch and further away. These genes were expressed at basal levels both in the untreated healthy tissue and in the BM controls. The group of genes displayed second in the table was upregulated in GvHD as compared to the BM controls, but these genes were also initially expressed at a high level in healthy untreated tissue. This cluster comprised mostly MHC molecules and those involved in antigen processing for presentation (Tap1, Tap2, Cd74), and some Type I inflammatory molecules (Igtp, Irf1, Irgm2).

Table 4-1 Heatmap of RNAseq data significantly altered between GvHD and bone marrow control.

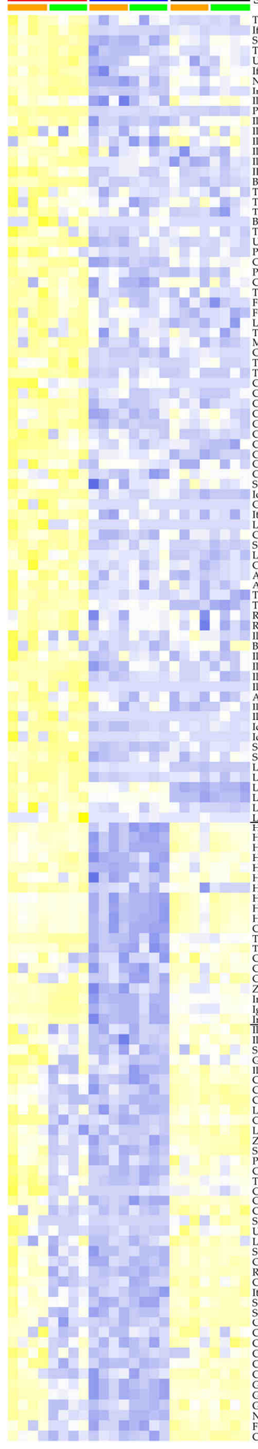

Gene symbol	Gene name	Gene function	RNAseq p-value	RNAseq log2FC	Mass-spec log2FC	Category	
Tnf	Tumor-necrosis-factor	proinflammatory molecule secreted by macrophages, induces Il12 and Th1 polarization	6.E-08	1.86		Type 1 inflammation (GvHD signature)	Upregulated in GvHD
Ifng	Interferon gamma	key GvHD inflammatory mediator, activates macrophages, Th1 polarization	6.E-23	5.16			
Stat1	Signal Transducer And Activator Of Transcription 1	IFN response	9.E-11	1.69	0.57		
Tgtp2	T-cell-specific guanine nucleotide triphosphate-binding protein 2	IFNg-inducible, antiviral response	7.E-26	3.34			
Usp18	Ubiquitin Specific Peptidase 18	type I interferon, inflammation	1.E-11	2.71	0.00		
Ifit2	Interferon Induced Protein With Tetratricopeptide Repeats 2	IFNg signaling, inhibits expression of viral mRNA	4.E-14	2.18			
Nlrc5	NLR Family CARD Domain Containing 5	induced by IFNg, MHC I transactivator	8.E-28	2.54			
Irgm1	Immunity Related GTPase M	regulates autophagy in response to intracellular pathogens, involved in Crohn's disease	4.E-50	2.76	1.65		
Il12rb1	Interleukin 12 Receptor Subunit Beta 1	low-affinity subunit of IL12R, also associates with IL23R.	3.E-05	1.56			
Pla2g4c	Phospholipase A2 Group IV C	macrophage differentiation, activated upon inflammation	2.E-116	6.71	5.74		
Il15ra	Interleukine 15 receptor α	similar to CD25, pairs with IL2Rb+c to induce T and NK cell activation	2.E-16	1.52			
Il18rap	Interleukin 18 Receptor Accessory Protein	enhances IL18-binding activity of the IL18R, involved in Crohn's disease and IBD	1.E-02	1.40			
Il1a	Interleukine 1α	inflammatory cytokine	2.E-03	1.56			
Il1b	Interleukin 1 beta	major inflammatory cytokine secreted by macrophages, activating T cells	5.E-04	1.35			
Il1r2	Interleukin 1 Receptor Type 2	non-signaling decoy receptor for IL1a, IL1b and IL1rn	4.E-07	1.77			
IL2ra	Interleukin 2 receptor alpha (CD25)	induced in T cells upon inflammation to generate the high-affinity IL2 receptor, constitutive on Tregs	1.E-09	3.32			
Batf2	Basic Leucine Zipper ATF-Like Transcription Factor 2	involved in differentiation of CD8+ DCs, not expressed by T cells	2.E-39	1.48			
Tnfrsf18	Glucocorticoid-Induced TNFR-Related Protein (GITR)	costimulatory receptor on CD25+ CD4 T cells	4.E-04	1.62			
Tnfrsf4	TNF Receptor Superfamily Member 4 (OX40)	costimulatory molecule on T cells implicated in long-term T-cell immunity, inhibits apoptosis	2.E-04	1.68			
Tnfsf9	TNF Superfamily Member 9 (4-1BB Ligand)	reactivates anergic T cells, promotes proliferation	2.E-03	1.33			
Btn1a1	Butyrophilin Subfamily 1 Member A1	B7-family-like, may validate TCR recognition in a non-classical innate-like fashion	3.E-02	1.52		T cell costimulation	
Treml2	Triggering Receptor Expressed On Myeloid Cells Like 2	interacts with CD276 on T cells and may enhance their activation	5.E-05	2.43			
Ubash3b	Ubiquitin Associated And SH3 Domain Containing B	interferes with degradation of RTKs, such as the TCR, and dephosphorylates SYK and ZAP70	1.E-16	2.46		T cell costimulation, inhibitory	
Pdcd1 (PD1)	Programmed Cell Death 1	on T cells, ligand binding inhibits T cell proliferation	1.E-21	1.47			
Cd274	Programmed Cell Death 1 Ligand 1	ligand for PD-1 on T cells, inhibits T cell proliferation	1.E-35	3.06			
Pdcd1lg2	Programmed Cell Death 1 Ligand 2 (PDL2)	inhibits T cell proliferation	8.E-05	2.17			
Cd40		costimulatory molecule on antigen-presenting cells	8.E-04	1.71			
Tnfsf13b	B-Cell-Activating Factor (BAFF)	potent B cell activator	1.E-12	1.83		Activation of antigen-presenting cells	
Fcgr2b	Fc Gamma Receptor IIb	low-affinity Fc receptor, inhibitory	1.E-05	1.09			
Fcgr4	Fc Gamma Receptor IV	activatory counterpart of FcgR2b	2.E-07	1.53			
Ly96	MD-2	co-receptor for TLR4 recognizing LPS	8.E-05	1.54			
Tlr2	Toll Like Receptor 2	recognizes lipoproteins of bacteria	5.E-03	1.06			
March9	Membrane-Associated RING Finger Protein 9	E3 ubiquitin-protein ligase, may mediate endocytosis of MHC-I, CD4 and ICAM1	1.E-06	1.40			
Cd47		"don't eat me" signal	1.E-80	1.57	0.57		
Tuba8	Tubulin alpha 8	microtubules	3.E-10	3.69			
Tubb3	Tubulin Beta 3 Class III	microtubules, primarily in neurons for neurogenesis and axon guidance	3.E-06	2.72	0.00		
Cxcl2	C-X-C Motif Chemokine Ligand 2	produced by activated monocytes and neutrophils in inflammation, attracts granulocytes	1.E-02	1.72			
Cxcl5	C-X-C Motif Chemokine Ligand 5	binds CXCR2 on neutrophils	8.E-06	2.70			
Cxcl9	C-X-C Motif Chemokine Ligand 9	early inflammatory cytokine, recruits T cells but not neutrophils	3.E-30	3.73			
Cxcl10	C-X-C Motif Chemokine Ligand 10	early inflammatory cytokine, recruits T cells, neutrophils, monocytes	1.E-12	2.68			
Cxcl11	C-X-C Motif Chemokine Ligand 11	early inflammatory cytokine, recruits T cells, neutrophils, monocytes	5.E-29	3.78			
Ccl7	C-C Motif Chemokine Ligand 7	binds to CCR1, 2 and 3 on monotytes and eosinophils, but not neutrophils	6.E-04	2.25			
Ccl8	C-C Motif Chemokine Ligand 8	attracts a broad range of immune cells	2.E-08	2.45			
Ccl11	C-C Motif Chemokine Ligand 11 (eotaxin)	recruits eosinophils	2.E-19	1.66			
Ccl17	C-C Motif Chemokine Ligand 17	chemotactic for T cells, binds to CCR4 and CCR8	1.E-02	1.31			
Ccrl2	C-C Motif Chemokine Receptor Like 2	expressed in activated neurophils and monocytes, inflammatory immune cell recruitment	8.E-11	2.31			
S1pr1	Sphingosine-1-Phosphate receptor 1	T, NK and B cell egress signal to leave lymphoid tissues	4.E-04	1.10			
Icam1	Intercellular Adhesion Molecule 1	binds to LFA1 on leukocytes, inflammatory trafficking molecule	4.E-29	2.30	0.91		
Ceacam12		rhodent-specific adhesion molecule	4.E-04	2.39			
Itgb1bp1	Integrin Subunit Beta 1 Binding Protein 1	binds to cytoplasmic domain of beta1 integrin and inhibits activation	7.E-12	1.17			
Lgals7	Galectin 7	beta-galactoside-binding protein modulating cell-cell and cell-matrix interations	2.E-04	2.47			
Clec10a	C-Type Lectin Domain Containing 10A	cell adhesion, Ca-dependent binding to terminal galactose and GalNAc (Tn-Ag expressed by carcinoma cells)	7.E-09	2.67			
St3gal4	ST3 Beta-Galactoside Alpha-2,3-Sialyltransferase 4	involved in Sialyl-Lewis X expression	2.E-43	3.57			
Lrg1	Leucine Rich Alpha-2-Glycoprotein 1	involved in cell adhesion, granulocyte differentation	5.E-10	2.40			
Cd38		glycoprotein involved in cell adhesion, signal transduction and calcium signaling. Mostly on B cells, but also on some macrophages, gd T cells and IEL	4.E-08	1.04			
Adam8	ADAM Metallopeptidase Domain 8	disintegrin and metalloprotease family	6.E-11	2.20			
Adamts4	ADAM Metallopeptidase With Thrombospondin Type 1 Motif 4	degradation of aggrecan (cartilage) and brevican (brain)	2.E-07	2.10			
Timp3	Tissue Inhibitor Of Metalloproteinases 3	metalloproteinase inhibitor	1.E-23	2.14			
Tnfrsf12a	TNF-Related Weak Inducer Of Apoptosis (TWEAK)	induces IEC apoptosis in GvHD	3.E-12	1.43			
Reg3b	Regenerating Islet-Derived 3 beta	protects intestinal stem cells in GvHD	3.E-05	1.24		Mucosal integrity	
Reg3g	Regenerating Islet-Derived 3 gamma	protects intestinal stem cells in GvHD	7.E-06	1.44	0.99		
Il11	Interleukin 11	development of T and B cells, proliferation of B cells and megakaryocyte maturation, mucosal integrity	1.E-02	1.28			
Batf	Basic Leucine Zipper ATF-Like Transcription Factor	differentiation of Th17 cells	3.E-04	1.49			
Il17d	Interleukin 17D	induces IL6, CXCL8, GM-CSF in endothelium	8.E-03	1.54			
Il18bp	Interleukin 18 Binding Protein	binds the pro-inflammatory IL18 and inhibits receptor binding, associated with Crohn's disease	5.E-19	2.20			
Il4ra	Interleukin 4 Receptor Alpha	binds IL4 and IL13, regulates IgE production	9.E-27	1.28			
Il13	Interleukin 13	produced by activated Th2 cells, promotes IgE switching	7.E-09	3.72		Th17, Th2, Treg induction	
Arg1	Arginase 1	expressed in macrophages promoting type 2 immunity	4.E-03	1.66			
Il33	Interleukin 33	alarmin, binds ST2 receptor, promotes Th2 cells	3.E-08	1.41			
Il10	Interleukin 10	anti-inflammatory cytokine	3.E-06	3.10			
Ido1	Indoleamine 2,3-Dioxygenase 1	Treg induction by tryptophane depletion	9.E-66	4.55	2.59		
Ido2	ndoleamine 2,3-Dioxygenase 2	Treg induction by tryptophane depletion	3.E-05	2.77			
Socs1	Suppressor Of Cytokine Signaling 1	downregulates cytokine signaling such as IL2, IL3	1.E-130	5.18			
Socs3	Suppressor Of Cytokine Signaling 3	downregulates cytokine signaling such as IL6, IL10, IFNg	3.E-18	2.06			
Ly6a	Lymphocyte antigen 6 complex, locus A	upregulated by IEC in colitis	1.E-101	4.40		Ly6 family	
Ly6c1	Lymphocyte antigen 6 complex, locus C1	induced by IFNg in IEC; leads to chemokine secretion. Activation of T cells in LP, LN-homing of memory CD8 T cells, marker for monocytes	2.E-38	3.14			
Ly6d	Lymphocyte antigen 6 complex, locus D	may differentiate between early developmental stages of T cells vs. B cells	2.E-04	1.64			
Ly6e	Lymphocyte antigen 6 complex, locus E	modulator of acetylcholine receptor activity	2.E-13	1.23			
Ly6g	Lymphocyte antigen 6 complex, locus G	marker for monocytes, granulocytes, neutrophil entry into inflamed tissue	4.E-04	2.40			
Ly6i	lymphocyte antigen 6 complex, locus I	maturation marker of B and T cells	1.E-02	1.75			
H2.DMa		classical MHC I	3.E-27	1.91	-0.55	Antigen presentation	Downregulated in BM
H2.DMb1		classical MHC I	5.E-35	2.22			
H2.DMb2		classical MHC I	7.E-30	2.10			
H2.Q4		non-classical MHC I	1.E-19	1.11			
H2.Q5		non-classical MHC I	6.E-25	1.02			
H2.Q7		non-classical MHC I	1.E-07	1.29			
H2.M3		non-classical MHC I	1.E-12	1.29			
H2.Aa		classical MHC II	1.E-21	1.47	0.21		
H2.Ab1		classical MHC II	2.E-29	1.59	1.27		
H2.Eb1		classical MHC II	4.E-26	1.60			
Cd74	HLA-DR Antigens-Associated Invariant Chain	involved in MHCII peptide loading	5.E-35	1.69	1.77		
Tap1	Transporter 1, ATP Binding Cassette Subfamily B Member	extended peptide loading machinery of MHC I	8.E-64	2.27	0.70		
Tap2	Transporter 2, ATP Binding Cassette Subfamily B Member	extended peptide loading machinery of MHC I	2.E-21	1.51	0.20		
Cd79b		B cell antigen receptor complex	2.E-03	1.08			
Cd53		complexes with integrins, contributes to CD2-generated signals in T cells	3.E-06	1.52		Homing and migration	
Ccl22	C-C Motif Chemokine Ligand 22	binds to CCR4, trafficking of activated/ effector T cells to inflammatory sites	8.E-07	2.16			
Zbp1	Z-DNA Binding Protein 1	DNA sensor, induces type I interferon	6.E-27	2.32	0.17		
Irf1	Interferon Reulatory Factor 1	antiviral response	4.E-45	1.53			
Igtp	Interferon gamma induced GTPase	induced by IFNg	2.E-54	4.15	1.77		
Irgm2	Immunity-related GTPase family member 2	interferon-induced, involved in IBD and Crohn's Disease	9.E-42	2.43	1.10		
Il2rb	Interleukin 2 Receptor Subunit Beta	intermediate to high-affinity IL2R, induces activation and proliferation of T cells	2.E-04	1.32		T cell activation and inflammation	Upregulated near the PP and in untreated
Il2rg	Interleukin 2 Receptor Subunit Gamma	part of the IL2, IL4, IL7 and IL21 receptor	2.E-08	1.43			
Stat4	Signal Transducer And Activator Of Transcription 4	downstream signaling of IL12	4.E-06	2.29			
Gata3	GATA Binding Protein 3	transcriptional activator for TCR alpha and beta genes. Required for Th2 differentiation	8.E-06	2.56			
Il21r	Interleukin 21 Receptor	proliferation of T, B NK cells	4.E-04	1.62			
Cd3d	CD3 delta	part of TCR complex	3.E-09	2.50		T cell activation	
Cd3e	CD3 epsilon	part of TCR complex	7.E-04	1.21			
Cd3g	CD3 gamma	part of TCR complex	8.E-04	1.01			
Lat	Linker For Activation Of T Cells	links TCR signaling to MAPK phosphorylation	8.E-09	2.39			
Cd247	T cell receptor zeta chain	TCR activation	1.E-05	2.35			
Lck	Lymphocyte Cell-Specific Protein-Tyrosine Kinase	intracellularly associated with CD4 or CD8, phosphorylates the TCR/CD3 complex	4.E-03	1.12			
Zap70	Zeta Chain Of T Cell Receptor Associated Protein Kinase 70	key tyrosine kinse downstream of the TCR	2.E-06	1.55			
Sh2d2a	SH2 Domain Containing 2A	TCR downstream signaling	3.E-07	2.14			
Prkcq	Protein Kinase C theta	TCR signaling in effector T cells	2.E-05	2.12			
Cd8b1	CD8 antigen, beta chain 1	part of the CD8 coreceptor for the TCR on MHC I restricted T cells	9.E-13	3.43			
Thy1	Thy-1 Cell Surface Antigen (CD90)	expressed by T cells and neuronal cells, involved in cell adhesion and T cell activation.	2.E-10	2.78			
Cd2	LFA-2	costimulatory receptor in T and NK cells, binds CD58 (LFA3) on APC	1.E-06	3.06			
Cd48	Signaling Lymphocytic Activation Molecule 2	CD2 family, low-affinity ligand for CD2, interaction between activated lymphocytes, regulating T cell activation	6.E-10	1.97			
Cd5	(scavenger receptor cystein-rich superfamily)	expressed by B1-a and T cells, regulates T cell proliferation	2.E-02	1.42			
Slamf1	Signaling Lymphocytic Activation Molecule Family Member 1	costimulatory receptor on B and T cells	8.E-03	1.85			
Ubash3a	Ubiquitin Associated And SH3 Domain Containing A	negatively regulates T cell signaling, promotes accumulation of activated TCR on the cell surface	1.E-04	2.39			
Ly9	SLAM Family Member 3	may participate in ahesive functions in T cells, promotes Th17 polarizaion	2.E-02	1.13			
Spn	Sialophorin	antigen-specific activation of T cells, polarization towards Th1	1.E-07	1.95			
Coro1a	Coronin-1-alpha	interacts with actin, involved in cytoskeletal dynamics and phagocytosis	1.E-07	1.53	-0.10	Migration	
Rac2	Rac Family Small GTPase 2	cytoskeletal reorganization and migration	2.E-07	1.51	-0.12		
Cd52	CAMPATH-1 Antigen	expressed on mature lymphocytes, potentially anti-cell-adhesive	9.E-04	1.17			
Itgb7	Integrin beta 7	pairs with integrin alpha 4 to form the gut-homing integrin a4b7	3.E-08	1.71		Trafficking	
Skap1	Src Kinase Associated Phosphoprotein 1	inside-out signaling of integrins in T cells	6.E-09	2.20			
Selplg	P-selectin Glycoprotein Ligand-1 (PSGL-1)	expressed on leukocytes, ligand for P-Selectin on endothelium	5.E-06	1.52			
Ccr9	C-C Motif Chemokine Receptor 9	expressed on 1 cells and DCs, binds to CCL25 for intestinal homing	3.E-03	1.02			
Ccr7	C-C Motif Chemokine Receptor 7	tethering of T cells in the T cells zones of SLO, binds CCL19 and CCL21	2.E-02	1.57			
Ccr5	C-C Motif Chemokine Receptor 5	binds the early inflammatory chemokines CCL3, 4, 5	3.E-03	1.01			
Ccl3	C-C Motif Chemokine Ligand 3	early inflammatory chemokine, binds to CCR1, 4, 5	6.E-05	2.37			
Ccl4	C-C Motif Chemokine Ligand 4	early inflammatory cytokine, binds to CCR5	2.E-07	2.47			
Cxcr6	C-X-C Motif Chemokine Receptor 6	receptor on T cells for CXCL16	2.E-02	1.15			
Gzma	Granzyme A	cytolytic protein released from cytotoxic T cell granules	7.E-21	2.43	-0.07	Cytotoxicity	
Gzmb	Granzyme B	cytolytic protein released from cytotoxic T cell granules	9.E-23	3.00	0.60		
Gzmk	Granzyme K	cytolytic protein released from cytotoxic T cell granules	4.E-03	1.79			
Nkg7	Natural Killer Cell Granule Protein 7	expressed in T and NK cells	8.E-10	2.12			
Fasl	Fas Ligand	expressed on T cells, mediates apoptosis in Fas-expressing cells	9.E-05	1.74			
Cd160	Natural Killer Cell Receptor BY55	expressed by cytolytic T cells and highly by IEL	2.E-02	1.03			

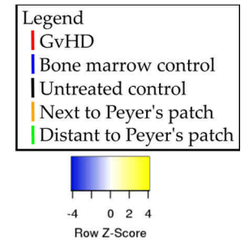

Some genes were significantly upregulated in the comparison between GvHD and BM control, but notably the heatmap revealed that these genes were only upregulated near the Peyer's patch in GvHD and not as much further away into the intestinal mucosa. The majority of the genes in this cluster are related to T cell activation and T cell mediated inflammatory mechanisms. Genes related to cell migration, trafficking and cytotoxicity were also included in this cluster. All of these genes were also expressed at a high level in healthy untreated tissue, which will be elaborated on in the discussion. These genes that were significantly increased between GvHD and bone marrow control but that were only expressed to a high extent near the Peyer's patch in GvHD mostly overlapped with the list of genes that were significantly upregulated in the respective statistical comparison. Even so, some of the genes were found only in one or the other list.

In summary, we found genes known to be upregulated in GvHD which validated our results. The functions of the upregulated genes were mainly Type I inflammation, antigen presentation, T cell activation and T cell trafficking/ homing, and we found an array of chemokines and migration-related molecules.

4.6.2 Genes upregulated near the Peyer's patch in GvHD

To find genes enriched in the recently egressed T cells, the second statistical evaluation compared the mucosa near the Peyer's patch versus the mucosa further away in GvHD samples. 143 genes were differentially expressed between the mucosa near the Peyer's patch *versus* the mucosa distant from the Peyer's patch (Table 4-2). Many transcripts of which the proteins are involved in migration and cytoskeletal rearrangement were upregulated (Parvg, Coro1a, Rac2, Dock2), as well as molecules in trafficking and migration (Ccl4, Xcr1, Ccr9, Itgb7, Itgal). Furthermore, Ccr7 was significantly upregulated in GvHD and the heatmap in Table 4-1 indicated upregulation only near the Peyer's patch. However, CCR7 was not part of the significantly upregulated genes of the second analysis of near *vs.* far to the Peyer's patch in GvHD, likely because of one outlier sample. Of note, most of the chemokines were upregulated both near and far from the Peyer's patch in GvHD, whereas the chemokine receptor transcripts only increased near the Peyer's patch.

Table 4-2 Heatmap of RNAseq data significantly altered between areas near the Peyer's patch and further away.

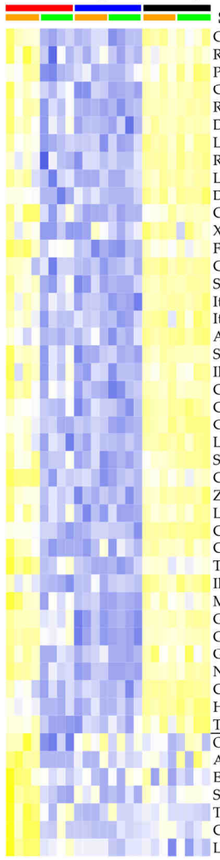

RNAseq heatmap	Gene symbol	Gene name	Gene function	RNAseq p-value	RNAseq log2FC	Category
	Cd52	CAMPATH-1 Antigen	may be anti-adhesive, expressed on mature lymphocytes, monocytes/MΦ, DCs	3E-06	1,85	
	Rasgrp2	RAS Guanyl Releasing Protein 2	inside-out integrin activation in lymphocytes	2E-03	2,01	
	Parvg	Parvin gamma	cell adhesion and cytoskeleton organization, leukocyte-substrate interaction	1E-04	2,44	
	Coro1a	Coronin 1A	interacts with actin, involved in cytoskeletal dynamics and phagocytosis	6E-04	1,40	
	Rac2	Rac family small GTPase 2	cytoskeletal reorganization and migration	5E-07	1,61	Migration/ cytoskeleton
	Def6	DEF6, Guanine Nucleotide Exchange Factor	highly expressed in B and T cells, regulates cell morphology, role in Th2 polarization	8E-02	1,20	
	Lsp1	Lymphocyte-Specific Protein 1	cell motility, adhesion to fibrinogen matrix proteins, transendothelial migration	2E-04	1,41	
	Rinl	Ras And Rab Interactor Like	vesicle-mediated transport	9E-02	1,13	
	Limd2	LIM Domain Containing 2	regulates cell motility in metastatic lesions, binding and activating integrin-linked kinase	1E-03	1,44	
	Dock2	Dedicator Of Cytokinesis 2	cytoskeleton remodeling for migration to chemokines, in hematopoietic cells	4E-02	1,75	
	Ccl4	C-C Motif Chemokine Ligand 4	early inflammatory cytokine, binds to CCR5	7E-02	1,95	
	Xcl1	X-C Motif Chemokine Ligand 1	antimicrobial, chemotactic for T cells but not for Mo or Neutro, self-tolerance	8E-05	1,22	
	Fxyd5	FXYD Domain Containing Ion Transport Regulator 5	upregulates chemokine production, reduces cell adhesion via E-cadherin downregulation	6E-02	1,26	
	Ccr9	C-C Motif Chemokine Receptor 9	expressed on T cells and DCs, binds to CCL25 for intestinal homing	5E-03	1,45	Trafficking and migration
	Selplg	Selectin P Ligand	expressed on leukocytes, ligand for P-Selectin on endothelium, fast rolling of leucocytes	5E-03	1,31	
	Itgb7	Integrin Subunit Beta 7	pairs to a4b7 (gut-homing) or to aEb7(endothelial localization)	1E-02	1,35	
	Itgal	Integrin Subunit Alpha L	pairs with β2 to form LFA-1, binds do ICAMs	8E-02	1,07	
	Acap1	ArfGAP With Coiled-Coil, Ankyrin Repeat And PH Domains 1	endocytosis, clathrin-dependent export of proteins such as ITGB1	2E-03	1,69	
	Spn	Sialophorin	antigen-specific activation of T cells, polarization towards Th1	8E-02	1,28	
	Il2rb	IL2 receptor subunit beta	part of the low (and high) affinity IL2 receptor. Also associates with IL23R	9E-02	1,49	
	Cd3d	in TCR complex	part of TCR complex in gd T cells	8E-02	1,26	
	Cd3e	in TCR complex	part of TCR complex	2E-06	1,48	
	Cd3g	TCR complex	part of TCR complex in gd T cells	3E-04	1,81	
	Lck	Lymphocyte Cell-Specific Protein-Tyrosine Kinase	intracellularly associated with CD4 or CD8, phosphorylates the TCR/CD3 complex	4E-03	1,77	
	Sh2d2a	SH2 Domain Containing 2A	TCR downstream signaling	2E-07	3,02	
	Cd247	CD3 zeta	TCR activation	2E-03	1,44	T cell activation
	Zap70	zeta-chain-of-TCR-associated protein kinase	key tyrosine kinse downstream of the TCR	7E-02	1,52	
	Lat	Linker For Activation Of T-Cells	major adapter molecule, links TCR signaling to MAPK phosphorylation	1E-04	1,26	
	Cd8a		part of the CD8 coreceptor for the TCR on MHC I restricted T cells	4E-03	2,39	
	Cd27		costimulation on T cells, particularly in lamina propria, ligand is CD70 on APC and T cells	2E-06	2,28	
	Thy1	Thy-1 Cell Surface Antigen	expressed by T cells and neuronal cells, involved in cell adhesion and T cell activation	1E-03	2,00	
	Il27ra	Interleukin 27 Receptor α	IL-12 cytokine family, Th1 differentiation when IFN is present, upregulation of IL-10	4E-02	1,99	
	Ms4a4b	membrane-spanning 4-domains, subfamily A, member 4B	inhibits T cell proliferation	2E-03	1,25	
	Gzma	Granzyme A	cytolytic protein released from cytotoxic T cell granules	2E-05	1,48	
	Gzmb	Granzyme B	cytolytic protein released from cytotoxic T cell granules, in activated IEL	5E-02	1,99	
	Gzmk	Granzyme K	cytolytic protein, in memory and effector CD8+ T cells, ativated gd-IEL	5E-10	2,07	Cytotoxicity
	Nkg7	Natural Killer Cell Granule Protein 7	expressed in T and NK cells	7E-02	1,51	
	Cd160		expressed by cytolytic T cells and highly by IEL	4E-03	1,07	
	Hmha1	Histocompatibility (Minor) HA-1 (ARHGAP45)	Rho-type GTPase, may negatively regulate actin cytoskeleton, precursor of miHA HA-1	6E-03	1,54	
	Traf1	TNF Receptor Associated Factor 1	TNF signaling to NFkappaB	2E-04	1,48	
	Ogdhl	Oxoglutarate Dehydrogenase-Like	degrades glucose and glutamate	2E-03	2,39	
	Aqp9	Aquaporin 9	aquaglyceroporin, transport of non-charged solutes incl. glucose, neutrophil migration	6E-02	2,06	
	Emp3	Epithelial Membrane Protein 3	cell proliferation, cell-cell interactions, may inhibit cytotoxic T lymphocytes	9E-02	1,15	
	Serpinb6b	Serpin Family B Member 6	placental thrombin inhibitor, expressed in hair cells of inner ear, mut: hair loss	8E-05	1,85	
	Tnfrsf9	TNF Superfamily Member 9 (4-1BB Ligand)	reactivates anergic T cells, promotes proliferation	6E-02	1,57	
	Cd2	LFA-2	costimulatory receptor in T and NK cells, binds CD58 (LFA3) on APC	5E-03	2,46	Costimulation
	Lgals1	Galectin 1	induces T-cell apoptosis, inhibits CD45 phosphatase, which dephosphorylates Lyn	2E-04	1,47	

Legend
- GvHD
- Bone marrow control
- Untreated control
- Next to Peyer's patch
- Distant to Peyer's patch

-4 0 2 4
Row Z-Score

Upregulated in GvHD near the PP and in untreated control

Upregulated near PP in GvHD only

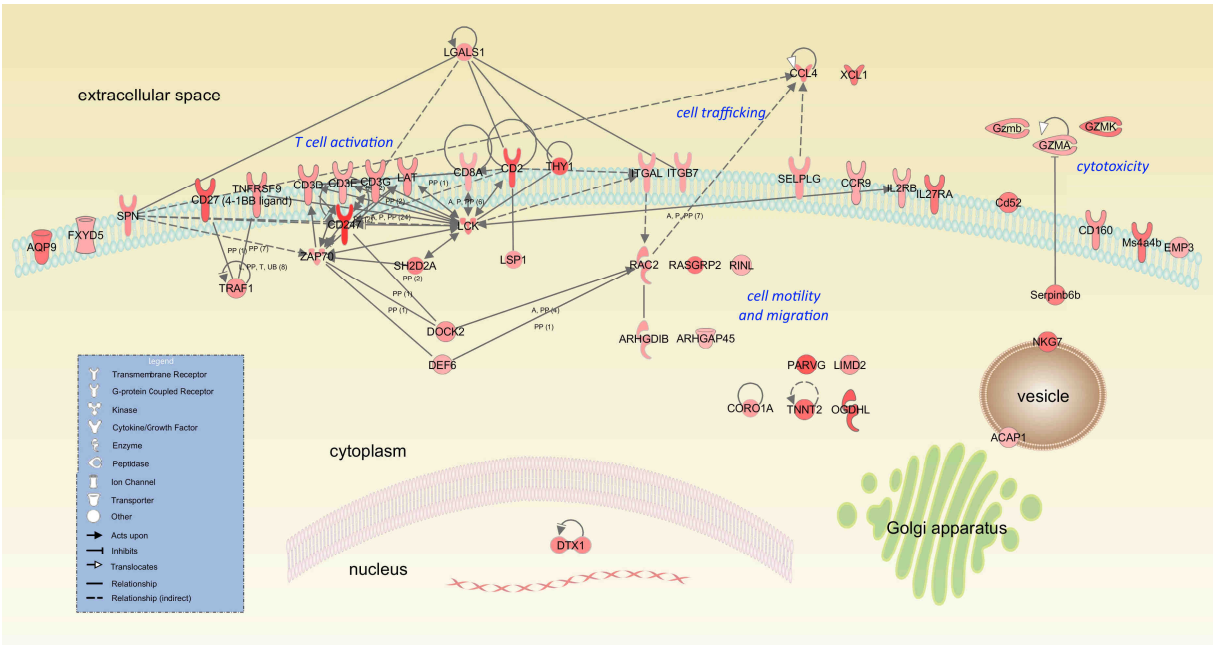

Figure 4-13 Subcellular localization and relationships of gene products upregulated near the Peyer's patch in GvHD. The intensity of red color indicates higher expression of the molecule near the Peyer's patch as compared to further away. The T cell receptor, associated signaling molecules and co-receptors form a cluster of upregulated transcripts. Moreover, a large group of gene products involved in cell trafficking and migration were highly expressed near the Peyer's patch. Furthermore, molecules involved in cytotoxicity were increased. A Activation, P Phosphorylation/ Dephosphorylation, PP Protein-Protein binding, L Proteolysis, T Transcription, UB Ubiquitination. The graph was generated with the help of the IPA software.

A major cluster of proteins upregulated near the Peyer's patch are T cell receptor-associated genes, as can be seen in Figure 4-13. The CD3 complex (Cd3d, Cd3e, Cd3g), as well as downstream signaling molecules (Cd247= CD3 ζ, Zap70, Sh2d2a), co-receptors and TCR regulators (Cd8a, Lat), and costimulatory molecules (Cd27, 4-1BB, Cd2) increased specifically near the Peyer's patch. Lastly, a couple of genes were increased that can be combined by their relation to cytotoxicity (Gzma, Gzmb, Gzmk, Nkg7) or because of their known expression in cytotoxic T and NK cells (Cd160).

Most of the genes mentioned for the comparison near *vs.* far to the Peyer's patch were also expressed to a high degree in the healthy untreated mucosa (Table 4-2). Only a very small number of genes were specifically upregulated near the Peyer's patch only in the GvHD setting and not in the healthy untreated tissue. Of these genes, 4-1BB, Cd2 and Galectin are known to play a major role in immune responses.

In summary, the genes upregulated near the Peyer's patch in GvHD were dominated by T cell activation genes and contained also molecules involved in T cell trafficking, migration and cytotoxicity. Some costimulatory molecules were upregulated near the Peyer's patch only in GvHD.

Overall, the GvHD *vs.* bone marrow comparison yielded many genes involved in inflammation, antigen presentation and costimulation. These results point to candidate chemokines that may be involved in attracting T cells from circulation as well as directly from the Peyer's patch to the surrounding mucosa. In contrast, particularly the mucosa near the Peyer's patch was strongly enriched by T cell associated genes. The genes upregulated specifically here point to some chemokine receptors and costimulatory details about the T cells that had recently egressed from the Peyer's patch to the *lamina propria*.

Taken together, the experiments of this thesis provided evidence for a previously unknown migration shortcut from the Peyer's patch directly into the *lamina propria* of the small intestine. This direct access to the target tissue bypasses lymphatic and vascular trafficking of the T cells.

This study showed that T cells migrate from the Peyer's patches directly to the adjacent *lamina propria* of the small intestine. They may possibly serve as seeder cells attracting further circulating T cells from the blood to the early inflammation site.

5 Discussion

5.1 The Peyer's patch lacks a capsule

The tissue around the Peyer's patch is directly accessible to the cells present in the patch. In contrast to lymph nodes, no capsule or basement membrane encapsulates the Peyer's patch. Staining of laminin, which is an integral part of all basement membranes, revealed a continuous migration space from the Peyer's patch to the adjacent villi of the *lamina propria*. Therefore, the extracellular organization allows for unhindered passage of migrating cells.

We cannot exclude that there may be other cell types, such as dense macrophage networks or reticular cells that form barriers at the edge of the Peyer's patch; this remains to be investigated. Nevertheless, the open boundary of the Peyer's patch supports the assumption of our main hypothesis that T cells may be able to leave the Peyer's patch directly to the adjacent *lamina propria*.

The main function attributed to the mostly fibrous lymph node capsule is that it gives mechanical stability to the small organ. In ruminants, the capsule additionally harbors smooth muscle cells and can contract (Thornbury *et al.*, 1990). The capsule thus fosters lymph flow through this dense tissue, which presents a high hydrodynamic resistance and hinders lymph flow (Browse *et al.*, 1984). Many lymph nodes are positioned between soft tissues, which may not provide enough pressure onto the lymph nodes to propel lymphatic flow. Therefore, the stable capsule can sustain the required pressure to transport lymphatics through the nodules towards the venous drainage. In the intestine, the pressure to drain the lymphatics may be produced and sustained by the muscle layers on the serosal side of the Peyer's patch, which produce the frequent peristaltic movement of the bowels. The architecture of the Peyer's patch, with draining lymph vessels towards the muscular layer of the intestine, may support efficient drainage of fluids from the efferent lymphatics.

Another difference between lymph nodes and the Peyer's patches is their location respective to the tissues they drain. Unlike Lymph nodes, which are positioned mostly distant to their draining site, Peyer's patches are embedded inside the organ they survey immunologically. Therefore, in contrast to lymph nodes, in Peyer's patches the direct access to the surrounding tissue can provide a shortcut for immune cells that traffic from activation- to effector site.

Table 5-1 Comparison of Peyer's patches and lymph nodes and in respect to their lymphatics.

Organ	Peyer's patch	Lymph node	Lymph vessel
Afferent lymphatics	no	yes	not applicable
Efferent lymphatics	yes	yes	not applicable
contraction	intestinal peristalsis	in some animals	in large collecting vessels
capsule	no	yes	no

Taken together, the Peyer's patch architecture can support efficient lymphatic drainage on the muscular side, while allowing access into the soft surrounding mucosal tissue.

5.2 T cells form a gradient around Peyer's patches

T cells form a gradient around the Peyer's patch early in the phase of intestinal infiltration during GvHD. Gradients generally develop by diffusion of particles from a point source to the adjacent areas. In this case, the Peyer's patch is the high-concentration source densely populated with T cells, and the *lamina propria* is the space the particles diffuse into. The gradient around the Peyer's patch indicates that the T cells migrate out laterally into the adjacent *lamina propria*.

We excluded the possibility that the T cells forming the gradient occupy the efferent lymphatics of the Peyer's patches instead of the *lamina propria* tissue. When we co-stained the lymphatic vasculature, the vast majority of T cells were located outside of the lymphatic vasculature.

Therefore, we have to reject the currently accepted theory that trafficking through lymphatics and blood followed by extravasation is the only access route for T cells to enter the small intestine.

5.3 T cells directly egress from the Peyer's patch to the *lamina propria*

There is a limitation to the previous experiment. The Peyer's patch is highly vascularized and bears many gut-specific homing factors. Hence there is an alternative explanation how the cell gradient may form around the Peyer's patch: At some of the later time points after transplantation when the gradient was observed, the very first cells already homed via the blood vessels to the intestinal *lamina propria* (Bäuerlein *et al.*, 2013). These circulating cells may preferentially have entered the MAdCAM-1^{high} high endothelial venules at the edge of the Peyer's patches to enter the *lamina propria*. This would mean that the cells forming the gradient did not necessarily emerge directly from the Peyer's patch. They would rather have extravasated from the vessels surrounding the Peyer's patch.

This possibility was ruled out by the photoconversion experiments, which showed that cells directly egressed from the Peyer's patch to the surrounding tissue. When we photoconverted T cells in the Peyer's patches, they migrated in the adjacent *lamina propria* after a few hours. They did not appear in areas more distant to the Peyer's patch nor adjacent to non-photoconverted Peyer's patches. Lack of converted T cells around unconverted Peyer's patches means that the photoconverted cells near the Peyer's patch did not come from circulation. Furthermore, we observed single T cells egressing from the Peyer's patches directly into the adjacent *lamina propria*.

To rule out that imprecise photoconversion also switches cells that had already infiltrated the adjacent mucosa at the time point of conversion, we chose conversion time points when there were no or only single cells outside the Peyer's patch. Furthermore, in some experiments, only the central spot of the Peyer's patches was converted, and the converted cells were still detected outside the Peyer's patch 12 hours later, despite completely unconverted Peyer's patch edges. The converted cells were still able to traffic to and migrate inside the intestine. They also still efficiently lysed tumor cells in culture. It can be expected that the cells detected in the mucosal tissue around the Peyer's patch are in the *lamina propria* and not inside lymphatic vessels. Although the lymphatics were not stained in these experiments, the results will presumably correlate with those from the light sheet microscope acquisitions where the cells were located inside the tissue and not in lymph vessels. Furthermore, in intravital migration experiments, the few T cells inside lymphatic or blood vessels had a rounded shape and fast flow-like kinetics when compared to the T cells in the tissue. These precautionary measures validated that this method yields reliable results.

Both irradiation and photoconversion can be damaging to stromal cell types in the border of the Peyer's patches that were not analyzed in this study. These could be macrophages, fibroblastic reticular cells, or other stromal cells. We cannot exclude that this opened up new migration spaces and influenced the migration behavior of the T cells in these experiments.

Approximately half of the cells counted around converted Peyer's patches carried only green fluorescent Dendra2 protein. There are two possibilities for the origin of these cells. (1) They may have been activated in lymphoid organs other than the converted Peyer's patches during photoconversion and may have entered the tissue by extravasation afterwards, or (2) they were activated in the Peyer's patch but photoconversion induced only dim red fluorescence that had diluted out due to cell divisions within the 12 h – 24 h until analysis. However, considering the highly

efficient photoconversion (Figure 4-7), the first explanation seems more realistic. This would mean that close to the Peyer's patch, approximately half of the cells originated directly from the Peyer's patch, and half of the cells had entered the tissue from the circulation.

In conclusion, a small population of the T cells directly enters the adjacent *lamina propria* from the Peyer's patch by migration. These cells do not pass through the circulatory system to enter the target tissue. This local infiltration path opens up new possibilities of intestinal subsegment-specific infiltration of immune cells. If a pathogen intrudes through the mucous layer and enters the mucosal tissue, this barrier breach does not necessarily occur in all parts of the intestine to the same extent. Different microbes inhabit different niches along the intestine (Bashir *et al.*, 2016; Suzuki and Nachman, 2016; Zilberstein *et al.*, 2007), and intruders of a certain bacterial species may not penetrate to the same extent in the duodenum and the ileum. A rapid and localized immune response is more likely to prevent dissemination of the intruders to distant body sites. Thus, this localized immune response may avoid spreading of the pathogen and infection of other organs or individuals. It is tempting to speculate that in addition to resident immune cell populations and fast-recruited neutrophils, this may be realized by directly egressing, potentially highly specific T cells directly from the Peyer's patches.

Most of the homing receptors are expressed rather uniformly throughout the intestine. During a local immune reaction, broadly acting inflammatory mediators upregulate early homing receptors such as P-selectin (Ley *et al.*, 1995), CXCL8 (Utgaard *et al.*, 1998) and ICAM-1 (Dustin *et al.*, 1986; Lane *et al.*, 1989). Some of these alterations occur within minutes, such as for CXCL8. In contrast, other homing molecules such as ICAM-1 reach their full expression level only 24 h after an inflammatory stimulus (Pober *et al.*, 1987). Moreover, there are some differentially expressed chemokines in the different parts of the small intestine, such as CCL5, CCL6 and CCL28 (Shang *et al.*, 2009), but there are no unique molecules directing trafficking only to some parts of the small intestine. Thus, it is difficult to guide circulating T cells directly into the segment in which a barrier breach has very recently occurred and microbiota threaten the tissue integrity. The direct egress from local Peyer's patches may provide this spatial specificity by directly providing a source of T cells able to infiltrate the surrounding mucosal tissue before eliciting a major infection. This mechanism would strongly couple the detection of antigens in the Peyer's patches to localized immunity. It would provide a difference in antigen recognition and removal between Peyer's patches and mesenteric lymph nodes, which are so far believed to play partly redundant roles in

intestinal immunity (Hashizume *et al.*, 2008; Macpherson and Smith, 2006; Spahn *et al.*, 2002).

5.4 T cells that have egressed from the Peyer's patch migrate randomly

The alloreactive T cells migrated from the Peyer's patch directly to the adjacent *lamina propria* in a random pattern. The directionality measurements of T cells on day 3 indicated random motion. In general, T cell migration appears to be random in lymph nodes (Miller *et al.*, 2002) and Peyer's patches. This is because in these lymphoid organs, T cells migrate on a three-dimensional network of fibroblastic reticular cells and often encounter other cells so they frequently change their direction of motion. Hence, when the cell is regarded as an isolated phenomenon, the migration pattern presents as random (Beltman *et al.*, 2007; Miller *et al.*, 2002). Since the T cells in the *lamina propria* on day 3 had a confinement ratio comparable to the cells in the Peyer's patch, they also migrated randomly.

On day 4 after transplantation, the donor T cells had a higher confinement ratio both inside and outside of the Peyer's patches, indicating more directed migration. It may seem surprising that the confinement ratio was also higher in the Peyer's patch on day 4 as compared to day 3. This might be due to the advanced immune response in the Peyer's patch. Most of the donor T cells inside the Peyer's patch on day 4 are expected to be alloresponsive and activated (Beilhack *et al.*, 2005). On day 3 in contrast, the T cells had not divided as much yet and may partly still have been in the process of activation. Naïve T cells migrate almost purely random during their search of antigen, whereas recently activated T cells perform informed motion (Krummel *et al.*, 2016). For instance, recently activated $CD8^+$ T cells upregulate CCR5 and thereafter perform chemotaxis towards antigen-presenting cells producing CCL3/4. Moreover, $CD4^+$ T cells destined to provide B cell help during an immune reaction upregulate CXCR5 and perform chemotaxis towards CXCL13 (Campbell *et al.*, 2001) produced by follicular dendritic cells in the B cell follicle. These mechanisms may have contributed to directional migration of T cells in the Peyer's patch four days after transplantation.

Outside of the Peyer's patch, the donor T cells migrated also much more directed on day 4 as compared to day 3. Most of the T cells in the *lamina propria* followed the collagen network on day 4 and they migrated much slower, which may indicate a more integrin-mediated migration in contrast to an amoeboid, pushing-and-squeezing-like behavior on day 3 (Lammermann *et al.*, 2008; Liu *et al.*, 2015; Wolf *et al.*, 2003). Alternatively, chemokines deposited on heparan sulphate can also induce haptokinesis on the extracellular matrix. This guided walk along fibers leads to highly

directed motion (Krummel *et al.*, 2016; Matheu *et al.*, 2008). In a 3D environment, leukocytes have been observed to migrate slower with haptokinesis as compared to amoeboid migration (Toyjanova *et al.*, 2015), although this may only apply to target organs and not to secondary lymphoid organs (Katakai *et al.*, 2013; Katakai and Kinashi, 2016). Furthermore, increased interactions of highly specific T cells with target cells may lead to a higher arrest rate. Thus, haptokinetic migration and higher arrest rate may contribute to the overall slower of T cell migration. The migration on the collagen network inside the tissue is likely to be guided by a mixture of haptic and soluble cues, as it has been analyzed in detail for dendritic cells (Schumann *et al.*, 2010; Schwarz *et al.*, 2017).

The reduced migration speed is in agreement with previous observations of activated T cells (Eickhoff *et al.*, 2015; Moreau *et al.*, 2015). Higher arrest rates on antigen-presenting cells in the Peyer's patch (Moreau *et al.*, 2015) or on target cells in the *lamina propria* (Boissonnas *et al.*, 2007) may in part explain why the at this time point highly antigen-specific T cells migrate overall slower. The time point of slower migration at day 4 is much later than in the mentioned literature, where the T cells already slowed down 6 h after infection. This may result from differences in the models employed: the models from the literature differ to this GvHD model in the type of antigen, have a high T cell specificity and larger number of transferred T cells. Furthermore, they may not be comparable in terms of antigen availability and numbers of antigen-presenting cells. In a minor mismatch GvHD model, slower migration of T cells in the lymph nodes was observed 7 days after transplantation (Michonneau *et al.*, 2016).

There are some alternative explanations for the migration patterns of the T cells. Regarding the low directionality of the T cells in the *lamina propria* on day 3 after transplantation, we cannot exclude that the cues promoting directional migration may be present in an irregular pattern inside the tissue. Additionally, physical obstacles such as other immune cells, extracellular matrix, vasculature or neurons affect the T cell migration tracks (Beltman *et al.*, 2007). Circumventing these obstacles could lead to seemingly random migration of the T cells although in fact they follow one or more directional migration cues.

Furthermore, we cannot exclude that the lymph flow around the Peyer's patch was partly slowed down during intravital microscopy. The blood flow was always ascertained to be fast and perfusing the tissue very well before starting imaging, and T cells were observed flowing inside vessels during the acquisitions. However, no tracers for lymph flow were used and anesthesia as well as handling of the organs may affect the lymph flow rate in the observed Peyer's patches. This may alter the T cell

egress behavior during imaging, because efficient lymphatic egress from lymph nodes depends on functional lymph flow (Grigorova *et al.*, 2008). Therefore, especially the T cells leaving the Peyer's patch during imaging may be affected by altered lymph flow, whereas the photoconverted cells that were already outside of the Peyer's patch before the start of imaging were completely unaffected by this potential artifact.

Taken together, these findings add a second T cell entry route to the small intestine. The T cells were able to migrate from the Peyer's patches directly to the adjacent *lamina propria*. This mechanism may foster more rapid and direct T cell infiltration into the intestinal tissue. It also provides an efficient mechanism to subregion-restricted immune responses in the intestine, such as duodenal ulcers infected with *Helicobacter pylori* (Hobsley and Tovey, 2001), or ulcerative colitis in the terminal ileum (Caprilli, 2008; Counsell, 1956). This direct migration may enrich for T cell infiltration in areas where threats such as bacteria invade the tissue or are sampled into the Peyer's patches via the M-cells. Thus, the immediate entry to the target organ may enable a more efficient eradication of pathogens at their primary entry site.

This immediate and early infiltration also calls for a hypothesis about the function of the egressed cells in the *lamina propria*. In addition to direct effector mechanisms, these cells may also serve as seeder cells to attract more cells to the region. Local secretion of chemoattractants, defensins or other soluble mediators may be a plausible mechanism for this secondary recruitment. They might be secreted directly by the T cells or indirectly by other cells in the local intestinal environment. This could be a mechanism to direct the systemic immunological attention to these subregions.

In summary, the T cells migrated non-directionally next to the Peyer's patch in the *lamina propria*. This mechanism of direct egress can nonetheless lead to efficient immunity due to fast recruitment of specific T cells, subregion-restricted immune reactions and may initiate secondary recruitment of further blood-borne lymphocytes.

5.5 The T cell egress to the tissue does not depend on S1PR1

Egressing T cells did not depend on S1PR1 for direct migration to the adjacent *lamina propria*. Systemic inhibition of S1PR1 did not alter the number of converted T cells around converted Peyer's patches or their migration behavior. The number of unconverted Dendra2-green cells around converted Peyer's patches tended to be slightly lower than around unconverted Peyer's patches. However, fingolimod treatment did not eradicate the Dendra2-green T cells around the Peyer's patches. This contradicts the point discussed earlier that the Dendra2-green T cells around the

Peyer's patch have likely entered the tissue from circulation. It rather speaks for the fact that some of the Dendra2-green T cells around the Peyer's patch have egressed directly from there, because the vascular T cells were vastly reduced in these experiments.

Alternatively, the Dendra2-green T cells around the Peyer's patch may have originated from the sparse cells left in circulation after fingolimod treatment. This accumulation near the directly emigrated cells would emphasize a strong recruitment of vascular T cells specifically to this region, since areas further away from the Peyer's patch were not infiltrated to the same extent.

S1P produced by the lymphatic endothelium promotes T cell egress towards the lymphatic sinus of lymphoid organs. At the time when this dogma was not yet so well established, one early study investigated the role of S1P for lymphocyte homing by measuring accumulation of transferred labeled lymphocytes into secondary lymphoid organs (Halin *et al.*, 2005). Using either FTY720 treatment or cells deficient for S1PR1, the researchers found that sticking to the high endothelial venules was significantly impaired in the lymph nodes but not in the Peyer's patches. Until today, there are no more detailed reports on the effect of S1PR1 on homing into lymph nodes and Peyer's patches, but our results may offer an explanation for this finding. Considering the limited space inside a lymph node, blocking lymphocyte egress quickly leads to overpopulation and lack of space for incoming cells. In this case, the endothelial pockets of the high endothelial venules become jammed with T cells. In consequence, they limit entry into the lymph node stroma (Mionnet *et al.*, 2011). This could be a mechanism leading to the reduced homing to the peripheral lymph nodes observed by Halin *et al.*. However, if we assume that in contrast to the lymph nodes, the Peyer's patches have a second exit route for T cells into the *lamina propria* that is independent of S1PR1, the unreduced entry into Peyer's patch could be a result of this T cell efflux specific for the Peyer's patches. This explanation is particularly tempting considering that the effects of FTY720 on homing into the LN were independent of S1PR1 expression on the homing lymphocytes, whereas the recipient mice in their study were proficient for the receptor, allowing for efficient overpopulation of lymph nodes before adoptive transfer.

A recent report associated the egress of γδ T cells from the Peyer's patch with the G-protein coupled receptor GPR55 (Sumida *et al.*, 2017). Upon blockade of this receptor, the authors observed a drop in γδ T cell numbers in the Peyer's patch that could not be explained by increased efflux of cells to the mesenteric lymph nodes. Potentially, these cells have exited the Peyer's patch directly into the adjacent lamina propria to become

intraepithelial lymphocytes. This or similar mechanisms may contribute to the direct egress of also other immune cell populations from the Peyer's patch.

To conclude, the mechanism of direct egress to the tissue differs from lymphatic egress from Peyer's patches because it does not require S1PR1.

5.6 RNAseq screen reveals migration-promoting factors in the *lamina propria*

The inflammation during GvHD induces migration-promoting factors in the *lamina propria*. Early inflammatory chemokines and other migration-promoting factors may attract the T cells directly from the Peyer's patch. These cells are highly activated and harbor some specific costimulatory molecules that may hint towards an alternative activation pathway. The T cell attracting chemokine CCL4 was produced in vicinity of these cells and may be a factor recruiting further circulating T cells.

5.6.1 Factors potentially attracting T cells from the Peyer's patch to the adjacent mucosa

The RNAseq results revealed a strong Th1 inflammatory milieu, as it was expected for the GvHD setting. The intestinal mucosa may induce inflammatory factors non-specifically in response to the damage resulting from the conditioning regimen. We excluded this possibility by comparing the GvHD mice to BM transplanted mice, which also received irradiation. The signature cytokines Ifng and Tnf were upregulated, along with an array of genes induced by them (Stat1, Tgtp2, Usp18, Ifit2, Nlrc5, Il12rb1, Irf1, Igtp, Irgm2). IFNγ is important for particularly gastrointestinal GvHD, although conversely absence of IFNγ aggravates overall GvHD (Coghill *et al.*, 2011). The authors attribute this effect to the immunoregulatory mechanisms that IFNγ also initiates. Many migration-related transcripts were upregulated in the mucosa (Coro1a, Dock2, Rac2, CD47, tubulins, chemokines and receptors, S1PR1, Integrins and -related proteins, Lgals7, Clec1a, St3gal4, Lrg1, Cd38, and metalloproteinases) indicating early infiltration of neutrophils (Hulsdunker *et al.*, 2018) and possibly the T cells. Furthermore, several mechanisms that counteract and therefore inhibit the aGvHD reaction were detected, such as Treg induction (Il10, Ido1, Ido2, Socs1, Socs3) and Th2 polarization (Il4ra, Il13, Arg, Il33). These two polarizations lead to general dampening of an immune response through the action of regulatory T cells and to a diminished Th1 response, respectively, and counter-regulatory mechanisms are an essential part of every ongoing immune reaction. These results convinced us that the findings from the RNAseq screen were well representative of the overall

immunological situation and that it is possible to derive more detailed information from this experiment.

In the overall mucosa, there were two prominent groups of genes induced: those involved in chemoattraction and those in antigen presentation and costimulation. Chemoattractant molecules (Cxcl2, Cxcl5, Cxcl9, Cxcl10, Cxcl11, Ccl3, Ccl4, Ccl7, Ccl8, Ccl11, Ccl17, Ccl22 and the alarmin Il33) may play a role in attracting the alloreactive donor T cells from the Peyer's patch to the adjacent mucosa, despite dominating random migration in the *lamina propria*. The surprisingly straight cell tracks at the border of the Peyer's patches may hint in this direction. IFNγ induces CCL3-5 and CXCL9-11, which play an important role in early recruitment of immune cells to the inflamed intestine (Bouazzaoui *et al.*, 2009; Wysocki *et al.*, 2005). CCL17 and CCL22 bind to CCR4 on T cells and may also attract them from the Peyer's patch to the adjacent *lamina propria*. Alternatively, the T cells may also access the mucosa due to a loss-of-gradient, such as downregulation of CCL21 and CXCL13 as a response to IFNγ (Mueller *et al.*, 2007). CXCL2 and CXCL5 attract neutrophils which precedes T cell infiltration in time. CCL7 recruits monocytes, which are important for clearance of cell debris from the tissue as macrophages, although work from the Beilhack laboratory points to intestinal macrophages that are rather tissue-resident (Le *et al.*, manuscript in preparation). CCL8 attracts a broad range of immune cells, whereas CCL11 attracts eosinophils (Jose *et al.*, 1994). Eosinophils are mostly related to Th2 inflammation and therefore play a more dominant role in chronic GvHD (Kalaycioglu and Bolwell, 1994), although eosinophils have also been associated with upper gastrointestinal acute GvHD (Daneshpouy *et al.*, 2002). The alarmin IL-33 recognizes ST2, which mediates Th2 polarization in its membrane bound form or Th1 polarization when soluble (Garlanda *et al.*, 2013). Therefore, IL-33 plays diverse but important roles in GvHD. Many of these chemokines expressed in the mucosa attract T cells and potentially promote the direct migration of the T cells from the Peyer's patch to the adjacent *lamina propria*.

Most of these infiltration-related genes were increased specifically in GvHD and were not expressed at this high level in the untreated healthy tissue. Therefore, these genes represent the inflammatory environment during the alloreaction, and differ from the tolerogenic immune-cell rich environment that is naturally present in the steady-state intestine.

Another prominent group of genes induced in the overall mucosa were related to antigen-presentation and costimulation. A whole range of classical and non- classical MHC I and II molecules were upregulated, which on one hand reflect stressed cells in

the case of MHC I upregulation, and increased antigen presentation in the case of MHC II. Furthermore, the peptide loading machinery of both MHC classes was highly expressed (CD74, Tap1, Tap2). Further antigen presentation in the mucosa can deliver confirming survival signals for the infiltrating T cells. The costimulatory molecules upregulated in the mucosa were GITR, OX40 and 4-1BB Ligand. GITR on T cells enhances $CD8^+$ T cell proliferation whereas it inhibits conventional $CD4^+$ T cell proliferation in GvHD (Muriglan *et al.*, 2004). OX40 is expressed on activated T cells and 4-1BB Ligand on antigen presenting cells, which binds to 4-1BB on T cells. 4-1BB expression was high particularly near the Peyer's patch in our screen, as discussed below. Both OX40 and 4-1BB promote GvHD (Briones *et al.*, 2011). Also coinhibitory molecules increased, such as PD1 expressed by T cells that binds the also upregulated molecules PD-L1 and PD-L2 on antigen-presenting cells. Btn1a1 belongs to the B7 family and may function as a validation signal of γδTCR recognition in an innate-like fashion, as it has been shown for BTN3A1 (Vantourout *et al.*, 2018). Since different costimulatory cues promote different responses in T cells, it is conceivable that these mechanisms contribute not only to the activation, but also to the adhesive and migratory phenotype of the T cells activated in the Peyer's patch. Some studies tried to differentiate the induction of migratory mechanisms from the proliferation that different costimulatory molecules initiate, but the number of reports is still scarce (Mirenda *et al.*, 2007; Walker *et al.*, 1999).

The five most upregulated genes from the RNAseq analysis comparing GvHD with bone marrow controls included some molecules intuitive to immunologists and some less studied in this field. The top upregulated gene, Pla2g4c, was almost the only candidate that was also found upregulated with mass spectrometry, also by a factor of more than 5. The Phospholipase A2 Group IV C (Pla2g4c) is involved in eicosanoid signaling and may regulate macrophage differentiation. The Suppressor Of Cytokine Signaling 1 (Socs1) downregulates chemokine signaling and is part of the anti-inflammatory counter-regulatory mechanisms initiated during the immune response. Restistin-like beta (Retnlb) is highly expressed in colitis and ileitis and seems to play a role in mucosal integrity (Hogan *et al.*, 2006). Ifng is the signature cytokine of GvHD and induces the overshooting type I immunity, and was an expected upregulated gene. The pseudogene gasdermin C-like is on the antisense strand between the genes Gasdermin C4 (Gsdmc4) and Family with sequence similarity 49b (Fam49b) (Chattaragada *et al.*, 2017) and may be involved in their regulation. Fam49b has recently been associated with actin dynamics and T cell activation (Shang *et al.*, 2018). This the pseudogene may be expressed due to an open and accessible chromatin

structure, which resulted from expression of another gene in close proximity. Fam49b was not detected which may have been due to technical reasons.

Most of these antigen-presenting genes upregulated in GvHD were also expressed in the healthy untreated mucosa, hinting at the immune-cell rich environment in the steady state. After transplantation conditioning, many of the immune cell populations are lost. Therefore, the influx of immune cells to the intestine may partly be interpreted as replacement of the local immune system, were it not for the alloreactive reaction that attacks and destroys the host tissue.

In summary, there is a group of migration-promoting genes upregulated only in GvHD as compared to the bone marrow control and the untreated healthy control. Another group of genes involved in antigen presentation and costimulation was present in the healthy untreated control, was eradicated by irradiation but reappears after GvHD induction. The cytokines and costimulatory molecules are potential candidates fostering the migration of T cells into the adjacent mucosa.

5.6.2 Factors likely expressed in the T cells near the Peyer's patch

When comparing the mucosa near the Peyer's patch and further away, the area near the Peyer's patch was expected to be enriched for genes expressed by T cells, which accumulate in this region due to the direct efflux from the Peyer's patch. Except for a few single exceptions, all genes upregulated specifically near the Peyer's patch in GvHD were also expressed in the healthy untreated mucosa.

Next to the Peyer's patch, T cell marker genes (Cd3γ, δ, ε, Cd8a) factors for T cell activation (Cd3ζ, Zap70, Lat, Cd27, Cd2, Lck) and migration (Parvinγ, Rac2, Dock2) were increased. Furthermore, chemokines that T cells produce were increased near the Peyer's patch (Xcl-1, Ccl4). The integrins α_L recognizing ICAM-1 and integrin β_7, which pairs with integrin α_4 for intestinal homing, were also increased near the Peyer's patch and likely represent the T cell population in this location. In the course of his medical doctoral thesis, Lukas Scheller confirmed the expression of Cxcl9, Ccl4, Cd27, Cd2, Dock2 and Parvinγ in immunofluorescence microscopy, and the sensitivity of allogenic T cells from the mesenteric lymph nodes to Cxcl11 and Ccl4 in a transwell assay or chemotaxis chamber (all data will be presented in his thesis).

$CD4^+$ T cell infiltration precedes $CD8^+$ T cell infiltration in this GvHD model and $CD4^+$ T cells are good producers of cytokines attracting more T cells. Therefore, we expected to find predominantly $CD4^+$ T cells around the Peyer's patch early during GvHD. However, the RNAseq results rather point to a gradient of $CD8^+$ T cells around the

Peyer's patch. The expression of Cd8a and cytotoxic molecules such as granzymes and Nkg7 was increased near the Peyer's patch, and no strictly $CD4^+$ T cell associated genes were found. The reason for this may lie in the time point chosen for this analysis. As discussed earlier, the first T cells migrate out of the Peyer's patch three days after transplantation, whereas one day later on day 4, the first T cells already enter the intestinal tissue via blood circulation. Therefore, at the time point of the RNAseq analysis, the population of T cells is likely already a mixture between directly egressed cells and those from circulation. Hence, the $CD8^+$ T cell gradient may originate directly from egressed cells or may also represent the T cells that have entered from circulation.

The chemokine receptors expressed near the Peyer's patch included CXCR6, CCR5, CCR7 and CCR9. CXCR6 is expressed on T cells and can be upregulated on neutrophils in inflamed tissue and likely represents their infiltration into this tissue area (Gaida *et al.*, 2008). The frequency of neutrophils in the Peyer's patch lies below 5% (Jung *et al.*, 2010), and although this migration route may also be conceivable for other cell types, the Peyer's patch is not a likely a source of directly migrating neutrophils for the adjacent mucosa. Therefore, $CXCR6^+$ neutrophils would probably have entered the tissue from circulation. CCR5 is an important early inflammatory recruitment receptor on T cells and recognizes CCL3-5, which is secreted primarily by T cells, B cells and monocytes after activation. Since CCL4 is expressed particularly near the Peyer's patch, this may be a mechanism how the egressed T cells recruit cells from circulation and induce a secondary infiltration at this site.

CCR7 is constitutively expressed on naïve T cells and downregulated after activation in secondary lymphoid organs. Although CCR7 was not significantly upregulated near the Peyer's patch, it showed a strong increase in three out of four replicates. This strong expression of CCR7 near the Peyer's patch was unexpected in the light of the hypothesis that activated T cells migrate out of the Peyer's patch, which would likely express CCR7 only at low levels. However, receptor density at the surface is also modulated by internalization and does not necessarily have to correlate with expression levels. Also, other cell types such as dendritic cells upregulate CCR7 after activation to be able to home to the lymphoid organs to present antigen to T cells (Ohl *et al.*, 2004). Therefore, antigen-presenting cells may be another source of CCR7 in the mucosa. Activated B cells can also upregulate CCR7 after activation, but are not a plausible source after irradiation. Furthermore, activated neutrophils can also express CCR7 (Beauvillain *et al.*, 2011).

CCR9 is the classical gut-homing molecule on T cells and B cells, and expression on T cells is high in gastrointestinal GvHD (Beilhack *et al.*, 2008). The increased CCR9

expression near the Peyer's patch may be attributed both to the cells migrating from the Peyer's patch as well as those from circulation.

Surprisingly, we did not find increased expression of the classical gut-homing chemokine CCL25, although immunofluorescence stainings of the mucosa around Peyer's patches showed a marked increase of CCL25 from day 2 to day 4 after allogenic hematopoietic cell transplantation. The epithelium ad mid-height of the villi, and particularly around ileal Peyer's patches including the follicle-associated epithelium expressed marked levels of CCL25 (Annex Figure 7-2). This was counter-intuitive as in the steady state, CCL25 is expressed mainly in the crypts of the proximal intestine (Kunkel *et al.*, 2000; Wurbel *et al.*, 2000). However, the CCL25 gene may be transcribed earlier than when it is presented on the cell surface and picked up by microscopy, therefore, the RNA analysis at this time point may simply miss a difference due to the time point. Therefore, the role of CCL25 for the Peyer's patch egress remains elusive.

The three costimulatory molecules CD27, CD2 and 4-1BB were transcriptionally elevated near the Peyer's patch. CD27 was expressed near the Peyer's patch in GvHD and throughout the whole mucosa in the healthy untreated tissue. In contrast, both CD2 and 4-1BB were expressed only near the Peyer's patch in GvHD and not in the healthy untreated tissue. This means that likely these molecules represent the inflammatory stimulus during GvHD and that potentially these cells acquired a phenotype different to those that populate the intestine in the steady state.

CD27 is upregulated on recently activated T cells and recognizes CD70 expressed on antigen-presenting cells (Watts, 2005). Ligation of CD27 promotes effector T cell survival after activation. Conversely, in GvHD, host-derived CD70 suppresses the donor T cell reaction (Leigh *et al.*, 2017). CD70 is also upregulated on activated alloreactive T cells and limits the T cell response (O'Neill *et al.*, 2017). In contrast, CD70-expressing non-hematopoietic cells in the *lamina propria* provide survival signals to T cells in a *Listeria monocytogenes* infection model (Laouar *et al.*, 2005). Therefore, whether CD27 promotes or dampens the immune response seems to strictly depend on the location (Peyer's patch *vs. lamina propria*) and the type of inflammation. Transcriptional profiling of steady-state intraepithelial lymphocyte and lamina propria lymphocyte populations revealed expression of CD27 in the $CD8^+$ lamina propria lymphocytes population and 4-1BB expression in $CD4^+$ and $CD8^+$ lamina propria lymphocytes (Raine *et al.*, 2014). This speaks for the survival-promoting role of CD27 in homeostasis of the tissue-resident cells in the steady state, which may also play a role for the recently egressed T cells from the Peyer's patch.

4-1BB, like CD27, belongs to the TNF family and was increased near the Peyer's patch, whereas 4-1BB ligand was upregulated throughout the mucosa in GvHD. 4-1BB is expressed on T cells and natural killer cells, whereas the ligand is expressed on antigen-presenting cells. 4-1BB is upregulated after T cell activation and preferentially acts on $CD8^+$ T cells, but can also activate $CD4^+$T cells (Briones *et al.*, 2011). 4-1BB promotes alloreactive T cells in acute GvHD by upregulation of granzyme, perforin, IL-2 and IFNγ (Blazar *et al.*, 2001), but dampens the Th2 response in chronic GvHD (Nozawa *et al.*, 2001). Furthermore, 4-1BB promotes inflammatory bowel disease (Maerten *et al.*, 2004). Since 4-1BB promotes rather a Th1 phenotype, it fits well with the GvHD pathology. Unfortunately, not much is known about the induced effector mechanisms after 4-1BB stimulation, which may hint to a mechanism of Peyer's patch egress.

CD2 belongs to the SLAM family of receptors and expressed on T cells and NK cells. It binds to CD58 in humans which is the homolog for CD48 in mice. Both 4-1BB and CD2 were expressed selectively near the Peyer's patch in GvHD, making them interesting molecules for the sideways migration of the T cells. CD2 can activate T cells in absence of CD28 by promoting TCR-proximal signaling (Hünig *et al.*, 1987; Leitner *et al.*, 2015; Skånland *et al.*, 2014). Many of genes involved in proximal TCR signaling were induced, which speaks for the fact that the cells did not only express CD2, but also received signals through this receptor, which particularly upregulates receptor-proximal signaling molecules when compared to CD28 (Skånland *et al.*, 2014). Costimulation with CD2 induces strong adhesion of T cells as compared to CD28 (Parra *et al.*, 1994), which may be beneficial for migrating cells. CD2 is normally expressed on all T cells, but in the intestine, the majority of CD8αα IEL lacks CD2 expression (Van Houten *et al.*, 1993). The authors claimed that these cells were hyporesponsive to proliferative stimuli. However this may be due to other characteristics of this autoreactive tolerogenic CD8αα population (Qiu *et al.*, 2016) and may not necessarily result directly from the lack of CD2.

The costimulatory molecules upregulated only near the Peyer's patch in GvHD are likely important candidates for initiating this direct migration from the Peyer's patch. It would be interesting to see whether protein levels of the T cells isolated from the Peyer's patch or the surrounding tissue confirm this hypothesis, and whether these cells behave differently in terms of chemoattraction or general migratory properties.

The five most upregulated genes near the Peyer's patches were Cd247 (Cd3ζ), Cd2, Parvg (Parvin γ), Cd27 and Ogdhl (Oxoglutarate Dehydrogenase Like). The first two speak for strong activation of the T cells and emphasize the potential role of alternative

costimulation for the activation and maintenance of these cells. Parvin γ is a central intracellular migratory molecule, and confirms the migratory phenotype of the cells near the Peyer's patch. Ogdhl localizes to the mitochondria, and plays a role in glucose and glutamate utilization, which may be linked to an effector phenotype of the egressed T cells, which are known to utilize glucose to generate ATP rather than oxidative phosphorylation (Nguyen *et al.*, 2018; van der Windt and Pearce, 2012).

To sum up, the T cells near the Peyer's patch likely had a highly activated phenotype and expressed alternative costimulatory molecules. They produced the chemokines XCL-1 and CCL4, which may be involved in secondary recruitment of circulating T cells.

The migratory factors induced in the mucosa and the properties that can likely be attributed to the T cells around the Peyer's patch hint at mechanisms that may attract the T cells from the Peyer's patch to the adjacent *lamina propria*, despite the random migration observed for the egressed T cells. Nevertheless, it still needs to be tested individually what the driving source for the direct egress from Peyer's patch to *lamina propria* is. Furthermore, it will be fundamental to the concept whether these early emigrants are able to attract additional specific or unspecific lymphocytes and therefore serve as seeder cells.

5.7 Conclusion

So far, T cells were considered to enter the small intestine only via extravasation from the blood vessels. Our findings add a second T cell entry route to the intestinal *lamina propria*: a fraction of T cells enters the *lamina propria* directly by migrating from the Peyer's patches. We hypothesize that these cells may be necessary to initiate a fast immune response in specific regions of the small intestine. They are key candidates to recruit additional circulating T cells to the site of inflammation and thereby lead to a secondary strong influx of activated T cells.

This concept would affect treatment strategies against gastrointestinal GvHD, and may provide an answer to the question why it is so difficult to prevent T cell infiltration by only blocking extravasation, even via multiple receptors. Furthermore, intestinal infections and inflammatory bowel diseases such as ulcerative colitis of Crohn's disease may be influenced by this mechanism in a rather non-profitable way. Antigen-specific cells may successfully protect against invaders or harmfully cause pathologies against commensal bacteria or intestinal antigens. However, this direct migration mechanism may also be exploited by smart vaccination strategies targeting the

antigens to the Peyer's patches which may induce a protective local T cell memory close to the prime pathogen entry site. Finally, this direct migration may conceivably play a role in oral tolerance, where induced regulatory T cells subsequently populate the intestinal *lamina propria*.

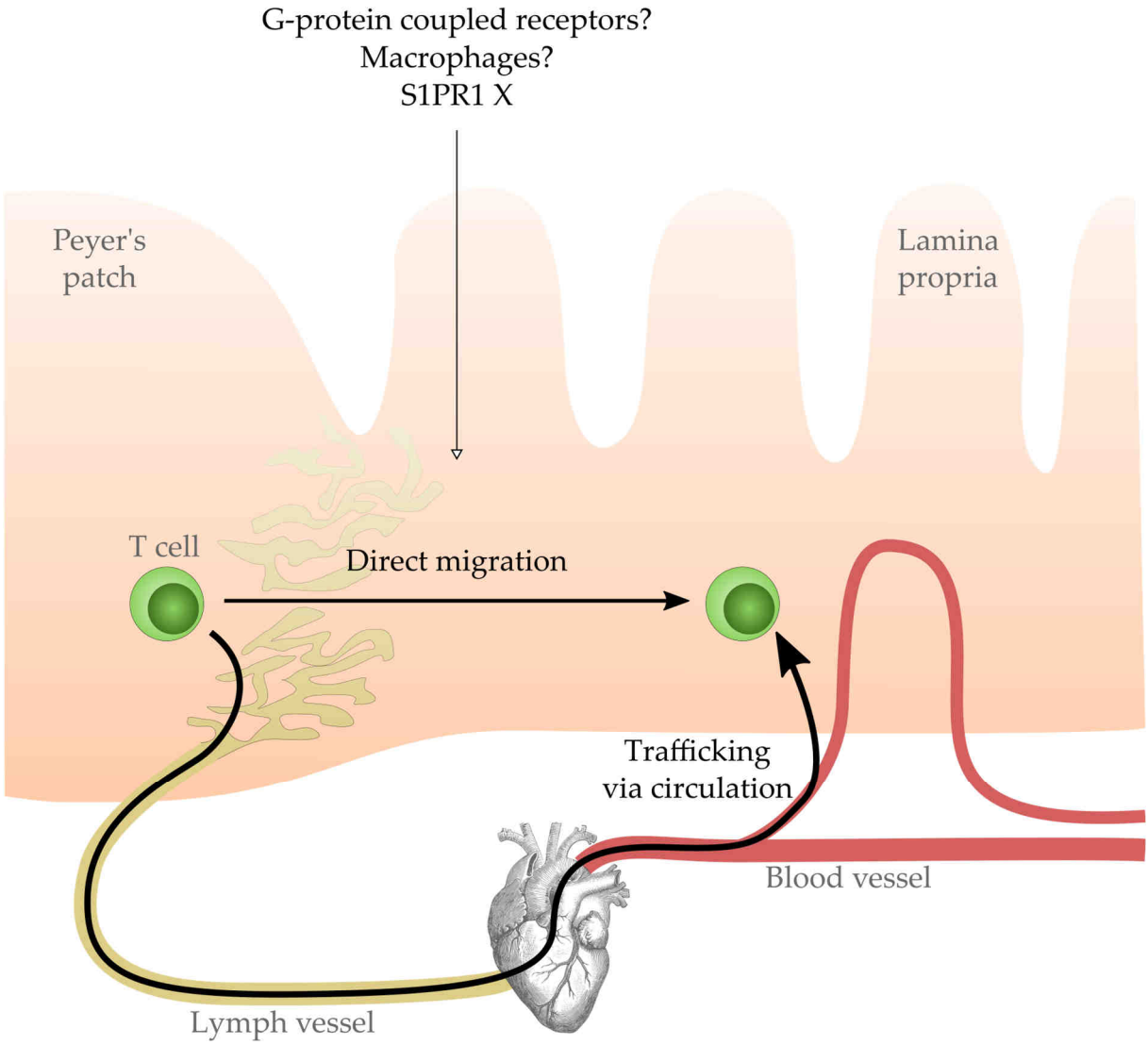

Figure 5-1 Proposed model. T cells traffic from the Peyer's patch to the *lamina propria* via the lymphatics and enter the mucosa from blood vessels. We demonstrated that a small fraction of cells accesses the *lamina propria* adjacent to the Peyer's patch directly by migration inside the tissue. It remains unclear, which mechanism mediates this direct migration. It is unlikely related to S1PR1. Possible candidates fostering direct T cell egress are G-protein coupled receptors, such as chemokine receptors, on T cells responding to soluble environmental cues. Alternatively, stromal-like cells such as tissue-resident macrophages may facilitate the observed T cell migration patterns.

In light of these findings, clinicians and experimentalists may have to revisit the treatments to block or modify cell trafficking to the small intestine. Current strategies that insufficiently block intestinal trafficking may improve by addressing both access routes to the small intestine.

6 References

Annunziato, F., Cosmi, L., Liotta, F., Lazzeri, E., Romagnani, P., Angeli, R., . . . Romagnani, S. (2006). CXCR3 and alphaEbeta7 integrin identify a subset of CD8+ mature thymocytes that share phenotypic and functional properties with CD8+ gut intraepithelial lymphocytes. Gut *55*, 961-968.

Babicki, S., Arndt, D., Marcu, A., Liang, Y., Grant, J.R., Maciejewski, A., and Wishart, D.S. (2016). Heatmapper: web-enabled heat mapping for all. Nucleic acids research *44*, W147-W153.

Baekkevold, E.S., Yamanaka, T., Palframan, R.T., Carlsen, H.S., Reinholt, F.P., von Andrian, U.H., . . . Haraldsen, G. (2001). The Ccr7 Ligand ELC (Ccl19) Is Transcytosed in High Endothelial Venules and Mediates T Cell Recruitment. The Journal of Experimental Medicine *193*, 1105-1112.

Bajénoff, M., Egen, J.G., Koo, L.Y., Laugier, Jean P., Brau, F., Glaichenhaus, N., and Germain, R.N. (2006). Stromal Cell Networks Regulate Lymphocyte Entry, Migration, and Territoriality in Lymph Nodes. Immunity *25*, 989-1001.

Bashir, M., Prietl, B., Tauschmann, M., Mautner, S.I., Kump, P.K., Treiber, G., . . . Pieber, T.R. (2016). Effects of high doses of vitamin D3 on mucosa-associated gut microbiome vary between regions of the human gastrointestinal tract. European journal of nutrition *55*, 1479-1489.

Bäuerlein, C.A., Riedel, S.S., Baker, J., Brede, C., Garrote, A.L., Chopra, M., . . . Beilhack, A. (2013). A diagnostic window for the treatment of acute graft-versus-host disease prior to visible clinical symptoms in a murine model. BMC medicine *11*, 134.

Beauchemin, C., Dixit, N.M., and Perelson, A.S. (2007). Characterizing T Cell Movement within Lymph Nodes in the Absence of Antigen. The Journal of Immunology *178*, 5505-5512.

Beauvillain, C., Cunin, P., Doni, A., Scotet, M., Jaillon, S., Loiry, M.-L., . . . Jeannin, P. (2011). CCR7 is involved in the migration of neutrophils to lymph nodes. Blood *117*, 1196-1204.

Beelen, D., Haralambie, E., Brandt, H., Linzenmeier, G., Muller, K., Quabeck, K., . . . Schaefer, U. (1992). Evidence that sustained growth suppression of intestinal anaerobic bacteria reduces the risk of acute graft-versus-host disease after sibling marrow transplantation. Blood *80*, 2668-2676.

Beilhack, A., and Rockson, S.G. (2003). Immune traffic: a functional overview. Lymphat Res Biol *1*, 219-234.

Beilhack, A., Schulz, S., Baker, J., Beilhack, G.F., Nishimura, R., Baker, E.M., . . . Negrin, R.S. (2008). Prevention of acute graft-versus-host disease by blocking T-cell entry to secondary lymphoid organs. Blood *111*, 2919-2928.

Beilhack, A., Schulz, S., Baker, J., Beilhack, G.F., Wieland, C.B., Herman, E.I., . . . Negrin, R.S. (2005). In vivo analyses of early events in acute graft-versus-host disease reveal sequential infiltration of T-cell subsets. Blood *106*, 1113-1122.

Beltman, J.B., Maree, A.F., Lynch, J.N., Miller, M.J., and de Boer, R.J. (2007). Lymph node topology dictates T cell migration behavior. J Exp Med *204*, 771-780.

Beltman, J.B., Maree, A.F.M., and de Boer, R.J. (2009). Analysing immune cell migration. Nat Rev Immunol *9*, 789-798.

Blazar, B.R., Kwon, B.S., Panoskaltsis-Mortari, A., Kwak, K.B., Peschon, J.J., and Taylor, P.A. (2001). Ligation of 4-1BB (CDw137) Regulates Graft-Versus-Host Disease, Graft-Versus-Leukemia, and Graft Rejection in Allogeneic Bone Marrow Transplant Recipients. The Journal of Immunology *166*, 3174-3183.

Bleakley, M., and Riddell, S.R. (2004). Molecules and mechanisms of the graft-versus-leukaemia effect. Nature Reviews Cancer *4*, 371.

Boissonnas, A., Fetler, L., Zeelenberg, I.S., Hugues, S., and Amigorena, S. (2007). In vivo imaging of cytotoxic T cell infiltration and elimination of a solid tumor. The Journal of Experimental Medicine *204*, 345-356.

Bosgraaf, L., and Van Haastert, P.J.M. (2009). Navigation of Chemotactic Cells by Parallel Signaling to Pseudopod Persistence and Orientation. PLOS ONE *4*, e6842.

Bouazzaoui, A., Spacenko, E., Mueller, G., Miklos, S., Huber, E., Holler, E., . . . Hildebrandt, G.C. (2009). Chemokine and chemokine receptor expression analysis in target organs of acute graft-versus-host disease. Genes And Immunity *10*, 687.

Brede, C., Friedrich, M., Jordan-Garrote, A.L., Riedel, S.S., Bauerlein, C.A., Heinze, K.G., . . . Beilhack, A. (2012). Mapping immune processes in intact tissues at cellular resolution. J Clin Invest *122*, 4439-4446.

Briones, J., Novelli, S., and Sierra, J. (2011). T-Cell Costimulatory Molecules in Acute-Graft-Versus Host Disease: Therapeutic Implications. Bone Marrow Research *2011*.

Browse, N.L., Doig, R.L., and Sizeland, D. (1984). The resistance of a lymph node to lymph flow. The British journal of surgery *71*, 192-196.

Brucklacher-Waldert, V., Carr, E.J., Linterman, M.A., and Veldhoen, M. (2014). Cellular Plasticity of CD4+ T Cells in the Intestine. Frontiers in Immunology *5*.

Campbell, D.J., Kim, C.H., and Butcher, E.C. (2001). Separable effector T cell populations specialized for B cell help or tissue inflammation. Nature immunology *2*, 876.

Caprilli, R. (2008). Why does Crohn's disease usually occur in terminal ileum? Journal of Crohn's and Colitis *2*, 352-356.

Castellino, F., Huang, A.Y., Altan-Bonnet, G., Stoll, S., Scheinecker, C., and Germain, R.N. (2006). Chemokines enhance immunity by guiding naive CD8+ T cells to sites of CD4+ T cell-dendritic cell interaction. Nature *440*, 890-895.

Chattaragada, M.S., Riganti, C., Sassoe, M., Principe, M., Santamorena, M.M., Roux, C., . . . Novelli, F. (2017). FAM49B, a novel regulator of mitochondrial function and integrity that suppresses tumor metastasis. Oncogene *37*, 697.

Chen, Y., Corriden, R., Inoue, Y., Yip, L., Hashiguchi, N., Zinkernagel, A., . . . Junger, W.G. (2006). ATP Release Guides Neutrophil Chemotaxis via P2Y2 and A3 Receptors. Science *314*, 1792-1795.

Cheroutre, H., Lambolez, F., and Mucida, D. (2011). The light and dark sides of intestinal intraepithelial lymphocytes. Nat Rev Immunol *11*, 445-456.

Coelho, F.M., Natale, D., Soriano, S.F., Hons, M., Swoger, J., Mayer, J., . . . Stein, J.V. (2013). Naive B-cell trafficking is shaped by local chemokine availability and LFA-1–independent stromal interactions. Blood *121*, 4101-4109.

Coghill, J.M., Sarantopoulos, S., Moran, T.P., Murphy, W.J., Blazar, B.R., and Serody, J.S. (2011). Effector CD4⁺ T cells, the cytokines they generate, and GVHD: something old and something new. Blood *117*, 3268-3276.

Coombes, J.L., Siddiqui, K.R., Arancibia-Carcamo, C.V., Hall, J., Sun, C.M., Belkaid, Y., and Powrie, F. (2007). A functionally specialized population of mucosal CD103+ DCs induces Foxp3+ regulatory T cells via a TGF-beta and retinoic acid-dependent mechanism. J Exp Med *204*, 1757-1764.

Cornes, J.S. (1965). Number, size, and distribution of Peyer's patches in the human small intestine: Part I The development of Peyer's patches. Gut *6*, 225-229.

Counsell, B. (1956). Lesions of the ileum associated with ulcerative colitis. BJS *44*, 276-290.

Cyster, J.G. (1999). Chemokines and the homing of dendritic cells to the T cell areas of lymphoid organs. The Journal of experimental medicine *189*, 447-450.

Cyster, J.G., and Schwab, S.R. (2012). Sphingosine-1-phosphate and lymphocyte egress from lymphoid organs. Annu Rev Immunol *30*, 69-94.

Daneshpouy, M., Socie, G., Lemann, M., Rivet, J., Gluckman, E., and Janin, A. (2002). Activated eosinophils in upper gastrointestinal tract of patients with graft-versus-host disease. Blood *99*, 3033-3040.

DeFilipp, Z., Peled, J.U., Li, S., Mahabamunuge, J., Dagher, Z., Slingerland, A.E., . . . Chen, Y.-B. (2018). Third-party fecal microbiota transplantation following allo-HCT reconstitutes microbiome diversity. Blood advances *2*, 745-753.

Dustin, M.L., Rothlein, R., Bhan, A.K., Dinarello, C.A., and Springer, T.A. (1986). Induction by IL 1 and interferon-gamma: tissue distribution, biochemistry, and function of a natural adherence molecule (ICAM-1). The Journal of Immunology *137*, 245-254.

Eickhoff, S., Brewitz, A., Gerner, Michael Y., Klauschen, F., Komander, K., Hemmi, H., . . . Kastenmüller, W. (2015). Robust Anti-viral Immunity Requires Multiple Distinct T Cell-Dendritic Cell Interactions. Cell *162*, 1322-1337.

Fang, V., Chaluvadi, V.S., Ramos-Perez, W.D., Mendoza, A., Baeyens, A., Rivera, R., . . . Schwab, S.R. (2016). Gradients of the signaling lipid S1P in lymph nodes position natural killer cells and regulate their interferon-γ response. Nature immunology *18*, 15.

Ferrara, J.L.M., Levine, J.E., Reddy, P., and Holler, E. (2009). Graft-versus-host disease. The Lancet *373*, 1550-1561.

Förster, R., Schubel, A., Breitfeld, D., Kremmer, E., Renner-Müller, I., Wolf, E., and Lipp, M. (1999). CCR7 Coordinates the Primary Immune Response by Establishing Functional Microenvironments in Secondary Lymphoid Organs. Cell *99*, 23-33.

Fu, H., Ward, E.J., and Marelli-Berg, F.M. (2016). Mechanisms of T cell organotropism. Cellular and Molecular Life Sciences *73*, 3009-3033.

Fürth, R. (1920). Die Brownsche Bewegung bei Berücksichtigung einer Persistenz der Bewegungsrichtung. Mit Anwendungen auf die Bewegung lebender Infusorien. Zeitschrift für Physik *2*, 244-256.

Gaida, M.M., Günther, F., Wagner, C., Friess, H., Giese, N.A., Schmidt, J., . . . Wente, M.N. (2008). Expression of the CXCR6 on polymorphonuclear neutrophils in pancreatic carcinoma and in acute, localized bacterial infections. Clinical and experimental immunology *154*, 216-223.

Garlanda, C., Dinarello, Charles A., and Mantovani, A. (2013). The Interleukin-1 Family: Back to the Future. Immunity *39*, 1003-1018.

Geem, D., Medina-Contreras, O., Kim, W., Huang, C.S., and Denning, T.L. (2012). Isolation and Characterization of Dendritic Cells and Macrophages from the Mouse Intestine. Journal of Visualized Experiments : JoVE, 4040.

Gérard, A., Patino-Lopez, G., Beemiller, P., Nambiar, R., Ben-Aissa, K., Liu, Y., . . . Krummel, M.F. (2014). Detection of rare antigen-presenting cells through T cell-intrinsic meandering motility, mediated by Myo1g. Cell *158*, 492-505.

Glucksberg, H., Storb, R., Fefer, A., Buckner, C.D., Neiman, P.E., Clift, R.A., . . . Thomas, E.D. (1974). Clinical manifestations of graft-versus-host disease in human recipients of marrow from HL-A-matched sibling donors. Transplantation *18*, 295-304.

Gooley, T.A., Chien, J.W., Pergam, S.A., Hingorani, S., Sorror, M.L., Boeckh, M., . . . McDonald, G.B. (2010). Reduced Mortality after Allogeneic Hematopoietic-Cell Transplantation. New England Journal of Medicine *363*, 2091-2101.

Göppert-Mayer, M. (1931). Über Elementarakte mit zwei Quantensprüngen. Annalen der Physik *401*, 273-294.

Gorfu, G., Rivera-Nieves, J., and Ley, K. (2009). Role of beta7 integrins in intestinal lymphocyte homing and retention. Current molecular medicine *9*, 836-850.

Graubert, T.A., DiPersio, J.F., Russell, J.H., and Ley, T.J. (1997). Perforin/granzyme-dependent and independent mechanisms are both important for the development of graft-versus-host disease after murine bone marrow transplantation. J Clin Invest *100*, 904-911.

Grigorova, I.L., Panteleev, M., and Cyster, J.G. (2010). Lymph node cortical sinus organization and relationship to lymphocyte egress dynamics and antigen exposure. Proc Natl Acad Sci U S A *107*, 20447-20452.

Grigorova, I.L., Schwab, S.R., Phan, T.G., Pham, T.H.M., Okada, T., and Cyster, J.G. (2008). Cortical sinus probing, S1P1-dependent entry and flow-based capture of egressing T cells. Nature Immunology *10*, 58.

Grigorova, I.L., Schwab, S.R., Phan, T.G., Pham, T.H.M., Okada, T., and Cyster, J.G. (2009). Cortical sinus probing, S1P1-dependent entry and flow-based capture of egressing T cells. Nature immunology *10*, 58.

Gross, M., Salame, T.-M., and Jung, S. (2015). Guardians of the Gut – Murine Intestinal Macrophages and Dendritic Cells. Frontiers in Immunology *6*.

Gunn, M.D., Tangemann, K., Tam, C., Cyster, J.G., Rosen, S.D., and Williams, L.T. (1998). A chemokine expressed in lymphoid high endothelial venules promotes the adhesion and chemotaxis of naive T lymphocytes. Proceedings of the National Academy of Sciences *95*, 258-263.

Habtezion, A., Nguyen, L.P., Hadeiba, H., and Butcher, E.C. (2016). Leukocyte Trafficking to the Small Intestine and Colon. Gastroenterology *150*, 340-354.

Halin, C., Scimone, M.L., Bonasio, R., Gauguet, J.-M., Mempel, T.R., Quackenbush, E., . . . von Andrian, U.H. (2005). The S1P-analog FTY720 differentially modulates T-cell homing via HEV: T-cell–expressed S1P1 amplifies integrin activation in peripheral lymph nodes but not in Peyer patches. Blood *106*, 1314-1322.

Hällgren, R., Colombel, J.F., Dahl, R., Fredens, K., Kruse, A., Jacobsen, N.O., . . . Rambaud, J.C. (1989). Neutrophil and eosinophil involvement of the small bowel in patients with celiac disease and Crohn's disease: Studies on the secretion rate and immunohistochemical localization of granulocyte granule constituents. The American journal of medicine *86*, 56-64.

Hamada, H., Hiroi, T., Nishiyama, Y., Takahashi, H., Masunaga, Y., Hachimura, S., . . . Ishikawa, H. (2002). Identification of Multiple Isolated Lymphoid Follicles on the Antimesenteric Wall of the Mouse Small Intestine. The Journal of Immunology *168*, 57-64.

Hammerschmidt, S.I., Ahrendt, M., Bode, U., Wahl, B., Kremmer, E., Forster, R., and Pabst, O. (2008). Stromal mesenteric lymph node cells are essential for the generation of gut-homing T cells in vivo. J Exp Med *205*, 2483-2490.

Hansson, G.C. (2012). Role of mucus layers in gut infection and inflammation. Current opinion in microbiology *15*, 57-62.

Harris, T.H., Banigan, E.J., Christian, D.A., Konradt, C., Tait Wojno, E.D., Norose, K., . . . Hunter, C.A. (2012). Generalized Lévy walks and the role of chemokines in migration of effector CD8+ T cells. Nature *486*, 545.

Harrison, O.J., and Powrie, F.M. (2013). Regulatory T cells and immune tolerance in the intestine. Cold Spring Harbor perspectives in biology *5*, a018341.

Hartrampf, S., Dudakov, J.A., Johnson, L.K., Smith, O.M., Tsai, J., Singer, N.V., . . . van den Brink, M.R.M. (2013). The central nervous system is a target of acute graft versus host disease in mice. Blood *121*, 1906-1910.

Hashizume, T., Togawa, A., Nochi, T., Igarashi, O., Kweon, M.-N., Kiyono, H., and Yamamoto, M. (2008). Peyer's Patches Are Required for Intestinal Immunoglobulin A Responses to Salmonella spp. Infection and Immunity *76*, 927-934.

Higgins, J.M., Mandlebrot, D.A., Shaw, S.K., Russell, G.J., Murphy, E.A., Chen, Y.T., . . . Brenner, M.B. (1998). Direct and regulated interaction of integrin alphaEbeta7 with E-cadherin. J Cell Biol *140*, 197-210.

Hill, L., Alousi, A., Kebriaei, P., Mehta, R., Rezvani, K., and Shpall, E. (2018). New and emerging therapies for acute and chronic graft versus host disease. Therapeutic Advances in Hematology *9*, 21-46.

Hobsley, M., and Tovey, F.I. (2001). Helicobacter pylori: the primary cause of duodenal ulceration or a secondary infection? World Journal of Gastroenterology *7*, 149-151.

Hogan, S.P., Seidu, L., Blanchard, C., Groschwitz, K., Mishra, A., Karow, M.L., . . . Rothenberg, M.E. (2006). Resistin-like molecule beta regulates innate colonic function: barrier integrity and inflammation susceptibility. The Journal of allergy and clinical immunology *118*, 257-268.

Hons, M., Kopf, A., Hauschild, R., Leithner, A., Gaertner, F., Abe, J., . . . Sixt, M. (2018). Chemokines and integrins independently tune actin flow and substrate friction during intranodal migration of T cells. Nature immunology *19*, 606-616.

Hulsdunker, J., Ottmuller, K.J., Neeff, H.P., Koyama, M., Gao, Z., Thomas, O.S., . . . Zeiser, R. (2018). Neutrophils provide cellular communication between ileum and mesenteric lymph nodes at graft-versus-host disease onset. Blood *131*, 1858-1869.

Hünig, T., Tiefenthaler, G., zum Büschenfelde, K.H.M., and Meuer, S.C. (1987). Alternative pathway activation of T cells by binding of CD2 to its cell-surface ligand. Nature *326*, 298.

Iwata, M., Hirakiyama, A., Eshima, Y., Kagechika, H., Kato, C., and Song, S.-Y. (2004). Retinoic Acid Imprints Gut-Homing Specificity on T Cells. Immunity *21*, 527-538.

Jacobelli, J., Bennett, F.C., Pandurangi, P., Tooley, A.J., and Krummel, M.F. (2009). Myosin-IIA and ICAM-1 Regulate the Interchange between Two Distinct Modes of T Cell Migration. The Journal of Immunology *182*, 2041-2050.

Jarick, K.J., Mokhtari, Z., Scheller, L., Hartweg, J., Thusek, S., Le, D.-D., . . . Beilhack, A. (2018). Photoconversion of Alloreactive T Cells in Murine Peyer's Patches During Acute Graft-Versus-Host Disease: Tracking the Homing Route of Highly Proliferative Cells In Vivo. Frontiers in Immunology *9*.

Jenq, R.R., Taur, Y., Devlin, S.M., Ponce, D.M., Goldberg, J.D., Ahr, K.F., . . . van den Brink, M.R. (2015). Intestinal Blautia Is Associated with Reduced Death from Graft-versus-Host Disease. Biology of blood and marrow transplantation : journal of the American Society for Blood and Marrow Transplantation *21*, 1373-1383.

Johnsen, S., and Widder, E.A. (1999). The physical basis of transparency in biological tissue: ultrastructure and the minimization of light scattering. J Theor Biol *199*, 181-198.

Jose, P.J., Griffiths-Johnson, D.A., Collins, P.D., Walsh, D.T., Moqbel, R., Totty, N.F., . . . Williams, T.J. (1994). Eotaxin: a potent eosinophil chemoattractant cytokine detected in a guinea pig model of allergic airways inflammation. The Journal of Experimental Medicine *179*, 881-887.

Jung, C., Hugot, J.P., and Barreau, F. (2010). Peyer's Patches: The Immune Sensors of the Intestine. International journal of inflammation *2010*, 823710.

Jung, U., Bullard, D.C., Tedder, T.F., and Ley, K. (1996). Velocity differences between L- and P-selectin-dependent neutrophil rolling in venules of mouse cremaster muscle in vivo. The American journal of physiology *271*, H2740-2747.

Kadivar, M., Petersson, J., Svensson, L., and Marsal, J. (2016). CD8alphabeta+ gammadelta T Cells: A Novel T Cell Subset with a Potential Role in Inflammatory Bowel Disease. J Immunol *197*, 4584-4592.

Kalaycioglu, M.E., and Bolwell, B.J. (1994). Eosinophilia after allogeneic bone marrow transplantation using the busulfan and cyclophosphamide preparative regimen. Bone marrow transplantation *14*, 113-115.

Kastenmuller, W., Brandes, M., Wang, Z., Herz, J., Egen, J.G., and Germain, R.N. (2013). Peripheral prepositioning and local CXCL9 chemokine-mediated guidance orchestrate rapid memory CD8+ T cell responses in the lymph node. Immunity *38*, 502-513.

Katakai, T., Habiro, K., and Kinashi, T. (2013). Dendritic cells regulate high-speed interstitial T cell migration in the lymph node via LFA-1/ICAM-1. J Immunol *191*, 1188-1199.

Katakai, T., Hara, T., Sugai, M., Gonda, H., and Shimizu, A. (2004). Lymph Node Fibroblastic Reticular Cells Construct the Stromal Reticulum via Contact with Lymphocytes. The Journal of Experimental Medicine *200*, 783-795.

Katakai, T., and Kinashi, T. (2016). Microenvironmental Control of High-Speed Interstitial T Cell Migration in the Lymph Node. Frontiers in Immunology *7*, 194.

Kim, S.V., Xiang, W.V., Kwak, C., Yang, Y., Lin, X.W., Ota, M., . . . Littman, D.R. (2013). GPR15-mediated homing controls immune homeostasis in the large intestine mucosa. Science *340*, 1456-1459.

Krummel, M.F., Bartumeus, F., and Gérard, A. (2016). T cell migration, search strategies and mechanisms. Nature Reviews Immunology *16*, 193.

Kuhn, K.A., and Stappenbeck, T.S. (2013). Peripheral education of the immune system by the colonic microbiota. Seminars in immunology *25*, 364-369.

Kunkel, E.J., Campbell, J.J., Haraldsen, G., Pan, J., Boisvert, J., Roberts, A.I., . . . Agace, W.W. (2000). Lymphocyte CC chemokine receptor 9 and epithelial thymus-expressed chemokine (TECK) expression distinguish the small intestinal immune compartment: Epithelial expression of tissue-specific chemokines as an organizing principle in regional immunity. J Exp Med *192*, 761-768.

Lammermann, T., Bader, B.L., Monkley, S.J., Worbs, T., Wedlich-Soldner, R., Hirsch, K., . . . Sixt, M. (2008). Rapid leukocyte migration by integrin-independent flowing and squeezing. Nature *453*, 51-55.

Lane, T.A., Lamkin, G.E., and Wancewicz, E. (1989). Modulation of endothelial cell expression of intercellular adhesion molecule 1 by protein kinase c activation. Biochemical and Biophysical Research Communications *161*, 945-952.

Laouar, A., Haridas, V., Vargas, D., Zhinan, X., Chaplin, D., van Lier, R.A., and Manjunath, N. (2005). CD70+ antigen-presenting cells control the proliferation and differentiation of T cells in the intestinal mucosa. Nature immunology *6*, 698-706.

Lavagnino, Z., Sancataldo, G., d'Amora, M., Follert, P., De Pietri Tonelli, D., Diaspro, A., and Cella Zanacchi, F. (2016). 4D (x-y-z-t) imaging of thick biological samples by means of Two-Photon inverted Selective Plane Illumination Microscopy (2PE-iSPIM). Scientific Reports *6*, 23923.

Leigh, N.D., O'Neill, R.E., Du, W., Chen, C., Qiu, J., Ashwell, J.D., . . . Cao, X. (2017). Host-Derived CD70 Suppresses Murine Graft-versus-Host Disease by Limiting Donor T Cell Expansion and Effector Function. J Immunol *199*, 336-347.

Leishman, A.J., Gapin, L., Capone, M., Palmer, E., MacDonald, H.R., Kronenberg, M., and Cheroutre, H. (2002). Precursors of functional MHC class I- or class II-restricted CD8alphaalpha(+) T cells are positively selected in the thymus by agonist self-peptides. Immunity *16*, 355-364.

Leitner, J., Herndler-Brandstetter, D., Zlabinger, G.J., Grubeck-Loebenstein, B., and Steinberger, P. (2015). CD58/CD2 Is the Primary Costimulatory Pathway in Human CD28[−]CD8⁺ T Cells. The Journal of Immunology *195*, 477-487.

Ley, K., Bullard, D.C., Arbones, M.L., Bosse, R., Vestweber, D., Tedder, T.F., and Beaudet, A.L. (1995). Sequential contribution of L- and P-selectin to leukocyte rolling in vivo. J Exp Med *181*, 669-675.

Ley, K., Laudanna, C., Cybulsky, M.I., and Nourshargh, S. (2007). Getting to the site of inflammation: the leukocyte adhesion cascade updated. Nature Reviews Immunology *7*, 678.

Li, L., Nørrelykke, S.F., and Cox, E.C. (2008). Persistent cell motion in the absence of external signals: a search strategy for eukaryotic cells. PloS one *3*, e2093-e2093.

Lindquist, R.L., Shakhar, G., Dudziak, D., Wardemann, H., Eisenreich, T., Dustin, M.L., and Nussenzweig, M.C. (2004). Visualizing dendritic cell networks in vivo. Nature immunology *5*, 1243.

Liu, Y.-J., Le Berre, M., Lautenschlaeger, F., Maiuri, P., Callan-Jones, A., Heuzé, M., . . . Piel, M. (2015). Confinement and Low Adhesion Induce Fast Amoeboid Migration of Slow Mesenchymal Cells. Cell *160*, 659-672.

Lo, C.-M., Wang, H.-B., Dembo, M., and Wang, Y.-l. (2000). Cell Movement Is Guided by the Rigidity of the Substrate. Biophysical journal *79*, 144-152.

Luckey, A., Livingston, E., and Taché, Y. (2003). Mechanisms and treatment of postoperative ileus. Archives of Surgery *138*, 206-214.

MacMillan, M.L., Weisdorf, D.J., Wagner, J.E., DeFor, T.E., Burns, L.J., Ramsay, N.K.C., . . . Blazar, B.R. (2002). Response of 443 patients to steroids as primary therapy for acute graft-versus-host disease: Comparison of grading systems. Biology of Blood and Marrow Transplantation *8*, 387-394.

Macpherson, A.J., and Smith, K. (2006). Mesenteric lymph nodes at the center of immune anatomy. J Exp Med *203*, 497-500.

Maeda, Y., Levy, R.B., Reddy, P., Liu, C., Clouthier, S.G., Teshima, T., and Ferrara, J.L. (2005). Both perforin and Fas ligand are required for the regulation of alloreactive CD8+ T cells during acute graft-versus-host disease. Blood *105*, 2023-2027.

Maerten, P., Geboes, K., De Hertogh, G., Shen, C., Cadot, P., Bullens, D.M., . . . Ceuppens, J.L. (2004). Functional expression of 4-1BB (CD137) in the inflammatory tissue in Crohn's disease. Clinical immunology *112*, 239-246.

Maiuri, P., Rupprecht, J.-F., Wieser, S., Ruprecht, V., Bénichou, O., Carpi, N., . . . Voituriez, R. (2015). Actin Flows Mediate a Universal Coupling between Cell Speed and Cell Persistence. Cell *161*, 374-386.

Masopust, D., Choo, D., Vezys, V., Wherry, E.J., Duraiswamy, J., Akondy, R., . . . Ahmed, R. (2010). Dynamic T cell migration program provides resident memory within intestinal epithelium. J Exp Med *207*, 553-564.

Matheu, M.P., Beeton, C., Garcia, A., Chi, V., Rangaraju, S., Safrina, O., . . . Cahalan, M.D. (2008). Imaging of Effector Memory T Cells during a Delayed-Type Hypersensitivity Reaction and Suppression by Kv1.3 Channel Block. Immunity *29*, 602-614.

Matloubian, M., Lo, C.G., Cinamon, G., Lesneski, M.J., Xu, Y., Brinkmann, V., . . . Cyster, J.G. (2004). Lymphocyte egress from thymus and peripheral lymphoid organs is dependent on S1P receptor 1. Nature *427*, 355-360.

McDole, J.R., Wheeler, L.W., McDonald, K.G., Wang, B., Konjufca, V., Knoop, K.A., . . . Miller, M.J. (2012). Goblet cells deliver luminal antigen to CD103+ dendritic cells in the small intestine. Nature *483*, 345-349.

Mempel, T.R., Henrickson, S.E., and von Andrian, U.H. (2004). T-cell priming by dendritic cells in lymph nodes occurs in three distinct phases. Nature *427*, 154.

Michonneau, D., Sagoo, P., Breart, B., Garcia, Z., Celli, S., and Bousso, P. (2016). The PD-1 Axis Enforces an Anatomical Segregation of CTL Activity that Creates Tumor Niches after Allogeneic Hematopoietic Stem Cell Transplantation. Immunity *44*, 143-154.

Middleton, J., Neil, S., Wintle, J., Clark-Lewis, I., Moore, H., Lam, C., . . . Rot, A. (1997). Transcytosis and Surface Presentation of IL-8 by Venular Endothelial Cells. Cell *91*, 385-395.

Miller, M.J., Wei, S.H., Parker, I., and Cahalan, M.D. (2002). Two-photon imaging of lymphocyte motility and antigen response in intact lymph node. Science *296*, 1869-1873.

Mionnet, C., Sanos, S.L., Mondor, I., Jorquera, A., Laugier, J.-P., Germain, R.N., and Bajénoff, M. (2011). High endothelial venules as traffic control points maintaining lymphocyte population homeostasis in lymph nodes. Blood *118*, 6115-6122.

Mirenda, V., Jarmin, S.J., David, R., Dyson, J., Scott, D., Gu, Y., . . . Marelli-Berg, F.M. (2007). Physiologic and aberrant regulation of memory T-cell trafficking by the costimulatory molecule CD28. Blood *109*, 2968-2977.

Mokhtari, Z., Mech, F., Zitzmann, C., Hasenberg, M., Gunzer, M., and Figge, M.T. (2013). Automated characterization and parameter-free classification of cell tracks based on local migration behavior. PLoS One *8*, e80808.

Moreau, H.D., Lemaître, F., Garrod, K.R., Garcia, Z., Lennon-Duménil, A.-M., and Bousso, P. (2015). Signal strength regulates antigen-mediated T-cell deceleration by distinct mechanisms to promote local exploration or arrest. Proceedings of the National Academy of Sciences *112*, 12151-12156.

Mowat, A.M., and Agace, W.W. (2014). Regional specialization within the intestinal immune system. Nature Reviews Immunology *14*, 667.

Moy, R.H., Huffman, A.P., Richman, L.P., Crisalli, L., Wang, X.K., Hoxie, J.A., . . . Reshef, R. (2017). Clinical and immunologic impact of CCR5 blockade in graft-versus-host disease prophylaxis. Blood *129*, 906-916.

Mrass, P., Petravic, J., Davenport, M.P., and Weninger, W. (2010). Cell-autonomous and environmental contributions to the interstitial migration of T cells. Seminars in immunopathology *32*, 257-274.

Mueller, S.N., Hosiawa-Meagher, K.A., Konieczny, B.T., Sullivan, B.M., Bachmann, M.F., Locksley, R.M., . . . Matloubian, M. (2007). Regulation of Homeostatic Chemokine Expression and Cell Trafficking During Immune Responses. Science (New York, NY) *317*, 670-674.

Muller, W.A. (2011). Mechanisms of leukocyte transendothelial migration. Annual review of pathology *6*, 323-344.

Murai, M., Yoneyama, H., Ezaki, T., Suematsu, M., Terashima, Y., Harada, A., . . . Matsushima, K. (2003). Peyer's patch is the essential site in initiating murine acute and lethal graft-versus-host reaction. Nature immunology *4*, 154.

Muriglan, S.J., Ramirez-Montagut, T., Alpdogan, O., Van Huystee, T.W., Eng, J.M., Hubbard, V.M., . . . Van Den Brink, M.R.M. (2004). GITR activation induces an opposite effect on alloreactive CD4(+) and CD8(+) T cells in graft-versus-host disease. The Journal of experimental medicine *200*, 149-157.

Murphy, K.M., and Weaver, C. (2016). Janeway's immunobiology, 9th edition edn (New York, NY: Garland Science/Taylor & Francis Group, LLC).

Nestel, F.P., Price, K.S., Seemayer, T.A., and Lapp, W.S. (1992). Macrophage priming and lipopolysaccharide-triggered release of tumor necrosis factor alpha during graft-versus-host disease. The Journal of Experimental Medicine *175*, 405-413.

Ng, L.G., Hsu, A., Mandell, M.A., Roediger, B., Hoeller, C., Mrass, P., . . . Weninger, W. (2008). Migratory Dermal Dendritic Cells Act as Rapid Sensors of Protozoan Parasites. PLoS pathogens *4*, e1000222.

Nguyen, H.D., Kuril, S., Bastian, D., and Yu, X.-Z. (2018). T-Cell Metabolism in Hematopoietic Cell Transplantation. Frontiers in Immunology *9*.

Nguyen, L.P., Pan, J., Dinh, T.T., Hadeiba, H., O'Hara, E., 3rd, Ebtikar, A., . . . Habtezion, A. (2015). Role and species-specific expression of colon T cell homing receptor GPR15 in colitis. Nature immunology *16*, 207-213.

Nowarski, R., Jackson, R., and Flavell, R.A. (2017). The Stromal Intervention: Regulation of Immunity and Inflammation at the Epithelial-Mesenchymal Barrier. Cell *168*, 362-375.

Nozawa, K., Ohata, J., Sakurai, J., Hashimoto, H., Miyajima, H., Yagita, H., . . . Azuma, M. (2001). Preferential Blockade of CD8⁺ T Cell Responses by Administration of Anti-CD137 Ligand Monoclonal Antibody Results in Differential Effect on Development of Murine Acute and Chronic Graft-Versus-Host Diseases. The Journal of Immunology *167*, 4981-4986.

O'Neill, R.E., Du, W., Mohammadpour, H., Alqassim, E., Qiu, J., Chen, G., . . . Cao, X. (2017). T Cell-Derived CD70 Delivers an Immune Checkpoint Function in Inflammatory T Cell Responses. J Immunol *199*, 3700-3710.

Ohl, L., Mohaupt, M., Czeloth, N., Hintzen, G., Kiafard, Z., Zwirner, J., . . . Förster, R. (2004). CCR7 Governs Skin Dendritic Cell Migration under Inflammatory and Steady-State Conditions. Immunity *21*, 279-288.

Ohta, T., Sugiyama, M., Hemmi, H., Yamazaki, C., Okura, S., Sasaki, I., . . . Kaisho, T. (2016). Crucial roles of XCR1-expressing dendritic cells and the XCR1-XCL1 chemokine axis in intestinal immune homeostasis. Scientific Reports *6*, 23505.

Okada, T., Miller, M.J., Parker, I., Krummel, M.F., Neighbors, M., Hartley, S.B., . . . Cyster, J.G. (2005). Antigen-engaged B cells undergo chemotaxis toward the T zone and form motile conjugates with helper T cells. PLoS biology *3*, e150-e150.

Okada, T., Ngo, V.N., Ekland, E.H., Förster, R., Lipp, M., Littman, D.R., and Cyster, J.G. (2002). Chemokine Requirements for B Cell Entry to Lymph Nodes and Peyer's Patches. The Journal of Experimental Medicine *196*, 65-75.

Overstreet, M.G., Gaylo, A., Angermann, B.R., Hughson, A., Hyun, Y.-M., Lambert, K., . . . Fowell, D.J. (2013). Inflammation-induced interstitial migration of effector CD4+ T cells is dependent on integrin αV. Nature immunology *14*, 949.

Pabst, O., Herbrand, H., Worbs, T., Friedrichsen, M., Yan, S., Hoffmann, M.W., . . . Forster, R. (2005). Cryptopatches and isolated lymphoid follicles: dynamic lymphoid tissues dispensable for the generation of intraepithelial lymphocytes. European journal of immunology *35*, 98-107.

Paluch, E.K., Aspalter, I.M., and Sixt, M. (2016). Focal Adhesion–Independent Cell Migration. Annual review of cell and developmental biology *32*, 469-490.

Parra, E., Wingren, A.G., Hedlund, G., Björklund, M., Sjögren, H.O., Kalland, T., . . . Dohlsten, M. (1994). Costimulation of human CD4+ T lymphocytes with B7 and lymphocyte function-associated antigen-3 results in distinct cell activation profiles. The Journal of Immunology *153*, 2479-2487.

Pham, T.H., Okada, T., Matloubian, M., Lo, C.G., and Cyster, J.G. (2008). S1P1 receptor signaling overrides retention mediated by G alpha i-coupled receptors to promote T cell egress. Immunity *28*, 122-133.

Pober, J.S., Lapierre, L.A., Stolpen, A.H., Brock, T.A., Springer, T.A., Fiers, W., . . . Gimbrone, M.A. (1987). Activation of cultured human endothelial cells by recombinant lymphotoxin: comparison with tumor necrosis factor and interleukin 1 species. The Journal of Immunology *138*, 3319-3324.

Pospischil, A. (1989). Struktur und Funktion von Peyer'schen Platten im Darm verschiedener Tierarten. Schweiz Arch Tierheilk *131*, 595-603.

Przepiorka, D., Weisdorf, D., Martin, P., Klingemann, H.G., Beatty, P., Hows, J., and Thomas, E.D. (1995). 1994 Consensus Conference on Acute GVHD Grading. Bone marrow transplantation *15*, 825-828.

Qiu, Y., Peng, K., Liu, M., Xiao, W., and Yang, H. (2016). CD8alphaalpha TCRalphabeta Intraepithelial Lymphocytes in the Mouse Gut. Dig Dis Sci *61*, 1451-1460.

Raine, T., Liu, J.Z., Anderson, C.A., Parkes, M., and Kaser, A. (2014). Generation of primary human intestinal T cell transcriptomes reveals differential expression at genetic risk loci for immune-mediated disease. Gut.

Rastogi, R.P., Richa, Kumar, A., Tyagi, M.B., and Sinha, R.P. (2010). Molecular Mechanisms of Ultraviolet Radiation-Induced DNA Damage and Repair. Journal of Nucleic Acids *2010*.

Reboldi, A., and Cyster, J.G. (2016). Peyer's patches: organizing B-cell responses at the intestinal frontier. Immunological Reviews *271*, 230-245.

Reig, G., Pulgar, E., and Concha, M.L. (2014). Cell migration: from tissue culture to embryos. Development *141*, 1999-2013.

Röhrl, J., Yang, D., Oppenheim, J.J., and Hehlgans, T. (2010). Human β-Defensin 2 and 3 and Their Mouse Orthologs Induce Chemotaxis through Interaction with CCR2. The Journal of Immunology *184*, 6688-6694.

Ruggiu, M., Cuccuini, W., Mokhtari, K., Meignin, V., Peffault de Latour, R., Robin, M., . . . Michonneau, D. (2017). Case report: Central nervous system involvement of human graft versus host disease: Report of 7 cases and a review of literature. Medicine *96*, e8303.

Sallusto, F., Lenig, D., Förster, R., Lipp, M., and Lanzavecchia, A. (1999). Two subsets of memory T lymphocytes with distinct homing potentials and effector functions. Nature *401*, 708.

Schmidt, T.H., Bannard, O., Gray, E.E., and Cyster, J.G. (2013). CXCR4 promotes B cell egress from Peyer's patches. J Exp Med *210*, 1099-1107.

Schreder, A., Moschovakis, G.L., Halle, S., Schlue, J., Lee, C.-W., Schippers, A., . . . Koenecke, C. (2015). Differential Effects of Gut-Homing Molecules CC Chemokine Receptor 9 and Integrin-β7 during Acute Graft-versus-Host Disease of the Liver. Biology of Blood and Marrow Transplantation *21*, 2069-2078.

Schroeder, M.A., and DiPersio, J.F. (2011). Mouse models of graft-versus-host disease: advances and limitations. Disease models & mechanisms *4*, 318-333.

Schumann, K., Lammermann, T., Bruckner, M., Legler, D.F., Polleux, J., Spatz, J.P., . . . Sixt, M. (2010). Immobilized chemokine fields and soluble chemokine gradients cooperatively shape migration patterns of dendritic cells. Immunity *32*, 703-713.

Schwarz, J., Bierbaum, V., Vaahtomeri, K., Hauschild, R., Brown, M., de Vries, I., . . . Sixt, M. (2017). Dendritic Cells Interpret Haptotactic Chemokine Gradients in a Manner Governed by Signal-to-Noise Ratio and Dependent on GRK6. Current Biology *27*, 1314-1325.

Shallis, R.M., Terry, C.M., and Lim, S.H. (2018). Changes in intestinal microbiota and their effects on allogeneic stem cell transplantation. American journal of hematology *93*, 122-128.

Shamri, R., Grabovsky, V., Gauguet, J.-M., Feigelson, S., Manevich, E., Kolanus, W., . . . Alon, R. (2005). Lymphocyte arrest requires instantaneous induction of an extended LFA-1 conformation mediated by endothelium-bound chemokines. Nature immunology *6*, 497.

Shang, L., Thirunarayanan, N., Viejo-Borbolla, A., Martin, A.P., Bogunovic, M., Marchesi, F., . . . Lira, S.A. (2009). Expression of the chemokine binding protein M3 promotes marked changes in the accumulation of specific leukocytes subsets within the intestine. Gastroenterology *137*, 1006-1018, 1018 e1001-1003.

Shang, W., Jiang, Y., Boettcher, M., Ding, K., Mollenauer, M., Liu, Z., . . . Wang, H. (2018). Genome-wide CRISPR screen identifies FAM49B as a key regulator of actin dynamics and T cell activation. Proceedings of the National Academy of Sciences *115*, E4051-E4060.

Shiow, L.R., Rosen, D.B., Brdičková, N., Xu, Y., An, J., Lanier, L.L., . . . Matloubian, M. (2006). CD69 acts downstream of interferon-α/β to inhibit S1P1 and lymphocyte egress from lymphoid organs. Nature *440*, 540.

Shono, Y., Docampo, M.D., Peled, J.U., Perobelli, S.M., Velardi, E., Tsai, J.J., . . . Jenq, R.R. (2016). Increased GVHD-related mortality with broad-spectrum antibiotic use after allogeneic hematopoietic stem cell transplantation in human patients and mice. Science Translational Medicine *8*, 339ra371-339ra371.

Sigmundsdottir, H., Pan, J., Debes, G.F., Alt, C., Habtezion, A., Soler, D., and Butcher, E.C. (2007). DCs metabolize sunlight-induced vitamin D3 to 'program' T cell attraction to the epidermal chemokine CCL27. Nature immunology *8*, 285.

Sixt, M., Kanazawa, N., Selg, M., Samson, T., Roos, G., Reinhardt, D.P., . . . Sorokin, L. (2005). The Conduit System Transports Soluble Antigens from the Afferent Lymph to Resident Dendritic Cells in the T Cell Area of the Lymph Node. Immunity *22*, 19-29.

Skånland, Sigrid S., Moltu, K., Berge, T., Aandahl, Einar M., and Taskén, K. (2014). T-cell co-stimulation through the CD2 and CD28 co-receptors induces distinct signalling responses. Biochemical Journal *460*, 399-410.

Spahn, T.W., Weiner, H.L., Rennert, P.D., Lügering, N., Fontana, A., Domschke, W., and Kucharzik, T. (2002). Mesenteric lymph nodes are critical for the induction of high-dose oral tolerance in the absence of Peyer's patches. European journal of immunology *32*, 1109-1113.

Stegner, D., vanEeuwijk, J.M.M., Angay, O., Gorelashvili, M.G., Semeniak, D., Pinnecker, J., . . . Heinze, K.G. (2017). Thrombopoiesis is spatially regulated by the bone marrow vasculature. Nature Communications *8*, 127.

Streeter, P.R., Rouse, B.T., and Butcher, E.C. (1988). Immunohistologic and functional characterization of a vascular addressin involved in lymphocyte homing into peripheral lymph nodes. The Journal of Cell Biology *107*, 1853-1862.

Suchin, E.J., Langmuir, P.B., Palmer, E., Sayegh, M.H., Wells, A.D., and Turka, L.A. (2001). Quantifying the Frequency of Alloreactive T Cells In Vivo: New Answers to an Old Question. The Journal of Immunology *166*, 973-981.

Sumida, H., Lu, E., Chen, H., Yang, Q., Mackie, K., and Cyster, J.G. (2017). GPR55 regulates intraepithelial lymphocyte migration dynamics and susceptibility to intestinal damage. Science immunology *2*.

Sun, C.M., Hall, J.A., Blank, R.B., Bouladoux, N., Oukka, M., Mora, J.R., and Belkaid, Y. (2007). Small intestine lamina propria dendritic cells promote de novo generation of Foxp3 T reg cells via retinoic acid. J Exp Med *204*, 1775-1785.

Suzuki, T.A., and Nachman, M.W. (2016). Spatial Heterogeneity of Gut Microbial Composition along the Gastrointestinal Tract in Natural Populations of House Mice. PLoS One *11*, e0163720.

Teshima, T., Reddy, P., and Zeiser, R. (2016). Acute Graft-versus-Host Disease: Novel Biological Insights. Biology of blood and marrow transplantation : journal of the American Society for Blood and Marrow Transplantation *22*, 11-16.

Textor, J., Peixoto, A., Henrickson, S.E., Sinn, M., von Andrian, U.H., and Westermann, J. (2011). Defining the quantitative limits of intravital two-photon lymphocyte tracking. Proc Natl Acad Sci U S A *108*, 12401-12406.

Thornbury, K.D., McHale, N.G., Allen, J.M., and Hughes, G. (1990). Nerve-mediated contractions of sheep mesenteric lymph node capsules. The Journal of physiology *422*, 513-522.

Tomura, M., Yoshida, N., Tanaka, J., Karasawa, S., Miwa, Y., Miyawaki, A., and Kanagawa, O. (2008). Monitoring cellular movement in vivo with photoconvertible fluorescence protein “Kaede” transgenic mice. Proceedings of the National Academy of Sciences *105*, 10871-10876.

Toyjanova, J., Flores-Cortez, E., Reichner, J.S., and Franck, C. (2015). Matrix Confinement Plays a Pivotal Role in Regulating Neutrophil-generated Tractions, Speed, and Integrin Utilization. Journal of Biological Chemistry *290*, 3752-3763.

Tsuji, M., Suzuki, K., Kitamura, H., Maruya, M., Kinoshita, K., Ivanov, I.I., . . . Fagarasan, S. (2008). Requirement for Lymphoid Tissue-Inducer Cells in Isolated

Follicle Formation and T Cell-Independent Immunoglobulin A Generation in the Gut. Immunity *29*, 261-271.

Utgaard, J.O., Jahnsen, F.L., Bakka, A., Brandtzaeg, P., and Haraldsen, G. (1998). Rapid Secretion of Prestored Interleukin 8 from Weibel-Palade Bodies of Microvascular Endothelial Cells. The Journal of Experimental Medicine *188*, 1751-1756.

van der Windt, G.J.W., and Pearce, E.L. (2012). Metabolic switching and fuel choice during T-cell differentiation and memory development. Immunological reviews *249*, 27-42.

Van Houten, N., Mixter, P.F., Wolfe, J., and Budd, R.C. (1993). CD2 expression on murine intestinal intraepithelial lymphocytes is bimodal and defines proliferative capacity. International immunology *5*, 665-672.

Vantourout, P., Laing, A., Woodward, M.J., Zlatareva, I., Apolonia, L., Jones, A.W., . . . Hayday, A.C. (2018). Heteromeric interactions regulate butyrophilin (BTN) and BTN-like molecules governing γδ T cell biology. P Natl Acad Sci USA *115*, 1039-1044.

Via, C.S., Nguyen, P., Shustov, A., Drappa, J., and Elkon, K.B. (1996). A major role for the Fas pathway in acute graft-versus-host disease. J Immunol *157*, 5387-5393.

von Andrian, U.H., and Mempel, T.R. (2003). Homing and cellular traffic in lymph nodes. Nature Reviews Immunology *3*, 867.

Walker, L.S.K., Gulbranson-Judge, A., Flynn, S., Brocker, T., Raykundalia, C., Goodall, M., . . . Lane, P. (1999). Compromised Ox40 Function in Cd28-Deficient Mice Is Linked with Failure to Develop Cxc Chemokine Receptor 5–Positive Cd4 Cells and Germinal Centers. The Journal of Experimental Medicine *190*, 1115-1122.

Washington, K., and Jagasia, M. (2009). Pathology of graft-versus-host disease in the gastrointestinal tract. Human Pathology *40*, 909-917.

Watts, T.H. (2005). TNF/TNFR FAMILY MEMBERS IN COSTIMULATION OF T CELL RESPONSES. Annual Review of Immunology *23*, 23-68.

Wendt, E., and Keshav, S. (2015). CCR9 antagonism: potential in the treatment of Inflammatory Bowel Disease. Clinical and experimental gastroenterology *8*, 119-130.

Wolf, K., Muller, R., Borgmann, S., Brocker, E.B., and Friedl, P. (2003). Amoeboid shape change and contact guidance: T-lymphocyte crawling through fibrillar collagen is independent of matrix remodeling by MMPs and other proteases. Blood *102*, 3262-3269.

Woolf, E., Grigorova, I., Sagiv, A., Grabovsky, V., Feigelson, S.W., Shulman, Z., . . . Alon, R. (2007). Lymph node chemokines promote sustained T lymphocyte motility

without triggering stable integrin adhesiveness in the absence of shear forces. Nature immunology *8*, 1076-1085.

Worbs, T., Mempel, T.R., Bölter, J., von Andrian, U.H., and Förster, R. (2007). CCR7 ligands stimulate the intranodal motility of T lymphocytes in vivo. The Journal of Experimental Medicine *204*, 489-495.

Wurbel, M.-A., Philippe, J.-M., Nguyen, C., Victorero, G., Freeman, T., Wooding, P., . . . Naquet, P. (2000). The chemokine TECK is expressed by thymic and intestinal epithelial cells and attracts double- and single-positive thymocytes expressing the TECK receptor CCR9. European journal of immunology *30*, 262-271.

Wysocki, C.A., Panoskaltsis-Mortari, A., Blazar, B.R., and Serody, J.S. (2005). Leukocyte migration and graft-versus-host disease. Blood *105*, 4191-4199.

Yang, Y.G., Dey, B.R., Sergio, J.J., Pearson, D.A., and Sykes, M. (1998). Donor-derived interferon gamma is required for inhibition of acute graft-versus-host disease by interleukin 12. J Clin Invest *102*, 2126-2135.

Yoo, B.B., and Mazmanian, S.K. (2017). The Enteric Network: Interactions between the Immune and Nervous Systems of the Gut. Immunity *46*, 910-926.

Zarbock, A., and Ley, K. (2009). New insights into leukocyte recruitment by intravital microscopy. Current topics in microbiology and immunology *334*, 129-152.

Zilberstein, B., Quintanilha, A.G., Santos, M.A., Pajecki, D., Moura, E.G., Alves, P.R., . . . Gama-Rodrigues, J. (2007). Digestive tract microbiota in healthy volunteers. Clinics (Sao Paulo, Brazil) *62*, 47-54.

7 Annex

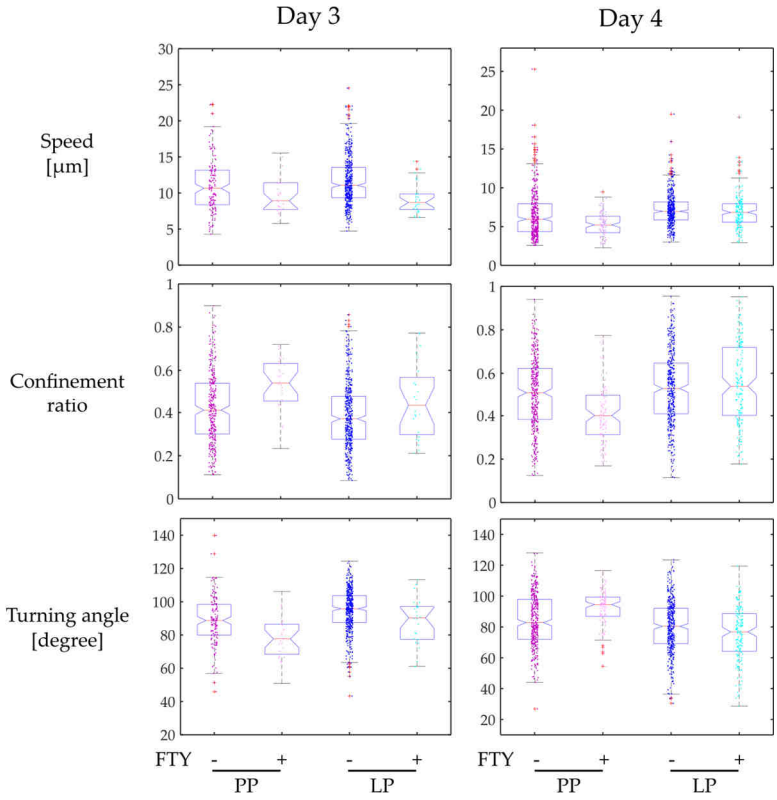

Figure 7-1 Preliminary results of migration patterns with fingolimod treatment. Analysis of the cell migration tracks inside and adjacent to Peyer's patches, with and without Fingolimod treatment. Fingolimod reduced the cell velocity both on day 3 and on day 4 inside and outside of the Peyer's patches. The confinement ration increased with fingolimod treatment on day 3 but was slightly reduced inside the Peyer's patch on day 4. The turning angle was antiproportionally altered. Data for day 3 and day 3.5 were pooled. One dot represents one cell track, n=5/ 1/ 13/ 2 mice for day 3 and 2/ 1/ 2/ 1 mice for day 4, left to right, outliers are indicated by a plus.

Table 7-1 Top five upregulated genes in the GvHD mucosa *vs.* bone marrow control

Gene names	padj	log2FoldChange BM+T *vs.* BM RNAseq
Pla2g4c	1,72E-116	6,711665312
Socs1	1,27E-130	5,175840504
Retnlb	1,02E-29	5,171271567
Ifng	6,34E-23	5,157368615
Gsdmcl-ps	1,45E-16	5,023157669

Table 7-2 Top five upregulated genes near the GvHD Peyer's patch

Gene names	padj	log2FoldChange Near PP *vs.* Far from PP
Cd247	1,83E-07	3,02049199
Cd2	0,0052	2,460315261
Parvg	0,0001	2,441031278
Cd27	0,0042	2,394772822
Ogdhl	0,0015	2,390875923

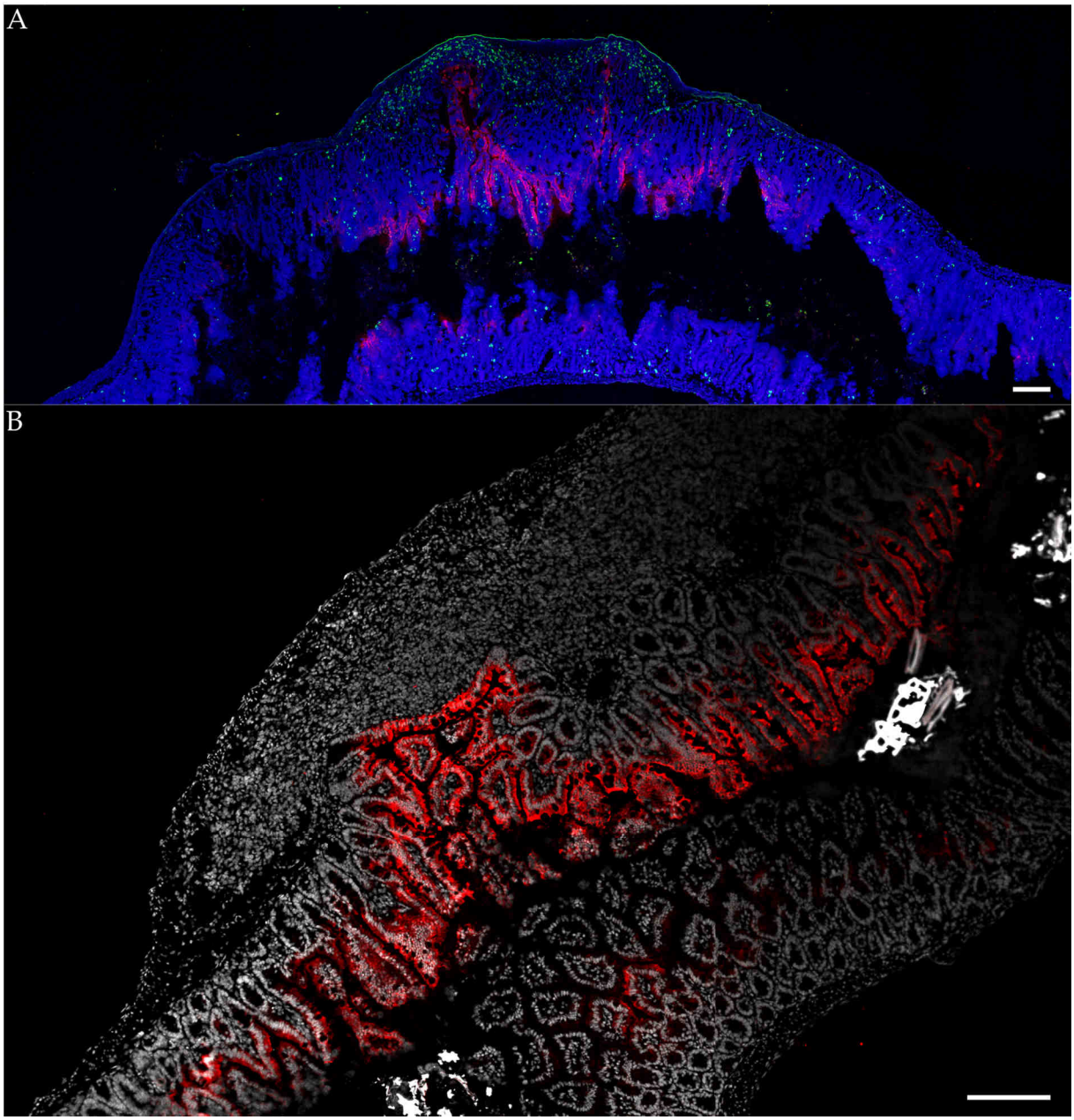

Figure 7-2 CCL25 expression around Peyer's patches 4 days after transplantation. **A** The intestinal epithelium around a Peyer's patch that contains donor T cells (CD90.1, green) expresses CCL25 (red). Cell nuclei were counter-stained with DAPI (blue). **B** Detail of CCL25 expression (red) by the follicle-associated epithelium and the epithelium of adjacent villi. Cell nuclei were counterstained with DAPI (white). Scale bar: 200 µm.

8 Publication list

Katja J Jarick, Zeinab Mokhtari, Lukas Scheller, Julia Hartweg, Sina Thusek, Duc-Dung Le, Maria Ranecky, Haroon Shaikh, Musga Qureischi, Katrin G Heinze, Andreas Beilhack.
Photoconversion of Alloreactive T Cells in Murine Peyer's Patches During Acute Graft-Versus-Host Disease: Tracking the Homing Route of Highly Proliferative Cells In Vivo.
Frontiers in Immunology 2018 Jun 27; Vol 9 (Issue 1468). doi: 10.3389/fimmu.2018.01468

Jan Hülsdünker, **Katja J Ottmüller**, Hannes P Neeff, Motoko Koyama, Zhan Gao, Oliver S Thomas, Marie Follo, Ali Al-Ahmad, Gabriele Prinz, Sandra Duquesne, Heide Dierbach, Susanne Kirschnek, Tim Lämmermann, Martin J Blaser, Brian T Fife, Bruce R Blazar, Andreas Beilhack, Geoffrey R Hill, Georg Hacker, Robert Zeiser
Neutrophils provide cellular communication between ileum and mesenteric lymph nodes at graft-versus-host disease onset.
Blood, 2018 April 19; Vol 131, (Issue 16), p. 1858-1869. doi: 10.1182/blood-2017-10-812891

Tobias Wertheimer, Enrico Velardi, Jennifer Tsai, Kirsten Cooper, Shiyun Xiao, Christopher C Kloss, **Katja J Ottmüller**, Zeinab Mokhtari, Christian Brede, Paul deRoos, Sinead Kinsella, Brisa Palikuqi, Michael Ginsberg, Lauren F Young, Fabiana Kreines, Sophia R Lieberman, Amina Lazrak, Peipei Guo, Florent Malard, Odette M Smith, Yusuke Shono, Robert R Jenq, Alan M Hanash, Daniel J Nolan, Jason M Butler, Andreas Beilhack, Nancy R Manley, Shahin Rafii, Jarrod A Dudakov, Marcel RM van den Brink
Production of BMP4 by endothelial cells is crucial for endogenous thymic regeneration.
Science immunology 2018 Jan12; Vol3 (Issue 19). doi: 10.1126/sciimmunol.aal2736.

Martin Chopra, Marlene Biehl, Tim Steinfatt, Andreas Brandl, Juliane Kums, Jorge Amich, Martin Vaeth, Janina Kuen, Rafaela Holtappels, Jürgen Podlech, Anja Mottok, Sabrina Kraus, Ana-Laura Jordan-Garrote, Carina A Bäuerlein, Christian Brede, Eliana Ribechini, Andrea Fick, Axel Seher, Johannes Polz, **Katja J Ottmüller**, Jenette Baker, Hidekazu Nishikii, Miriam Ritz, Katharina Mattenheimer, Stefanie Schwinn, Thorsten Winter, Viktoria Schäfer, Sven Krappmann, Hermann Einsele, Thomas D Müller, Matthias J Reddehase, Manfred B Lutz, Daniela N Mannel, Friederike Berberich-Siebelt, Harald Wajant, Andreas Beilhack
Exogenous TNFR2 activation protects from acute GvHD via host T reg cell expansion.
The Journal of experimental medicine, 2016 Aug 22; Vol 213 (Issue 9) 1881-1900.

Anke Schmidt, Sander Bekeschus, **Katja J Jarick**, Sybille Hasse, Thomas von Woedke, Kristian Wende
Cold physical plasma modulates p53 and mitogen-activated protein kinase signaling in keratinocytes.
Oxidative Medicine and Cellular Longevity; 2019 Jan 13, Volume 2019, Article ID 7017363. Doi: 10.1155/2019/7017363

Lena Bundscherer, Kristian Wende, **Katja Ottmüller**, Anne Barton, Anke Schmidt, Sander Bekeschus, Sybille Hasse, Klaus D Weltmann, Kai Masur, Ulrike Lindequist
Impact of non-thermal plasma treatment on MAPK signaling pathways of human immune cell lines.
Immunobiology 2013 Jun 6; Volume 218 (Issue 10), p. 1248-1255. Doi: 10.1016/j.imbio.2013.04.015

Anke Schmidt, Kristian Wende, Sander Bekeschus, Lena Bundscherer, Anne Barton, **Katja Ottmüller**, Klaus D Weltmann, Kai Masur
Non-thermal plasma treatment is associated with changes in transcriptome of human epithelial skin cells.
Free radical research 2013 May 15; Vol. 47 (Issue 8), p. 577-592. doi: 10.3109/10715762.2013.804623